Optimal Design of Variable-Stiffness Fiber-Reinforced Composites Using Cellular Automata

Shahriar Setoodeh

Dissertation submitted to the Faculty of the
Virginia Polytechnic Institute and State University
in partial fulfillment of the requirements for the degree of

Doctor of Philosophy
in
Engineering Mechanics

Zafer Gürdal, Chair
Romesh C. Batra
Michael W. Hyer
Robert M. Jones
Layne T. Watson

September 21, 2005
Blacksburg, Virginia

Keywords: Cellular Automata, Compliance Design,
Tow-placed laminates, lamination parameters.
Copyright 2005, Shahriar Setoodeh

Optimal Design of Variable-Stiffness Fiber-Reinforced Composites Using Cellular Automata

Shahriar Setoodeh

(ABSTRACT)

The growing number of applications of composite materials in aerospace and naval structures along with advancements in manufacturing technologies demand continuous innovations in the design of composite structures. In the traditional design of composite laminates, fiber orientation angles are constant for each layer and are usually limited to 0, 90, and ± 45 degrees. To fully benefit from the directional properties of composite laminates, such limitations have to be removed. The concept of variable-stiffness laminates allows the stiffness properties to vary spatially over the laminate. Through tailoring of fiber orientations and laminate thickness spatially in an optimal fashion, mechanical properties of a part can be improved. In this thesis, the optimal design of variable-stiffness fiber-reinforced composite laminates is studied using an emerging numerical engineering optimization scheme based on the cellular automata paradigm.

A cellular automaton (CA) based design scheme uses local update rules for both field variables (displacements) and design variables (lay-up configuration and laminate density measure) in an iterative fashion to convergence to an optimal design. In the present work, the displacements are updated based on the principle of local equilibrium and the design variables are updated according to the optimality criteria for minimum compliance design. A closed form displacement update rule for constant thickness isotropic continua is derived, while for the general anisotropic continua with variable thickness a numeric update rule is used.

Combined lay-up and topology design of variable-stiffness flat laminates is performed under the action of in-plane loads and bending loads. An optimality criteria based formulation is used to obtain local design rules for minimum compliance design subject to a volume constraint. It is shown that the design rule splits into a two step application. In the first step an optimal lay-up configuration is computed and in the second step the density measure is obtained. The spatial lay-up design problem is formulated using both fiber angles and lamination parameters as design variables. A weighted average formulation is used to handle multiple load case designs. Numerical studies investigate the performance of the proposed design methodology. The optimal lay-up configuration is independent of the lattice density with more details emerging as the density is increased. Moreover, combined topology and lay-up designs are free of checkerboard patterns.

The lay-up design problem is also solved using lamination parameters instead of the fiber orientation angles. The use of lamination parameters has two key features: first, the convexity of the minimization problem guarantees a global minimum; second, for both in-plane and bending problems it limits the number of design variables to four regardless of the actual number of layers, thereby simplifying the optimization task. Moreover, it improves the

convergence rate of the iterative design scheme as compared to using fiber angles as design variables. Design parametrization using lamination parameters provides a theoretically better design, however, manufacturability of the designs is not certain. The cases of general, balanced symmetric, and balanced symmetric with equal thickness layers are studied separately. The feasible domain for laminates with equal thickness layers is presented for an increasing number of layers. A restricted problem is proposed that maintains the convexity of the design space for laminates with equal thickness layers. A recursive formulation for computing fiber angles for this case is also presented.

On the computational side of the effort, a parallel version of the present CA formulation is implemented on message passing multiprocessor clusters. A standard parallel implementation does not converge for an increased number of processors. Detailed analysis revealed that the convergence problem is due to a Jacobi type iteration scheme, and a pure Gauss-Seidel type iteration through a pipeline implementation completely resolved the convergence problem. Timing results giving the speedup for the pipeline implementation were obtained for up to 260 processors.

This work was supported by Grant NAG-1-01105 from NASA Langley Research Center. Special thanks to our project monitor Dr. Damodar R. Ambur for his technical guidance.

To my mother Mehrangiz, and
my wife Valia.

Acknowledgments

On completion of this thesis, I feel obliged to all whose precious help made this work possible. My advisor, Professor Zafer Gürdal, whose continuous support and thorough supervision guided me throughout my research work. Special thanks to my colleague and best friend, Dr. Mostafa M. Abdalla, for his continuous inspiration and constructive suggestions. My greatest appreciations to Prof. Layne T. Watson for his guidance, particularly on numerical schemes. Also, I wish to extend my thanks to Prof. Robert M. Jones for his valuable insights and recommendations for better presentation, and to Professors Michael W. Hyer and Romesh C. Batra for serving in my dissertation committee.

Finally, I would like to thank my wife, Valia, for her unconditional support.

Contents

List of Figures

List of Tables

Chapter 1

Introduction

1.1 Motivation

Manufacturing fiber-reinforced composite laminates with spatially varying fiber orientation is possible using advanced tow-placement machines. Tow-placement machines are computer numerical controlled multi-axis machines that are capable of steering up to 36 parallel tows along prescribed paths [15]. Each tow can be placed at a different rate allowing a radius of curvature as low as 20 inches. Moreover, tows can be independently stopped and restarted permitting flexible coverage patterns to build laminated panels. Such flexibilities in steering fiber tows along customized paths provides new design possibilities that can be used to improve the mechanical properties of composite laminates.

Contrary to the classical stacking sequence design of composite laminates with constant ply-angles, each ply can be designed with spatially optimal fiber orientations resulting in variation of the mechanical properties over the structure. Such laminates are often termed as "variable-stiffness panels" in the literature [22, 80]. The idea of variable-stiffness plates is not limited to composite materials only. Isotropic plates with variable thickness, which are well studied in the theory of plates and shells [72], can also be viewed as variable-stiffness structures. By allowing the stiffness properties of composite laminates to vary from one point to another, the design space is expanded as compared to the classical stacking sequence design problem. As a consequence, stiffer and lighter structures can be designed.

Introducing an extended number of design variables to model the spatially varying mechanical properties of variable-stiffness panels in a global design formulation (e.g., minimum compliance, maximum frequency, maximum buckling load, etc.) would lead to a very difficult if not unsolvable problem. Several researchers have used a curvilinear fiber path definition to reduce the number of design variables to a very limited number of tuning parameters controlling the curvilinear fiber paths [35, 50].

The goal of this study is to present a combined topology and lay-up design methodology based on rigorous optimality criteria which can accurately model variable-stiffness laminates without being limited to a predefined family of fiber path curves. Besides, the emerging cellular automata paradigm is employed in a parallel computing environment to substantially reduce the computational costs.

1.2 Literature Review

Optimum filament orientation of fiber-reinforced composites was studied as early as 1970 by Brandmaier [11], where maximum composite strength was sought by aligning the fiber direction based on local stresses. The article was the first to point out that the optimal fiber orientation could be different from the intuitive principal stress direction depending on the strength properties of the lamina. In a series of publications, Pedersen [52, 53, 54, 55, 56] studied optimal fiber orientations by finding local and global extrema of the strain energy density analytically and showed that the optimal fiber orientation depends not only on the ratio of the two principal strains, but also on dimensionless material parameters.

Cooper [12] used energy methods to establish optimality conditions for fiber reinforcement. He defined trajectorial fiber reinforcement, or principal trajectories for the fibers, as the orientation that maximizes the stiffness or the strength for a given weight and given stress or strain state. Banichuk [6] formulated the compliance design problem in a variational form and derived the necessary extremum condition analytically for optimal orientation of the axes of orthotropy at any point in a two-dimensional medium. The classical compliance minimization problem was solved for optimal fiber orientations and fiber volume fraction, subject to a fiber-cost-function constraint by Duvaut et al. [14]. Although the fiber patterns presented appear to be realistic, it is not clear how composite panels with a variable fiber volume fraction can be manufactured.

The references cited above treated the design optimization as determining the spatial fiber orientation based on local stress states. A more interesting, and perhaps more challenging, design optimization problem is to determine the optimal distribution of fiber orientation angles to improve a global measure of performance for a structure or structural component. For example, global fiber path representation, using a linear combination of non-uniform rational B-splines (NURBS) passing through a fixed number of control points, was implemented by Nagendra et al. [50] for rectangular laminates. They studied optimal frequency and buckling design of laminated composites plates subject to deformations, ply failure, and interlaminar stress constraints. The design variables were scalar multipliers of the different basis fiber paths. An in-depth study of rectangular panels with curvilinear fiber paths, termed variable-stiffness panels, was performed in a series of publications by Gürdal et al. [22, 23, 69]. The curvilinear fiber paths in these publications were generated from a base curve that changes its orientation linearly from one end of the panel to the other, while taking constraints on the radius of curvature of the fiber paths into account. The authors

manufactured such panels by using an advanced tow-placement machine. Even though use of linearly varying fiber orientation along the panel length represents only a limited class of spatially varying fiber orientations, those studies showed that considerable improvements in laminate responses such as buckling load can be gained. Moreover, such panels are relatively easy to analyze and manufacture, and have few design variables, thereby simplifying the optimization task.

For more complex geometries, design optimization was performed utilizing finite element analysis models. For example, Hyer and Charette [30] used the intuitive principal stress design with constant-fiber-orientation finite elements to design a plate with a center cutout. For a similar geometry, Katz et al. [35] used sequential linear programming to maximize the failure load based on the maximum strain criterion. The plate was modeled by the finite element method, and sensitivity, with respect to fiber orientation, was calculated by variational methods. Results showed substantial improvements in load-carrying capacity. Improvements in buckling resistance of composite plates with a circular center hole is studied by Hyer and Lee [31] using curvilinear fiber format. They used traditional sensitivity studies to find conditions that maximize buckling performance of a plate with a central circular hole. A quarter model was used with selected regions of fixed fiber orientations. Ultimately, radial regions with fixed fiber orientations were studied. In a similar work, Banichuk et al. [7] used triangular finite elements to search for optimal angles of orthotropy, which maximizes the critical buckling parameter. Their numerical results for the compressed plates showed a significant increase in the critical buckling load just with reorientation of the orthotropic material in an optimal manner. Load paths used as a trajectory taken by a given load starting from the point of application and ending at an equilibrating reaction point were introduced by Kelly and Tosh [36]. They used this load path direction to design curvilinear fiber paths for a plate with a hole. This design approach, although in some sense ensures continuity of fiber tows, satisfies neither local nor global optimality conditions. In a more recent publication, Tosh and Kelly [73] studied design, manufacturing, and testing of a specimen containing an open hole.

Topology design of isotropic materials on the other hand, is also a well developed topic in the structural optimization community. Extensive mathematical models have been developed and successfully applied to design structures such as trusses, beams, and plates. In the case of two-dimensional plates, Solid Isotropic Material Penalization (SIMP) is a promising technique to generate black (full thickness) and white (zero thickness) designs almost free of any gray areas (intermediate thicknesses) [10]. On the contrary, relatively little effort has been made in simultaneous design for orientation and topology. Pedersen [54, 56] minimized elastic strain energy with two groups of design variables, the material orientation and thickness subjected to a volume constraint. Hansel and Becker [27] proposed a heuristic optimization algorithm for minimum weight design of composite laminates based on layer-wise removal of elements with low stress measures. Parnas et al. [51] studied minimum weight design of composite laminates subject to the Tsai-Hill failure criterion as stress constraints by sequential quadratic programming. They constructed a bi-cubic Bezier surface for layer

thickness representation and cubic Bezier curves for fiber angles and used coordinates of the control points as design variables for a reduced number of the design variables.

Despite the progress made, there are shortcomings of the previous studies. The above studies lack generality. First, the global curve-fitting technique often used to represent continuous fiber paths has limited tailorability, restricting the fiber paths to a narrow class of predefined curves, and cannot be easily generalized for irregular geometries. Second, topology design of laminated composites using evolutionary techniques lacks a rigorous mathematical basis for optimality. Moreover, variable thickness or density laminae are not practical from the manufacturing point of view because composite layers are usually produced with fixed thicknesses and fixed fiber volume fractions. Finally, repeated finite element analyses are usually required which make the design task computationally expensive especially for large-scale structures exhibiting nonlinear behavior.

A remedy to these drawbacks would be an algorithm in which the entire design space is explored by treating fiber angles at any point in the domain as a continuous design variable. This is possible by reducing the global coupled design problem into a set of uncoupled local optimization problems. As it will be shown in this study, by local interpretation of the optimality criteria for minimum compliance design simple local design rules can be obtained. Second, to reduce the computational costs in real-life design problems, use of parallel computing environments seems inevitable. Therefore, algorithms that can easily be implemented on massively parallel machines are very appealing in the field of structural design.

A potential methodology that seems to meet all these requirements is an algorithm that utilizes the cellular automata (CA) paradigm. Cellular automata are a novel methodology that are suitable for the present structural problem. A basic feature of the CA approach is to divide the domain of interest into a large number of cells that typically form a regular grid over the domain. The cells in the domain only interact with their neighboring cells performing local computations. This approach is inherently suitable for parallel implementations because of the local nature of information flow among the neighboring cells and data storage, which does not require keeping information other than local cell level data. Therefore, by employing massively parallel processor machines simulation costs can be considerably reduced.

Recent studies showed the effectiveness of CA-based analysis and design in structures such as trusses [23, 69], beams [3], two-dimensional isotropic continua [2], and fiber-angle design of composite laminae [67]. In the present study, those ideas are extended to the design of fiber-reinforced composite laminates through combined tailoring of the local fiber orientation angle and topology design. In this study, optimality criteria for combined fiber angle and topology design of a two-dimensional composite laminate using SIMP specialization are presented. Locally interpreted optimality criteria are implemented in a cellular automata (CA) frame work which allows the same level of discretization for both design variables and field variables without causing any numerical instabilities or checkerboards.

1.3 Problem Definition

Consider a linearly elastic fiber-reinforced composite laminate where the laminate lay-up, i.e., fiber orientation angles and laminate thickness, varies spatially over the domain. The objective of the present study is to obtain the optimal distribution of laminate lay-up and density measure such that compliance is minimized subjected to a constraint on the total volume. The design variables are local density measures and laminate lay-ups. The laminate lay-up can be represented with either layer thicknesses and fiber orientation angles or lamination parameters.

1.4 Thesis Layout

In the next chapter, first an introduction to structural design using cellular automata is given followed by description of the elements of CA in structural design. Then the previous CA applications in structural design, i.e., trusses and isotropic continua, are reviewed.

The idea of topology design of 2-D isotropic continua, is extended to anisotropic media in Chapter 3. The analysis update rule is essentially very similar to that of isotropic problems except that the effect of the anisotropy is included in the constitutive relations. The design update rule on the other hand, is based on general optimality criteria for minimum compliance design. As it will be shown in Section 3.3, the optimality criteria will be reduced to a two-level design update rule. In the first level, the lay-up is designed while in the second level the density is being updated. The lay-up design problem is studied by treating both fiber angles and lamination parameters as design variables is separate cases.

Chapter 4 presents briefly the implemented code based on the update rules as derived in Chapter 3. Also, the basic and pipeline parallel implementations are discussed. Next, a set of numerical examples are presented to show the performance of the proposed formulation. Chapter 5, summarizes the accomplishments and conclusions made.

Chapter 2

Cellular Automata in Structural Design

2.1 Introduction

The cellular automata (CA) paradigm was initially introduced as early as 1946 [82, 77, 78, 83, 84], but remained unpopular until recent times possibly due to limited available parallel computing resources and the difficulty of parallel programming. Massively parallel machines have made CA an attractive tool for many physical and mathematical applications. Currently, CA applications include digital image processing [57], heat transfer [42], structural design [23], and traffic flow simulations [79].

The basic idea of the CA is to decompose a seemingly complicated system into small components (cells) governed by simple rules. These cells then act together to predict the global behavior of the system. CA divides the domain of interest into a large number of cells that typically form a regular grid. The cells in the domain only interact with their neighboring cells performing local computations. This approach is trivially parallelizable because of the local nature of information flow among the neighboring cells and data storage. Besides, the local update rules are usually very simple (as compared to traditional techniques to solve the global system) making it easy to implement CA on massively parallel machines.

An important characteristic of the CA in 2-D structural design, initially implemented by Gürdal and Tatting [23], is the integration of the analysis and design in their numerical implementation. Local cell level rules are developed and implemented for the update of both the field variables, which corresponded to the displacement degrees of freedom of the cells, and the design variables, which were used to size the cells. Hence, CA methodology can be thought of as a simultaneous analysis and design approach [24], even if the cell level updates are implemented sequentially, thereby eliminating the need for repetitive finite element analyses that are required by the traditional optimization schemes. Moreover, earlier

studies [23] showed that the local analysis update rules can easily be written based on prior deformed states so that geometric or material nonlinearities can easily be taken into account during the design updates.

Recent studies have shown effectiveness of CA-based analysis and design of structural components such as trusses [23, 49], beams and columns [3], and two-dimensional isotropic continua [69, 39, 2]. In the present study, those ideas are extended to the design of fiber-reinforced laminated composite plates for optimal stiffness through the tailoring of local fiber orientation angle, which allow stiffness properties to be varied from one point in the domain to the next similar to the curvilinear fiber path design [50].

In this study, the cellular automaton paradigm is adopted for design of variable-stiffness laminates. CA are especially appealing in this context for several reasons. First, computational costs could be substantially reduced without much additional efforts by parallel computing. Second, the analysis and design processes can be combined at the local level to potentially cut back on the computational costs, specially for nonlinear problems. Finally, it is believed that some of the manufacturing issues can be addressed at the local level.

2.2 Elements of Cellular Automata

The elements of cellular automata are CA cell, lattice, neighborhood, and update rules. These elements will be discussed in the context of structural design in the following sections.

2.2.1 CA Cell

A cellular automaton consists of a grid of identical cell components governed by simple rules acting on them to predict complicated behavior of a system based on the local behavior of the cells. These small components (cells) interact with a group of adjacent cells known as a cell neighborhood. A CA cell is a point in the space which recognizes a group of its neighboring cells and carries self-descriptive information known as *cell states*.

In CA for structural design, quantities such as generalized displacements, generalized forces, density measure, lay-up information, i.e., fiber angles, or lamination parameters, and laminate stiffness matrices **ABD** (see [33] for the definitions) constitute the numeric state of a cell. Boolean cell states may also be used to store the convergence state of a cell as well as its failure status. Character cell states are used to define the boundary condition of the cell degrees of freedom. For instance, whether a cell has a fixed displacement, applied load, or is free. The primary field variables in such a formulation are the generalized displacements whereas cell density and lay-up information are the design variables.

2.2.2 CA Lattice

Any two-dimensional domain is discretized using a regular lattice of CA cells numbered in a row-wise fashion. For non-rectangular geometries, a polygon is defined to approximately model the geometry. Cells outside of this polygon are turned off by simply assigning a zero density to them. This is implemented by invoking a "point in polygon" routine in which the coordinates of cells are compared against those of the polygon vertices (after Slotta et al. [68]).

2.2.3 Cell Neighborhood

The cell neighborhood can be any group of cells, including cells that are beyond the immediately adjacent cells on the grid. Often what is called the classical *von Neumann* and *Moore* neighborhoods are used. The von Neumann neighborhood has five cells: the center cell C and the other four are usually described by the directions N, E, S, and W, as shown in Figure 2.1(a). The Moore neighborhood shown in Figure 2.1(b) is a 3×3 square grid of cells, again described by the center cell C and the directions N, NE, E, SE, S, SW, W, and NW. A CA cell has a list of quantities associated with it that specify its state and are updated in discrete time steps using prespecified rules. During this update process, a cell uses only its own state and state information of the neighboring cells.

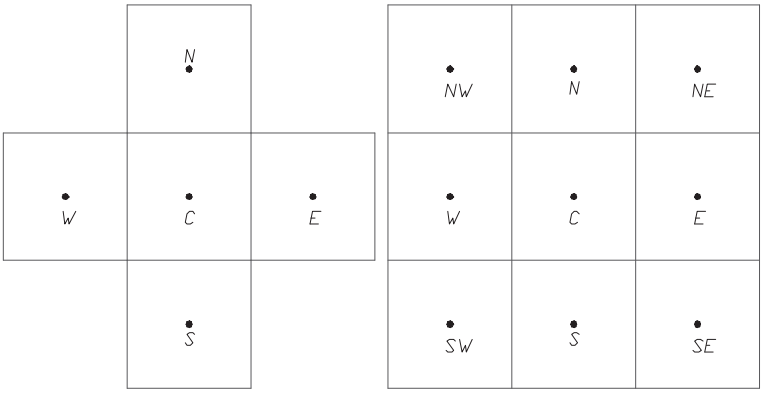

(a) von Neumann. (b) Moore.

Figure 2.1: CA cell neighborhoods

2.2.4 Update Rules

Basically, each cell update has two parts: *analysis update* and *design update*. The analysis rule updates the field variables based on the local equilibrium of cells, and the design rule

updates the design variables according to locally interpreted optimality criteria for minimum compliance design (see Section 3.3). These two rules can also be derived combined together in a simultaneous analysis and design fashion where both generalized displacements and design variables are computed from one single optimization problem. However, for the sake of simplicity in the present study, separate rules are used.

The analysis update rule updates the generalized displacements of the site cell given displacements of the neighboring cells. This rule is governed by the equilibrium of the local neighborhood which is fundamentally the same as minimization of the total potential energy over the cell neighborhood.

The design update on the other hand, seeks the optimal topology and lay-up that minimizes the compliance of a structure with a volume constraint. It will be shown in the next chapter that the optimality criteria for the minimum compliance design will be reduced into two levels of minimization at any point in the domain. The first level is local minimization of the complimentary strain energy density for which one can consider either fiber angles or lamination parameters as design variables. The second level is the topology design where density is being updated.

2.3 Iteration Schemes

In a CA-based analysis, an analysis update rule is applied to all cells in the lattice iteratively until displacements of all cells are converged in a relative sense. However, in a CA analysis and design, the design update rule is activated before full convergence in the displacement field is achieved. This activation occurs whenever the displacements are converged in a looser sense than the main termination criterion.

The process of lattice update can be done either in block Jacobi or Gauss-Seidel fashion. In Jacobi style updates, each cell uses neighboring cell information from the previous iteration, which in effect waits for all the cells to be updated synchronously before the next iteration of the update rules. With the Gauss-Seidel style scheme, the cell updates can be asynchronous, and new information is used if the neighboring cells are already updated. It can be shown that the CA analysis update is identical to a classical iterative solution of the equivalent global finite element model ($\mathbf{KX} = \mathbf{F}$) and is hence convergent ([68]).

In a CA-based structural analysis, the deformation starts propagating like a wave throughout the entire domain starting from the location of applied forces. The structural restraints are not sensed until this deformation wave reaches a support and bounces back. Such an oscillation will damp and eventually settle in the equilibrium deformed shape (the CA-based analysis is equivalent to an iterative solution of the global equilibrium equation and therefore is convergent). If the cell design update starts while the deformation still has large oscillations, divergence may occur. To prevent such a divergence, rather than performing cell design updates every iteration, the cell design update is performed every N iterations,

where N is also known as the design frequency [23, 68, 49]. Since the appropriate value of N which makes the design process convergent depends on the lattice size and the model, as initially suggested by Abdalla and Gürdal [2], the norm of the residual force on the structure could also be examined as a measure of the global equilibrium to activate the cell design update. Moreover, to improve convergence of the iterative CA scheme, move limits are usually imposed on the area sizing.

It is also important to emphasize that the lattice *design update* process is performed in a Jacobi sense. This means that once a cell design process is completed, the new values of the design variables are stored separately and they are updated only after the entire lattice had been designed.

2.4 Fully Stressed Design of Trusses

The first application of cellular automata in structural design that we are aware of was proposed by Gürdal et al. [23]. They used the CA paradigm for both linear and non-linear analysis and design of statically determinate truss structures. The Moore neighborhood was used with eight bar members as shown in Figure 2.2(b). Presuming bar members have the same behavior in tension and compression, a fully stressed design approach was used to design trusses, starting off from a ground structure as shown in Figure 2.2(a) (fully stressed design of statically determinate trusses is equivalent to minimum weight design of trusses subject to stress constraint [25]). The fully stressed design idea of trusses was later extended to design of 2-D isotropic continua with an equivalent truss model [69].

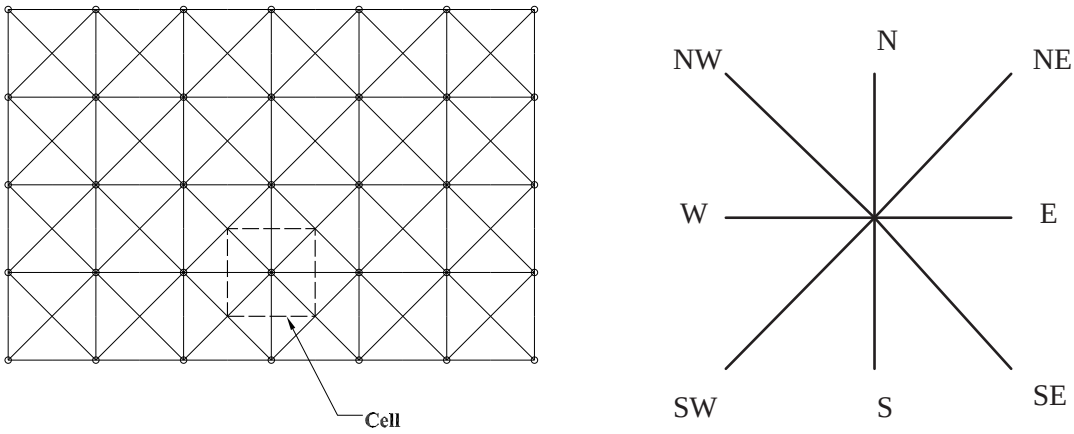

(a) Ground structure. (b) Moore neighborhood.

Figure 2.2: CA ground structure and Moore neighborhood for trusses.

In the present study, truss structures were used as an initial application of CA in structural design to implement a new generic cellular automata Fortran 90 code. Later on, the same

code was extended to 2-D anisotropic continua. Here for the sake of completeness, the truss application is briefly discussed along with a new local update scheme which would improve the rate of convergence [49].

In a CA lattice, cells are numbered in a row-wise fashion. For the i-th cell state in a Moore neighborhood is defined as follows

$$\phi_i = \{(u_i, v_i), (f_i^x, f_i^y), (A_i^{SW}, A_i^S, A_i^{SE}, A_i^W, A_i^E, A_i^{NW}, A_i^N, A_i^{NE})\} \tag{2.1}$$

where u_i and v_i are the horizontal and vertical displacements respectively. The reaction forces are denoted by f_i^x and f_i^y in the x and y directions respectively, and the member areas are represented by $A_i^{SW}, A_i^S, \ldots, A_i^{NE}$.

Given displacements of the neighboring cells, the center cell displacements can be easily obtained in closed form simply by minimizing the total potential energy [23]. Once the cell displacements are updated, strain and consequently stress in each member can be readily computed. According to the fully stressed design approach, the cross-sectional area of each member is then chosen to withstand the applied stress based on the allowable stress for the material used [25].

2.4.1 A New Local Update Scheme

An alternative approach to cell updates is to update cell displacements and design variables simultaneously through a single minimization problem. Missoum et al. [49] showed that the minimum-weight design of a ground truss structure subject to equilibrium and stress constraints is equivalent to satisfying the coupled conditions of equilibrium and the fully stressed design at the local cell level. The solution of this coupled system can be obtained by repeating the analysis and design update rules until convergence. However, it is not obvious that this process should actually be repeated until convergence at the cell level. For this reason, a number of "repeats", R, is introduced which represents the number of times the sequence of the analysis and design updates is repeated in each CA iteration. This defines a new local update for the CA process called the "repeat approach" here.

Experiments based on this scheme have been performed in a Gauss-Seidel and a Jacobi environment on several problem sizes and various numbers of repeats. The results show that the repeat approach is robust for small numbers of repeats with a near independency on the move limits. This statement is valid with Gauss-Seidel or Jacobi iterations. This represents a major improvement over the standard approach, which is very dependent on move limits, design update frequencies and exhibits marked convergence difficulties with Jacobi iterations (for thorough discussions see Missoum et al. [49]).

2.5 Topology Design of Isotropic Continua

Application of cellular automata in topology design of isotropic continua was initially suggested by Kita and Toyoda [39]. They used finite elements as the global deformation analysis tool and implemented a local density update rule for topology design. Tatting and Gürdal [69] also presented a CA-based topology design approach using an extended truss formulation, however, in their formulation both analysis and design were performed at the local level. Abdalla and Gürdal [2] used local minimization of the energy to obtain a local analysis update rule and optimality criteria based design rule for topology design of isotropic continua. The present study is essentially an extension of their formulation to anisotropic media.

Chapter 3

Extension of Cellular Automata to Anisotropic Continua

3.1 Introduction

The CA update rule in structural design has two parts. First, the analysis rule where displacements of the site cells are updated given displacements of the neighboring cells and, second, the design update rule where design variables are updated according to some local criterion. The analysis rule is governed by the physical principle of equilibrium of the local neighborhood. Depending on the structure under consideration, such an update rule would be different. The idea of the cellular automata is to implement an update rule in its simplest mathematical form (preferably a closed form) such that local updates can be performed at minimum computational costs. However, deriving a closed from update rule might or might not be possible for every type of structure. For example, in the case of truss structures, it is possible to find a closed form analysis rule [23]. However, for 2-D anisotropic continua, even if a closed explicit form exists, it will contain lengthy expressions which could be computationally as expensive as an implicit numerical rule. In this study, numerical analysis rules are presented for 2-D anisotropic continua for both in-plane and bending deformations. To implement a computational tool, the simple case of the truss structures where a closed form update rule is already available is considered first. Later, the same framework is extended to 2-D anisotropic continua.

3.2 In-Plane Analysis Update Rule

For in-plane analysis of anisotropic continua, we define the state of the i-th cell as:

$$\phi_i = \{(u_i, v_i), (f_i^x, f_i^y), (\rho_i, \theta_i), \mathbf{A}_i\} \tag{3.1}$$

where u_i and v_i are the cell displacements in the x and y directions respectively, f_i^x and f_i^y are the external forces acting on the i-th cell in the corresponding directions. Density measure and fiber angle of the cell are denoted by ρ_i and θ_i, and $\mathbf{A}_i$ is the in-plane laminae stiffness for which, due to symmetry, only the upper half diagonal of the matrix is stored (six elements). The reason for storing $\mathbf{A}_i$ is that between two consecutive design iterations the $\mathbf{A}_i$ matrix remains unchanged and a repeated material transformation, which is numerically expensive, should be avoided. In the following section, details of the update rules for the in-plane problem will be discussed.

3.2.1 A Numeric Analysis Rule

One can assume different neighborhoods and a variety of displacement interpolation models to derive the analysis update rule for a 2-D continuum. The simplest of all would be a von Neumann neighborhood, which is modeled with eight constant strain finite element triangles and nine nodes as shown in Figure 3.1(a). This model introduces auxiliary nodes (1 through 4) which have to be removed using a condensation technique at the price of additional computations [67]. In this study, to the avoid auxiliary nodes, a Moore neighborhood is used instead of von Neumann. Four square bilinear elements are used to construct a local analysis update model as shown in Figure 3.1(b).

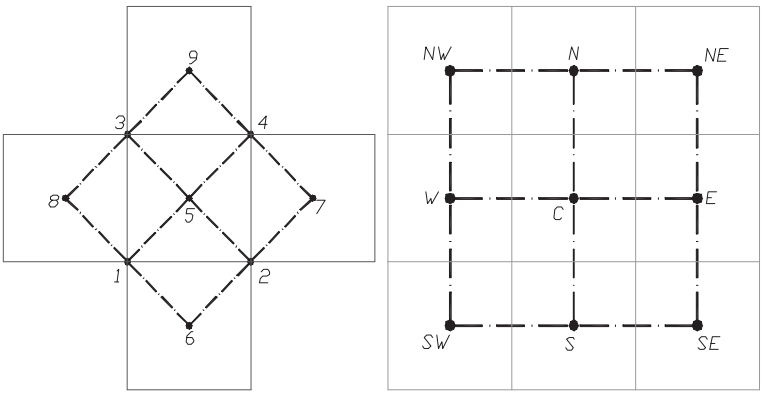

(a) Constant strain triangle model.

(b) Bilinear model.

Figure 3.1: Cell neighborhood models.

In this model, each bilinear element has constant thickness given by following reciprocal averaging formula as suggested by Abdalla and Gürdal [2]:

$$\frac{1}{\bar{\rho}^p} = \frac{1}{4}\sum_{i=1}^{4}\frac{1}{\rho_i^p}, \tag{3.2}$$

where ρ_i's are the density measures of the four nodes of the bilinear element such that $\varepsilon \leq \rho_i \leq 1$ and p is the so called SIMP penalization parameter and is usually chosen such that $p \geq 3$ [10]. This density interpolation scheme is chosen such that any node with a density measure below the threshold value ε would *turn off* all four elements in which the node participates. Such averaging scheme will later prove to automatically suppress the so called checkerboard patterns in topology design.

Stiffness properties for bilinear elements, on the other hand, are also constant and equal to the average of the stiffnesses at the four corners

$$[\overline{\mathbf{A}}, \overline{\mathbf{B}}, \overline{\mathbf{D}}] = \frac{1}{4}\sum_{i=1}^{4}[\mathbf{A}_i, \mathbf{B}_i, \mathbf{D}_i]. \tag{3.3}$$

In order to define elements with constant-stiffness properties, one could also suggest averaging fiber angles instead of stiffnesses. However, numerical studies showed that the latter approach generates smoother fiber paths with improved stiffness properties. In this section, the equilibrium equations for the bilinear model are derived for the in-plane deformation. The objective is to simplify these rules beforehand to make the cell update process computationally as inexpensive as possible.

For the case of constant thickness isotropic medium, it is possible to obtain a simple closed form displacement update rule using a symbolic processor such as *Mathematica*^{TM}. Denoting the applied forces on the site cell by f^x and f^y; the cell displacements u_C and v_C can be written in terms of the neighboring cells displacements as follows

$$\begin{aligned}
u_C &= \frac{3(1-\nu^2)}{2Eh(\nu-3)}f^x + \frac{(3+\nu)}{4(3-\nu)}(u^E + u^W) + \frac{-\nu}{2(3-\nu)}(u^N + u^S) \\
&+ \frac{1}{8}(u^{NW} + u^{SE} + u^{NE} + u^{SW}) \\
&+ \frac{3(1+\nu)}{16(3-\nu)}(v^{NE} + v^{SW} - v^{NW} - v^{SE}), \\
v_C &= \frac{3(1-\nu^2)}{2Eh(\nu-3)}f^y + \frac{(3+\nu)}{4(3-\nu)}(v^E + v^W) + \frac{-\nu}{2(3-\nu)}(v^N + v^S) \\
&+ \frac{1}{8}(v^{NW} + v^{SE} + v^{NE} + v^{SW}) \\
&+ \frac{3(1+\nu)}{16(3-\nu)}(u^{NE} + u^{SW} - u^{NW} - u^{SE}).
\end{aligned} \tag{3.4}$$

For neighborhoods with non-constant thicknesses and anisotropic material properties, it still would be possible to obtain similar closed forms. However, they would be rather lengthly, complicated, and computationally as expensive. Therefore, a numeric update rule has to be used.

A local finite element model with nine nodes and four bilinear elements (cf., Figure 3.1(b)) is constructed to derive the displacement update rule. The equilibrium of the local Moore neighborhood in such a model can be written in the following 18×18 matrix form:

$$\begin{bmatrix} \mathbf{K}_{nn} & \mathbf{K}_{nc} \\ \mathbf{K}_{cn} & \mathbf{K}_{cc} \end{bmatrix} \begin{Bmatrix} \mathbf{u}_n \\ \mathbf{u}_c \end{Bmatrix} = \begin{Bmatrix} \mathbf{f}_n \\ \mathbf{f}_c \end{Bmatrix}, \tag{3.5}$$

where $\mathbf{u}_c = \{u_i, v_i\}$ and $\mathbf{f}_c = \{f_i^x, f_i^y\}$ are the site cell displacements and external forces, respectively. Displacements of the neighboring cells are denoted by

$$\begin{aligned} \mathbf{u}_n = \quad & \{u^{SW}, v^{SW}, u^S, v^S, u^{SE}, v^{SE}, u^W, v^W, \\ & u^E, v^E, u^{NW}, v^{NW}, u^N, v^N, u^{NE}, v^{NE}\}, \end{aligned} \tag{3.6}$$

and $\mathbf{f}_n$ denotes the vector of the external forces, and the $\mathbf{K}$s are the stiffness matrices of the local model. The second row of this equation can be written as

$$\mathbf{K}_{cc}\mathbf{u}_c - \mathbf{f}_c = -\mathbf{K}_{cn}\mathbf{u}_n. \tag{3.7}$$

Knowing displacement of the neighboring cells and stiffness matrices, i.e., $\mathbf{u}_n$ and $\mathbf{K}$s, and given any pair of (u_i, v_i, f_i^x, f_i^y), Equation 3.7 is solved numerically for the remaining pair.

Equation 3.5 is obtained by assembling stiffnesses of the four bilinear elements of the Moore neighborhood model. The 8×8 stiffness matrix of each element can be expressed as

$$\mathbf{K}^e = \begin{bmatrix} \mathbf{K}^{11} & \mathbf{K}^{12} \\ sym. & \mathbf{K}^{22} \end{bmatrix}.$$

The above 4×4 sub-matrices are given in terms of the laminate extensional stiffness $\mathbf{A}$ as follows [58]:

$$\begin{aligned} \mathbf{K}^{11} = \quad & A_{11}\mathbf{S}^{xx} + A_{16}(\mathbf{S}^{xy} + \mathbf{S}^{yx}) + A_{66}\mathbf{S}^{yy}, \\ \mathbf{K}^{12} = \quad & A_{12}\mathbf{S}^{xy} + A_{16}\mathbf{S}^{xx} + A_{26}\mathbf{S}^{yy} + A_{66}\mathbf{S}^{yx}, \\ \mathbf{K}^{22} = \quad & A_{66}\mathbf{S}^{xx} + A_{26}(\mathbf{S}^{xy} + \mathbf{S}^{yx}) + A_{22}\mathbf{S}^{yy}. \end{aligned} \tag{3.8}$$

where the elements of the $\mathbf{S}$ matrix are defined as

$$S_{ij}^{\xi\eta} = \int_{\Omega_e} \frac{\partial \psi_i}{\partial \xi} \frac{\partial \psi_j}{\partial \eta} dxdy,$$

in which ψ_i $(i = 1, ..., 4)$ are the bilinear element interpolation functions [58] and Ω_e is the area of the element. In the case of square bilinear elements, $\mathbf{S}^{xx}$, $\mathbf{S}^{xy}$, and $\mathbf{S}^{yy}$ can be computed exactly as

$$\mathbf{S}^{xx} = \begin{bmatrix} \frac{1}{3} & -\frac{1}{3} & -\frac{1}{6} & \frac{1}{6} \\ -\frac{1}{3} & \frac{1}{3} & \frac{1}{6} & -\frac{1}{6} \\ -\frac{1}{6} & \frac{1}{6} & \frac{1}{3} & -\frac{1}{3} \\ \frac{1}{6} & -\frac{1}{6} & -\frac{1}{3} & \frac{1}{3} \end{bmatrix}, \mathbf{S}^{yy} = \begin{bmatrix} \frac{1}{3} & \frac{1}{6} & -\frac{1}{6} & -\frac{1}{3} \\ \frac{1}{6} & \frac{1}{3} & -\frac{1}{3} & -\frac{1}{6} \\ -\frac{1}{6} & -\frac{1}{3} & \frac{1}{3} & \frac{1}{6} \\ -\frac{1}{3} & -\frac{1}{6} & \frac{1}{6} & \frac{1}{3} \end{bmatrix},$$

$$\mathbf{S}^{xy} = \begin{bmatrix} \frac{1}{4} & \frac{1}{4} & -\frac{1}{4} & -\frac{1}{4} \\ -\frac{1}{4} & -\frac{1}{4} & \frac{1}{4} & \frac{1}{4} \\ -\frac{1}{4} & -\frac{1}{4} & \frac{1}{4} & \frac{1}{4} \\ \frac{1}{4} & \frac{1}{4} & -\frac{1}{4} & -\frac{1}{4} \end{bmatrix}, \mathbf{S}^{yx} = (\mathbf{S}^{xy})^T. \tag{3.9}$$

This ready-made form simplifies the analysis update rule and reduces the computational time as well. It is also worth mentioning that this update rule is independent of the lattice size s. This means that, for example, a Moore neighborhood with a lattice size of s will deform under the influence of an applied force F exactly the same as a neighborhood with lattice size of $2s$.

In a CA-based analysis, this update rule is applied to all cells in the lattice iteratively in a Gauss-Seidel fashion until displacements of all cells are converged in the following relative sense:

$$\|\mathbf{u}_c{}^{(t+1)} - \mathbf{u}_c{}^{(t)}\| \leq \epsilon \|\mathbf{u}_c{}^{(t)}\|, \tag{3.10}$$

where $\mathbf{u}_c^{(t)}$ and $\mathbf{u}_c^{(t+1)}$ are the cell displacements before and after update respectively. However, in a CA analysis and design, the design update rule is activated before full convergence of the displacement field is achieved. This activation is controlled by the norm of the residual forces on the structure as described in Section 2.3.

3.2.2 Recovering Cell Resultant Forces and Strain Energy

To compute the cell resultant forces, $\mathbf{N}$, the following formula is used

$$\mathbf{N} = \frac{1}{4}\sum_{j=1}^{4} \bar{\rho}_j^p \bar{\mathbf{A}}_j \cdot \boldsymbol{\epsilon}_j \tag{3.11}$$

in which $\bar{\rho}_j$ is the j-th quadrant density computed according to Equation 3.2 (see Figure 3.1(b)), $\bar{\mathbf{A}}_j$ is the element stiffness computed according to Equation 3.3, and $\boldsymbol{\epsilon}_j = \{\epsilon_{x_j}, \epsilon_{y_j}, 2\epsilon_{xy_j}\}$ is the vector of strains computed at the nearest Barlow [8] point (shown as solid squares in Figure 3.2(a)) to the center cell. Figure 3.2(b) depicts a bilinear element in local coordinate system with its Barlow points located at $\xi = \pm\frac{\sqrt{3}}{6}s,\ \eta = \pm\frac{\sqrt{3}}{6}s$ shown by solid squares. Once the nodal displacements are known, strains at any point (ξ, η) in the bilinear element are computed using the following relations

$$\begin{aligned}
\epsilon_x &= \frac{1}{2s}(-u_1 + u_2 + u_3 - u_4) + \frac{1}{s^2}(u_1 - u_2 + u_3 - u_4)\eta, \\
\epsilon_y &= \frac{1}{2s}(-v_1 - v_2 + v_3 + v_4) + \frac{1}{s^2}(v_1 - v_2 + v_3 - v_4)\xi, \\
\epsilon_{xy} &= \frac{1}{4s}(-u_1 - u_2 + u_3 + u_4 - v_1 + v_2 + v_3 - v_4) \\
&+ \frac{1}{2s^2}(u_1 - u_2 + u_3 - u_4)\xi + \frac{1}{2s^2}(v_1 - v_2 + v_3 - v_4)\eta.
\end{aligned} \tag{3.12}$$

The cell strain energy density is computed by averaging energy densities over the four quadrants by (see Figure 3.1(b))

$$\Phi^* = \frac{1}{4}\sum_{j=1}^{4}\frac{1}{2}\bar{\rho}_j^p \bar{\Phi}_j. \tag{3.13}$$

in which $\bar{\rho}_j$ is the j-th quadrant density and $\bar{\Phi}_j$ is the average quadrant strain energy density computed from (see Figure 3.2(b))

$$\Phi_j = \frac{\int_{\Omega_j} \boldsymbol{\epsilon}^T . \bar{\mathbf{A}}_j . \boldsymbol{\epsilon} d\xi d\eta}{s^2 h} \tag{3.14}$$

Here s is the element side, and h is the lamina thickness. For square bilinear elements, the above integral is computed in closed from and coded into the computer software.

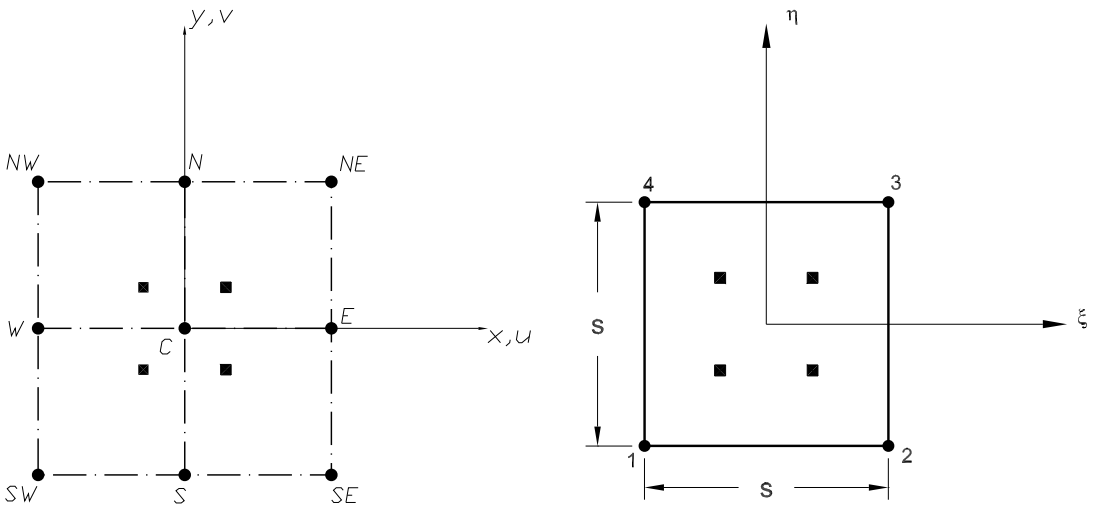

(a) Nearest Barlow points to center cell. (b) Barlow points in the local coordinate system.

Figure 3.2: CA Moore neighborhood.

3.3 Minimum Compliance Design Optimality Criteria

The structural design problem is well studied using mathematical programming techniques. Usually one or combination of several structural behaviors such compliance, natural frequency, buckling, or failure load are used as the objective or side constraints while thickness distribution, laminate lay-up, etc. are treated as design variables to improve the desired structural behavior. However, an increased number of design variables, would usually make the optimization problem difficult to solve. Evolutionary methods on the other hand, use heuristic update rules to update the design variables at the local level, but usually lack a rigorous mathematical basis. The goal of this study is to simplify the design problem into simpler local design problems while satisfying the optimality criteria.

In this section, the optimality criteria for general minimum compliance design problem are presented. A local interpretation of the optimality criteria are the mathematical basis for the CA design update rule as will be discussed later in this chapter. This section is essentially an extension of Abdalla and Gürdal [2] formulation for isotropic continua to an anisotropic one. This section was initially published in an AIAA paper [62] coauthored by Dr. M. M. Abdalla and Prof. Z. Gürdal.

3.3.1 Optimality Criteria for General Minimum Compliance Problems

We pose the design problem as a minimum compliance problem. The compliance of the structure is measured by the complementary work done by the external loads W_c, which is the negative of the total potential energy at equilibrium, Π_0 by,

$$W_c = -\Pi_0, \tag{3.15}$$

Thus the optimization problem is to find the distribution of design functions $\mathbf{b}(\mathbf{x})$ to minimize W_c, thus,

$$\min_{\mathbf{b}} -\Pi_0, \tag{3.16}$$

We also assume that the design functions $\mathbf{b}(\mathbf{x})$ have to satisfy local point by point constraints of the form,

$$\mathbf{g}(\mathbf{x}, \mathbf{b}(\mathbf{x})) \leq 0, \tag{3.17}$$

and a set of integral constraints,

$$\int_{\Omega} \left[\mathbf{f}(\mathbf{b}) - \mathbf{f}_0\right] \, d\Omega \leq 0, \tag{3.18}$$

where $\mathbf{f}_0$ is a constant vector.

Integral constraints define constraints on global resources, such as maximum material volume, while local constraints represent limits on available local resources, such as maximum possible thickness.

The equilibrium value of the total potential can be obtained by minimizing the total potential over kinematically admissible displacement fields $\mathbf{u}(\mathbf{x})$,

$$\Pi_0 = \min_{\mathbf{u}} \Pi, \tag{3.19}$$

where the total potential of the structure is defined by,

$$\Pi = \int_{\Omega} \Phi(\mathbf{x}, \boldsymbol{\gamma}; \mathbf{b}) \, d\Omega - \int_{\Gamma_1} \mathbf{t} \cdot \mathbf{u} \partial\Omega, \tag{3.20}$$

where $\mathbf{t}$ is the applied surface traction, Φ is the strain energy density of the structure, and $\boldsymbol{\gamma}(\mathbf{x}, \mathbf{u})$ is the generalized strain vector. Notice that the strain energy density Φ is parameterized by the design functions $\mathbf{b}(\mathbf{x})$.

Since the minimization of the total potential with respect to the displacement field (3.19) will reduce to the equilibrium equations, and since all the integral (3.18) and side point constraints (3.17) are not functions of the displacements, we will derive the optimality criteria by combining (3.16) and (3.19), and restricting ourselves to variations in the design functions, to obtain,

$$\min_{\mathbf{b}} -\Pi, \tag{3.21}$$

The Lagrangian is written as,

$$\mathcal{L} = \int_{\Omega} \left[-\Phi - \boldsymbol{\mu} \cdot \left(\mathbf{f} - \mathbf{f}_0 + \mathbf{c}^2 \right) + \boldsymbol{\lambda} \cdot \left(\mathbf{g} + \mathbf{s}^2 \right) \right] d\Omega, \tag{3.22}$$

where $\boldsymbol{\lambda}(\mathbf{x})$ is a vector of Lagrange multiplier functions associated with the point constraints (3.17), $\mathbf{s}(\mathbf{x})$ is the corresponding vector of slack functions, $\boldsymbol{\mu}$ is a constant vector of Lagrange multipliers associated with the integral constraints (3.18), and $\mathbf{c}$ is the corresponding constant vector of slack variables.

Setting the variation of the Lagrangian to zero, we obtain the first order necessary conditions as,

1. stationarity

$$-\frac{\partial \Phi}{\partial \mathbf{b}} + \boldsymbol{\mu} \cdot \frac{\partial \mathbf{f}}{\partial \mathbf{b}} + \boldsymbol{\lambda} \cdot \frac{\partial \mathbf{g}}{\partial \mathbf{b}} = 0. \tag{3.23}$$

2. switching conditions

$$\lambda_i(\mathbf{x})\, s_i(\mathbf{x}) = 0, \tag{3.24}$$

$$\mu_i\, c_i = 0. \tag{3.25}$$

3. non-negativity

$$\lambda_i \geq 0, \tag{3.26}$$

$$\mu_i \geq 0, \tag{3.27}$$

in addition to the integral (3.18) and side (3.17) constraints.

We introduce the generalized stresses $\boldsymbol{\sigma}$, defined by,

$$\boldsymbol{\sigma} = \frac{\partial \Phi}{\partial \boldsymbol{\gamma}}, \tag{3.28}$$

and we define the complementary energy density $\hat{\Phi}(\mathbf{x}, \boldsymbol{\sigma}; \mathbf{b})$ by the Legendre transformation,

$$\hat{\Phi}(\mathbf{x}, \boldsymbol{\sigma}; \mathbf{b}) = \boldsymbol{\sigma} \cdot \boldsymbol{\gamma} - \Phi(\mathbf{x}, \boldsymbol{\gamma}; \mathbf{b}), \tag{3.29}$$

It can be shown that [54],

$$\left.\frac{\partial \hat{\Phi}}{\partial \mathbf{b}}\right|_{\boldsymbol{\sigma}} = - \left.\frac{\partial \Phi}{\partial \mathbf{b}}\right|_{\boldsymbol{\gamma}} \tag{3.30}$$

Using (3.30), we can show that the first order conditions (3.23), (3.24), and (3.26) are equivalent to those of the following point-wise minimization problem,

$$\min_{\mathbf{b}} \ \hat{\Phi}_{(\mathbf{x},\boldsymbol{\sigma})} + \boldsymbol{\mu} \cdot \mathbf{f}, \tag{3.31}$$

subject to,

$$\mathbf{g}_{\mathbf{x}}(\mathbf{b}) \leq 0, \tag{3.32}$$

where the subscripts under different functions indicate variables that are held constant.

The Lagrange multipliers associated with the integral constraints, $\boldsymbol{\mu}$, are obtained by solving the active integral constraints of (3.18). In this fashion, the minimum compliance design problem is split into a set of local update rules (3.32), and a global iteration to obtain the Lagrange multipliers.

Multiple load cases

When the structure is acted upon by N sets of loads, the minimum compliance problem is posed as a weighted sum of individual compliances,

$$\min_{\mathbf{b}} \sum_{i=1}^{n} w_i \, W_c^{(i)}, \tag{3.33}$$

where w_i's are weights normalized such that,

$$\sum_{i=1}^{n} w_i = 1, \tag{3.34}$$

In this case, assuming the side and integral constraints are the same for all load cases, the local optimization problem is modified to take the form,

$$\min_{\mathbf{b}} \sum_{i=1}^{n} w_i \, \hat{\Phi}^{(i)}_{(\mathbf{x},\boldsymbol{\sigma})} + \boldsymbol{\mu} \cdot \mathbf{f}. \tag{3.35}$$

3.3.2 Combined Fiber Angle and SIMP Topology Design

The specific problem we are concerned with in this study is the combined topology and fiber angle design of a two-dimensional composite panel. We assume all the loads to be acting in the plane of the panel, so that no bending deformations are induced, and neglect body forces. We further assume that the material behavior is linearly elastic, and obeys plane stress equations,

$$\mathbf{N} = \overline{\mathsf{Q}}(\theta) \cdot \boldsymbol{\gamma}, \tag{3.36}$$

where $\mathbf{N}$ is the vector of in-plane stress resultants, and $\overline{\mathsf{Q}}$ is the reduced in-plane stiffness, which is a function of the local fiber angle θ.

For topology optimization using SIMP, we assume that the local stiffness of the structure is a function of a fictitious density $\rho(\mathbf{x})$. For the problem in hand, we can express the strain energy density, including the density, as,

$$2\Phi = \rho^p \, \boldsymbol{\gamma} \cdot \overline{\mathsf{Q}}(\theta) \cdot \boldsymbol{\gamma}, \tag{3.37}$$

For $\rho \equiv 1$, (3.37) reduces to the usual strain energy density for composite panels governed by (3.36). For $\rho = 0$, the strain energy density vanishes, signifying a void region. The exponent p is chosen high enough so that intermediate densities are penalized, and the final distribution of $\rho(\mathbf{x})$ will consist almost entirely of black ($\rho \approx 1$), and white ($\rho \approx 0$) regions.

The generalized stresses and the complementary energy are easily obtained as,

$$\boldsymbol{\sigma} = \rho^p \, \mathbf{N}, \tag{3.38}$$

$$\hat{\Phi} = \frac{\overline{\Phi}_{\boldsymbol{\sigma}}(\theta)}{\rho^p}, \tag{3.39}$$

where

$$2\overline{\Phi}_{\boldsymbol{\sigma}} = \boldsymbol{\sigma} \cdot \overline{\mathsf{Q}}^{-1}(\theta) \cdot \boldsymbol{\sigma} = \rho^{2p} \boldsymbol{\gamma} \cdot \overline{\mathsf{Q}}(\theta) \cdot \boldsymbol{\gamma}. \tag{3.40}$$

The total volume of the material is limited to a fraction η of the total volume of the domain. This constraint can be expressed in the standard form (3.18) as,

$$\int_{\Omega} (\rho - \eta) \, d\Omega \leq 0. \tag{3.41}$$

Thus the local optimization problem (3.35) reduces to,

$$\min_{\rho,\theta} \frac{\sum_{i=1}^{n} w_i \, \overline{\Phi}_{\boldsymbol{\sigma}}(\theta)^{(i)}}{\rho^p} + \mu\rho, \tag{3.42}$$

subject to,

$$\epsilon \leq \rho \leq 1, \tag{3.43}$$

where ϵ is a small number used to avoid numerical ill conditioning.

$\overline{\Phi}_{\boldsymbol{\sigma}}$ is evaluated based on the current value of the cell density ρ and the strain vector γ and then used to update the local density in a two step procedure. Due to its special mathematical form, this local optimization problem can be easily split into two problems, fiber angle design,

$$\Phi^* = \min_{\theta} \sum_{i=1}^{n} w_i \overline{\Phi}_{\boldsymbol{\sigma}}^{(i)}, \tag{3.44}$$

and, topology,

$$\min_{\rho} \frac{\Phi^*}{\rho^p} + \mu\rho \tag{3.45}$$

subject to,

$$\epsilon \leq \rho \leq 1 \tag{3.46}$$

The topology one-dimensional problem (3.45) is convex, and depending on the value of the parameter $\hat{\rho}$,

$$\hat{\rho} = \left(\frac{\Phi^*}{\overline{\mu}} \right)^{\frac{1}{p+1}}, \tag{3.47}$$

where $\overline{\mu} = \mu/p$ is a modified Lagrange multiplier that has units of energy density.

The solution of the local topology optimization problem is given by,

$$\rho = \begin{cases} \hat{\rho} & \varepsilon < \hat{\rho} < 1 \\ \varepsilon & \hat{\rho} < \varepsilon \\ 1 & \hat{\rho} > 1 \end{cases} \tag{3.48}$$

The modified Lagrange multiplier $\overline{\mu}$ can be loosely interpreted as an average strain energy density in the structure. So, instead of pre-specifying the volume fraction η, $\overline{\mu}$ may be specified as input. This eliminates the need to iteratively determine the Lagrange multiplier to satisfy the volume constraint.

The fiber angle design has an analytic solution for single load case, in the general case when multiple load cases are considered, the fiber design problem (3.44) is solved numerically.

3.4 In-Plane Design Rule Using Fiber Angles

The cell design update rule has two levels according to the optimality criteria derived in the previous section. The first level is the lay-up design level where the optimal lay-up configuration is computed at any cell and the second level is the density update rule. The two levels of the design update rule will be explained separately in the following sections.

3.4.1 The Lay-up Design Problem

In the lay-up design update, the complimentary strain energy density must be minimized at any cell while treating the fiber angle as a continuous design variable. In the case of in-plane loadings, this design problem is formulated as the following minimization problem ($i = 1, 2, \ldots, nc$ where nc is the number of cells)

$$\min_{\theta_i} \frac{1}{2} \mathbf{N}_i^T \cdot \mathbf{A}^{-1}(\theta_i) \cdot \mathbf{N}_i \tag{3.49}$$

$$\text{subject to} : -90^\circ \leq \theta_\text{i} \leq 90^\circ$$

It is well known that the optimal fiber angle orientation for "shear weak" materials coincides with the principal stress direction. According to Pedersen [52, 53], a composite material is shear weak if

$$1 + (E_2/E_1)(1 - 2\nu_{12}) - 4(G_{12}/E_1)(1 - \nu_{12}^2 E_2/E_1) \geq 0. \tag{3.50}$$

in which the engineering properties in the material coordinate system are denoted by E_1, E_2, G_{12}, and ν_{12}. For "shear strong" materials there exists a closed form solution for which depending on the principal strain ratio and material properties it might again coincide with principal stress direction or be different from the principal stress direction [6, 53, 20].

Gea and Luo [20] showed that the minimization problem of Equation 3.49 will reduce to a fourth order polynomial in $\tan(\theta)$ where θ is the optimal fiber orientation with respect to the principal stress direction. As mentioned earlier, for shear weak materials the principal stress direction is the optimal fiber orientation. In other words, either $\theta = 0^\circ$ or, $\theta = 90^\circ$. However, under special circumstances, both $\theta = 0^\circ$ and $\theta = 90^\circ$ could generate the same value of the objective function. This case of repeated global minima becomes very important in understanding the discontinuity of the optimal fiber orientation in numerical results. To investigate this further, let us consider a point where the principal stresses are σ_1 and σ_2. Now assume that the state of the stress in the material coordinate system is given by

$$\boldsymbol{\sigma} = \{\sigma_{xx}, \sigma_{yy}, \tau_{xy}\},$$

where

$$\begin{aligned} \sigma_{xx} &= \frac{(\sigma_1 + \sigma_2)}{2} + \frac{(\sigma_1 - \sigma_2)}{2}\cos(2\theta), \\ \sigma_{yy} &= \frac{(\sigma_1 + \sigma_2)}{2} - \frac{(\sigma_1 - \sigma_2)}{2}\cos(2\theta), \\ \tau_{xy} &= -\frac{(\sigma_1 - \sigma_2)}{2}\sin(2\theta). \end{aligned} \tag{3.51}$$

According to the definition, the complementary strain energy is defined by

$$\bar{U} = \frac{1}{2}\boldsymbol{\sigma}^T \cdot \bar{\mathbf{Q}}^{-1} \cdot \boldsymbol{\sigma}, \tag{3.52}$$

in which the reduced stiffness of the lamina $\bar{\mathbf{Q}}$ is

$$\bar{\mathbf{Q}} = \begin{bmatrix} \bar{Q}_{11} & \bar{Q}_{12} & 0 \\ \bar{Q}_{12} & \bar{Q}_{22} & 0 \\ 0 & 0 & \bar{Q}_{66} \end{bmatrix}. \tag{3.53}$$

Figure 3.3 depicts the nondimensional strain energy for a typical shear weak material for three different cases based on the value of $\sigma_1+\sigma_2$. First case in Figure 3.3(a) where $\sigma_1+\sigma_2 < 0$ we have $\theta = 90^\circ$ and second case in Figure 3.3(b) where $\sigma_1 + \sigma_2 > 0$ we have $\theta = 0^\circ$. Finally, as shown in Figure 3.3(c) where $\sigma_1 + \sigma_2 = 0$, there is a case of repeated global minima. Such a phenomenon explains sudden changes in the distribution of the optimal fiber angles for two adjacent points where the values of the stress are not significantly different however $\sigma_1+\sigma_2 \simeq 0$. Another important observation from these diagrams is that the sudden change in optimal value of the fiber orientation always happens by approximately 90°. The numerical results in Chapter 5 will later demonstrate this phenomenon.

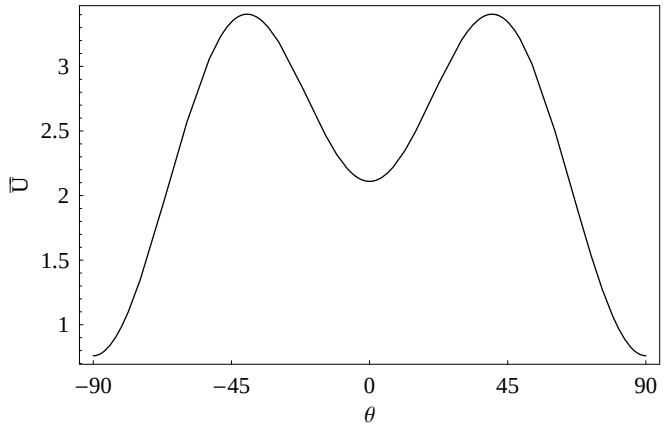

(a) $\sigma_1 + \sigma_2 < 0$

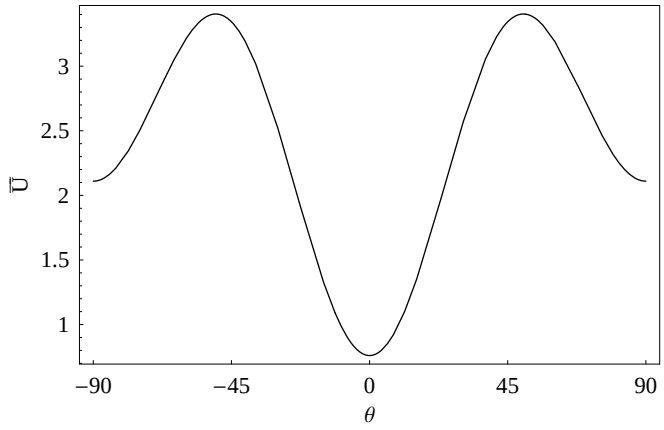

(b) $\sigma_1 + \sigma_2 > 0$

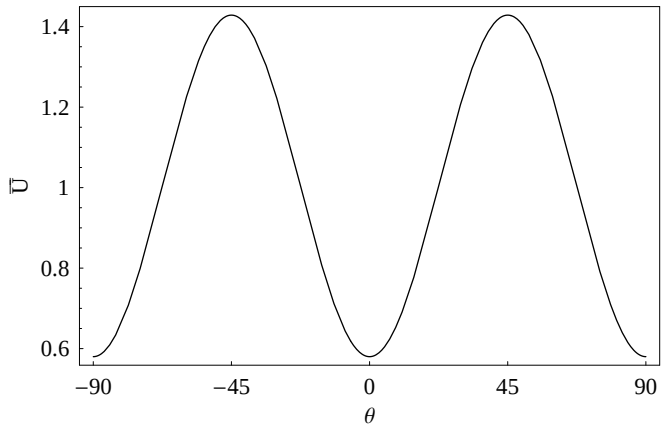

(c) $\sigma_1 + \sigma_2 = 0$

Figure 3.3: Nondimensional strain energy for different values of $\sigma_1 + \sigma_2$.

In the case of multiple loads, a weighted average formulation is used as suggested by Bendøe et al. [9] ($i = 1, 2, \ldots, nc$)

$$\min_{\theta_i} \frac{1}{2} \sum_{j=1}^{nlc} \mathbf{N}_i^{j^T} \cdot \mathbf{A}^{-1}(\theta_i) \cdot \mathbf{N}_i^j \tag{3.54}$$

$$\text{subject to} : -90^\circ \leq \theta_\text{i} \leq 90^\circ$$

in which nlc is the number of load cases, and $\mathbf{N}_i^j$ is the cell i resultant force for the j-th load case. This problem is solved numerically using a gradient-based minimizer[1]. In each design iteration, the minimizer starts from a random fiber angle and computes a candidate new fiber orientation. The cell fiber angle is updated using this new candidate only if it results in a lower value of the complimentary strain energy as compared to previous fiber orientation angle for the same values of resultant forces (notice that changes in the values of the resultant forces in Equation 3.54 are rather insignificant after the first few design iterations). Numerical studies show that this elite type of strategy is convergent.

3.4.2 The Density Design Problem

Once the optimal fiber angle is computed as explained in the previous section, Equation 3.48 is used to update the density measure of each cell. The cell complimentary strain energy density required in Equation 3.47 is computed by averaging energy densities over the cell neighborhood (see Section 3.2.2). In order to avoid numerical instabilities, a move limit is usually applied to the density sizing. In a hybrid cellular automata formulation however, no move limit is necessary.

3.5 In-Plane Design Using Lamination Parameters

The problem of minimum compliance design of variable-stiffness laminae is well studied in the literature using fiber angles as continuous spatial design variables. Numerical results show that substantial stiffness improvements can be gained only by reorientation of the orthotropic material in an optimal manner [11, 6, 30, 56, 66, 63, 67]. However, such a formulation requires repeated transformation of the material properties using the classical trigonometric transformations. These transformations are not only expensive in terms of the computational costs, but also can cause convergence problems. Besides, the dimension of the design space grows as the number of layers increase. An increased number of design

[1] DUVMID, IMSL Version 3.0.

variables makes the optimization process computationally expensive and cumbersome. A more general formulation for the same compliance design problem is to use the lamination parameters as design variables instead of the fiber angles. In general, the in-plane behavior of symmetric composite laminates can be fully modeled using only four lamination parameters regardless of the actual number of layers [21]. Moreover, the laminate extensional stiffness matrix is linear in terms of the lamination parameters. It can also be shown that compliance is convex in the lamination parameters space [61]. These characteristics are very beneficial in the optimal design of laminated composites in the sense that they substantially improve the computational efficiency as well as the accuracy.

Miki et al. [45, 46, 48] used lamination parameters for optimal design of constant-stiffness composite laminates. Convexity of the design problem in the lamination parameters space is discussed by Foldager et al. [16]. In the next section, the minimum compliance design problem of variable-stiffness composites is solved for in-plane loading using lamination parameters. First a brief introduction to the lamination parameters is given followed by the design formulation for different laminate lay-ups.

3.5.1 Definition of the Lamination Parameters

The in-plane lamination parameters as initially introduced by Tsai et al. [76, 75] represent the laminate lay-up configuration in a compact form for the in-plane stiffness by

$$(V_1, V_2, V_3, V_4) = \int_{-1/2}^{1/2} (\cos 2\theta(\bar{z}), \sin 2\theta(\bar{z}), \cos 4\theta(\bar{z}), \sin 4\theta(\bar{z}))d\bar{z}. \tag{3.55}$$

where $\bar{z} = z/h$ is the normalized z coordinate of the layers, and $\theta(\bar{z})$ is the fiber angle at $\bar{z}$ (see [33] for the definitions). The in-plane laminate stiffness matrix $\mathbf{A}$ is then a linear function of the lamination parameters as follows

$$\mathbf{A} = h(\mathbf{\Gamma_0} + V_1\mathbf{\Gamma_1} + V_2\mathbf{\Gamma_2} + V_3\mathbf{\Gamma_3} + V_4\mathbf{\Gamma_4}), \tag{3.56}$$

where the $\mathbf{\Gamma}_i$ $(i = 1, \ldots, 4)$ matrices in terms of the laminate invariants are given by:

$$\mathbf{\Gamma}_0 = \begin{bmatrix} U_1 & U_4 & 0 \\ U_4 & U_1 & 0 \\ 0 & 0 & U_5 \end{bmatrix}, \mathbf{\Gamma}_1 = \begin{bmatrix} U_2 & 0 & 0 \\ 0 & -U_2 & 0 \\ 0 & 0 & 0 \end{bmatrix}$$

$$\mathbf{\Gamma}_2 = \begin{bmatrix} 0 & 0 & U_2/2 \\ 0 & 0 & U_2/2 \\ U_2/2 & U_2/2 & 0 \end{bmatrix}, \mathbf{\Gamma}_3 = \begin{bmatrix} U_3 & -U_3 & 0 \\ -U_3 & U_3 & 0 \\ 0 & 0 & -U_3 \end{bmatrix},$$

$$\mathbf{\Gamma}_4 = \begin{bmatrix} 0 & 0 & U_3 \\ 0 & 0 & -U_3 \\ U_3 & -U_3 & 0 \end{bmatrix}. \tag{3.57}$$

The laminate invariants are, in turn, defined in terms of lamina reduced stiffnesses by [33]

$$\begin{aligned} U_1 &= (3\bar{Q}_{11} + 3\bar{Q}_{22} + 2\bar{Q}_{12} + 4\bar{Q}_{66})/8, \\ U_2 &= (\bar{Q}_{11} - \bar{Q}_{22})/2, \\ U_3 &= (\bar{Q}_{11} + \bar{Q}_{22} - 2\bar{Q}_{12} - 4\bar{Q}_{66})/8, \\ U_4 &= (\bar{Q}_{11} + \bar{Q}_{22} + 6\bar{Q}_{12} - 4\bar{Q}_{66})/8, \\ U_5 &= (\bar{Q}_{11} + \bar{Q}_{22} - 2\bar{Q}_{12} + 4\bar{Q}_{66})/8. \end{aligned} \tag{3.58}$$

The definition of the cell states in Equation 3.1, is modified here to replace the fiber angle by the vector of the lamination parameters $\mathbf{V}_i = \{V_{i1}, V_{i2}, V_{i3}, V_{i4}\}$

$$\phi_i = \{(u_i, v_i), (f_i^x, f_i^y), (\rho_i, \mathbf{V}_i), \mathbf{A}_i\}. \tag{3.59}$$

3.5.2 Feasible Domain for the Lamination Parameters

The lamination parameters are not independent since the trigonometric functions used in Equation 3.94 are related. The relation between the in-plane lamination parameters define their feasible domain and are expressed in the form of the following inequalities (see Hammer et al. [26])

$$\begin{aligned} (C_1): \quad & 2V_1^2(1 - V_3) + 2V_2^2(1 + V_3) + V_3^2 + V_4^2 - 4V_1V_2V_4 \leq 1 \\ & V_1^2 + V_2^2 \leq 1 \\ & -1 \leq V_i \leq 1 \ (i = 1, \ldots, 4), \end{aligned} \tag{3.60}$$

According to the definition of the lamination parameters in Equation 3.94, only two of the lamination parameters, namely V_1 and V_3, are required to fully model the in-plane stiffness of balanced symmetric laminates while $V_2 = V_4 = 0$. This would simplify the above set of inequality constraint (C_1) to (C_2) as

$$\begin{aligned} (C_2): \quad & V_3 \geq 2V_1^2 - 1 \\ & -1 \leq V_i \leq 1 \ (i = 1, 3) \end{aligned} \tag{3.61}$$

Using lamination parameters, the same analysis update rule (Equation 3.7) is used again except that the in-plane stiffness $\mathbf{A}$ is computed from the lamination parameters rather than fiber angles. However, for the design update rule, the minimum compliance design problem of Equation 3.49 is reformulated using lamination parameters as design variables instead of fiber orientations.

3.5.3 Constant Stiffness Panels Design

First, let us consider the case of constant-stiffness laminates where the cell in-plane laminate stiffness matrix $\mathbf{A}_i$ is constant over the entire domain. In this case, the minimum compliance design problem is formulated in its discrete form as

$$\min_{\mathbf{V}} \frac{1}{2} \sum_{i=1}^{nc} \mathbf{N}_i^T \cdot \mathbf{A}^{-1}(\mathbf{V}) \cdot \mathbf{N}_i \tag{3.62}$$

$$\text{Subject to: } (C_1)$$

in which $\mathbf{V} = \{V_1, V_2, V_3, V_4\}$ is the vector of the design variables, $\mathbf{N}_i$ is the vector of the resultant force at the cell i, $\mathbf{A}(\mathbf{V})$ is the in-plane stiffness of the laminate computed from Equation 3.56, and nc is the total number of the cells. To solve this problem a FSQP[2] (Feasible Sequential Quadratic Programming) solver is used where the exact gradient of the objective function is supplied to the solver as

$$\Phi_{,j} = -\frac{h}{2} \sum_{i=1}^{nc} \mathbf{N}_i^T \cdot \mathbf{A}^{-1} \mathbf{\Gamma}_j \mathbf{A}^{-1} \cdot \mathbf{N}_i \ (j = 1, .., 4). \tag{3.63}$$

3.5.4 General Variable-Stiffness Lay-up Design

For variable-stiffness laminates, the compliance design problem leads to the following local minimization problem at any cell in the two-dimensional domain ($i = 1, \ldots, nc$)

$$\min_{\mathbf{V}_i} \frac{1}{2} \mathbf{N}_i^T \cdot \mathbf{A}^{-1}(\mathbf{V}_i) \cdot \mathbf{N}_i \tag{3.64}$$

$$\text{Subject to: } (C_1)$$

[2]FFSQP Version 3.7, by Jian L. Zhou, André L. Tits, and Craig T. Lawrence.

where $\mathbf{N}_i$ is the vector of the resultant forces for the cell i,

$$\mathbf{V}_i = \{V_{i_1}, V_{i_2}, V_{i_3}, V_{i_4}\} \tag{3.65}$$

is the vector of the cell lamination parameters, and the constraints (C_1) as given in Equation 3.60 define the feasible lamination parameters space. In the present study, the optimal design problem of Equation 3.64 is numerically solved using a FSQP solver for all cells. The sensitivities of the complimentary strain energy density $\bar{\Phi}$ defined by

$$\bar{\Phi} = \frac{1}{2}\mathbf{N}^T \cdot \mathbf{A}^{-1} \cdot \mathbf{N}, \tag{3.66}$$

can be obtained exactly as follows:

$$\bar{\Phi}_{,i} = -\frac{h}{2}\mathbf{N}^T \cdot \mathbf{A}^{-1}\Gamma_i\mathbf{A}^{-1} \cdot \mathbf{N}, \tag{3.67}$$

$$\bar{\Phi}_{,ij} = \frac{h^2}{2}\mathbf{N}^T \cdot \mathbf{A}^{-1}(\Gamma_i\mathbf{A}^{-1}\Gamma_j + \Gamma_j\mathbf{A}^{-1}\Gamma_i)\mathbf{A}^{-1} \cdot \mathbf{N}. \tag{3.68}$$

An FSQP solver was used instead of a traditional SQP solver since initial numerical experiments showed that a SQP solver usually goes into the infeasible domain where the objective function (compliance) is not well defined since the $\mathbf{A}$ matrix is no longer positive definite. This resulted in divergence of the design process. On the other hand, an FSQP solver always stays in the feasible domain where the objective function is well defined and is therefore convergent. The first design iteration starts from a feasible point in the lamination parameters space, e.g. $V_1 = V_2 = V_3 = V_4 = 0.$, and for the next design steps, the optimizer starts from the previously obtained candidate. Since changes in the resultant forces are rather insignificant after first few design iterations and besides the design problem is convex, the iterative design process exhibits very fast convergence properties as compared to when the same problem is formulated used fiber orientation angles.

3.5.5 Balanced Symmetric Lay-up Design

Balanced symmetric laminates can be easily treated as a special case of Equation 3.64. According to the definition of the lamination parameters in Equation 3.94, only two of the lamination parameters, i.e., V_1 and V_3, are required to fully model the in-plane stiffness of balanced symmetric laminates. In this case, the minimization problem of Equation 3.64 reduces to the following problem:

$$\min_{\mathbf{V}_i} \frac{1}{2}\mathbf{N}^T \cdot \mathbf{A}^{-1}(\mathbf{V}_i) \cdot \mathbf{N} \tag{3.69}$$

Subject to: (C_2)

in which $\mathbf{V}_i = \{V_{i_1}, V_{i_3}\}$, and C_2 is defined in Equation 3.61.

The feasible lamination parameters domain for balanced symmetric laminates is graphically represented by the Miki diagram [45, 46]. The parabolic portion of the Miki diagram as shown in Figure 3.4(a), where $V_3 = 2V_1^2 - 1$, represents a two layer $[\pm\theta_1]_s$ balanced symmetric laminate with equal thickness layers [21].

3.5.6 Design of Balanced Symmetric Laminates with Equal Thickness Layers

Since the manufacturing practice is limited to fixed thickness of plies only, it is worth exploring subsets of the Miki diagram for which balanced symmetric laminates with equal thickness layers can be obtained for an increasing number of layers. For a $[\pm\theta_1/\pm\theta_2]_s$ lay-up, it can be easily shown that in addition to the general balanced symmetric constraint, i.e., $V_3 \geq 2V_1^2 - 1$, V_1 and V_3 should also satisfy $V_3 \leq 4V_1^2 \pm 4V_1 + 1$. The feasible domain for up to $[\pm\theta_1/\pm\theta_2/\pm\theta_3/\pm\theta_4]_s$ lay-ups are obtained numerically and depicted in the shaded areas of Figures 3.4(b) through 3.4(d). A quick examination of this family of diagrams reveals that a lay-up of $[\pm\theta_1/\pm\theta_2/\ldots/\pm\theta_k]_s$ represents $100(1-\frac{1}{k})\%$ of all possible general balanced symmetric configurations. Another useful information that can be extracted from Figure 3.4 is the minimum number of layers required to obtain a lamination parameters point (V_1, V_3) in the feasible domain. If in addition to $V_3 \geq 2V_1^2 - 1$ the following set of parabolic constraints are also satisfied for $p = 0, 1, 2, \ldots k-1$;

$$V_3 \leq 2k(V_1 - \frac{2p}{k})^2 + 4(k-1)(V_1 - \frac{2p}{k}) + (2k-3) \tag{3.70}$$

then a minimum number of k layers of equal thickness are required to obtain the (V_1, V_3) point in the balanced symmetric lamination parameters space.

3.5.7 Restricted Balanced Symmetric Lay-up Design

In order to generate designs with equal thickness layers, the inequalities of Equation 3.70 can be added as additional nonlinear constraints to the minimization problem of Equation 3.69. However, this would make the convex domain of the original problem nonconvex thereby

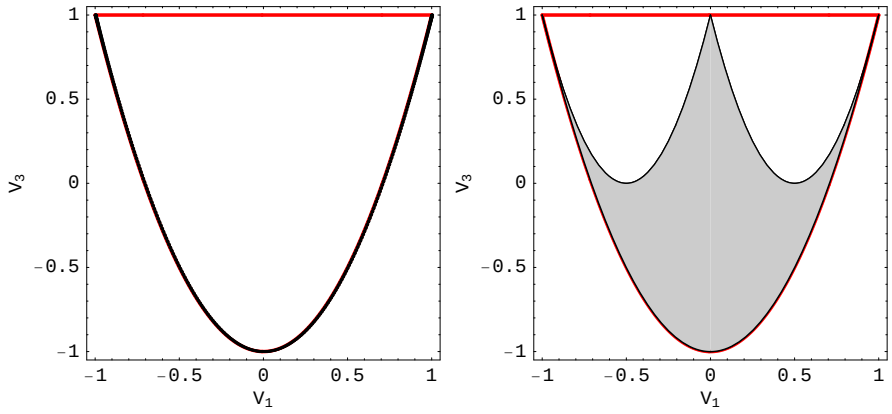

(a) $[\pm\theta_1]_S$ (b) $[\pm\theta_1/\pm\theta_2]_S$

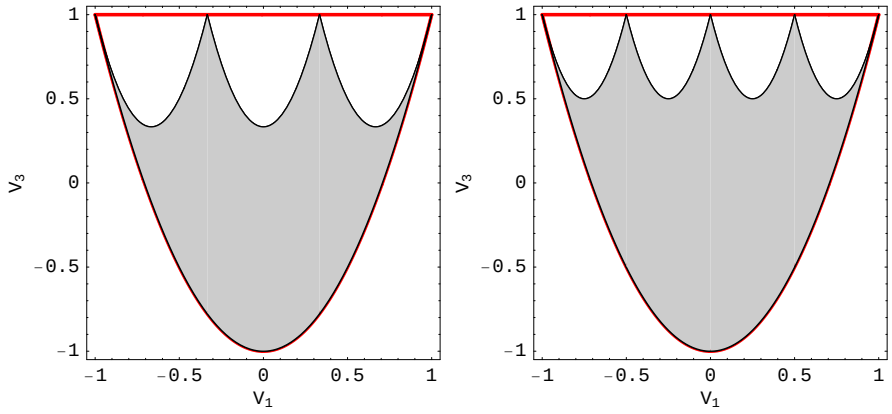

(c) $[\pm\theta_1/\pm\theta_2/\pm\theta_3]_S$ (d) $[\pm\theta_1/\pm\theta_2/\pm\theta_3/\pm\theta_4]_S$

Figure 3.4: Feasible domain for equi-thickness balanced symmetric laminates.

making the numerical solution very difficult. To maintain convexity of the original domain, a restricted problem is considered here in which rather than introducing the nonlinear constrains of Equation 3.70, only the following linear constraint is added to the problem

$$\begin{aligned} (C_3): \qquad & V_3 \geq 2V_1^2 - 1 \\ & V_3 \leq \tfrac{k-2}{k} \\ & -1 \leq V_i \leq 1 \ (i = 1, 3) \end{aligned} \tag{3.71}$$

in which k denotes the number of desired equi-thickness layers. This new linear constraint as shown in Figure 3.5 is basically the horizontal tangent to the equithickness parabolas of Figure 3.4.

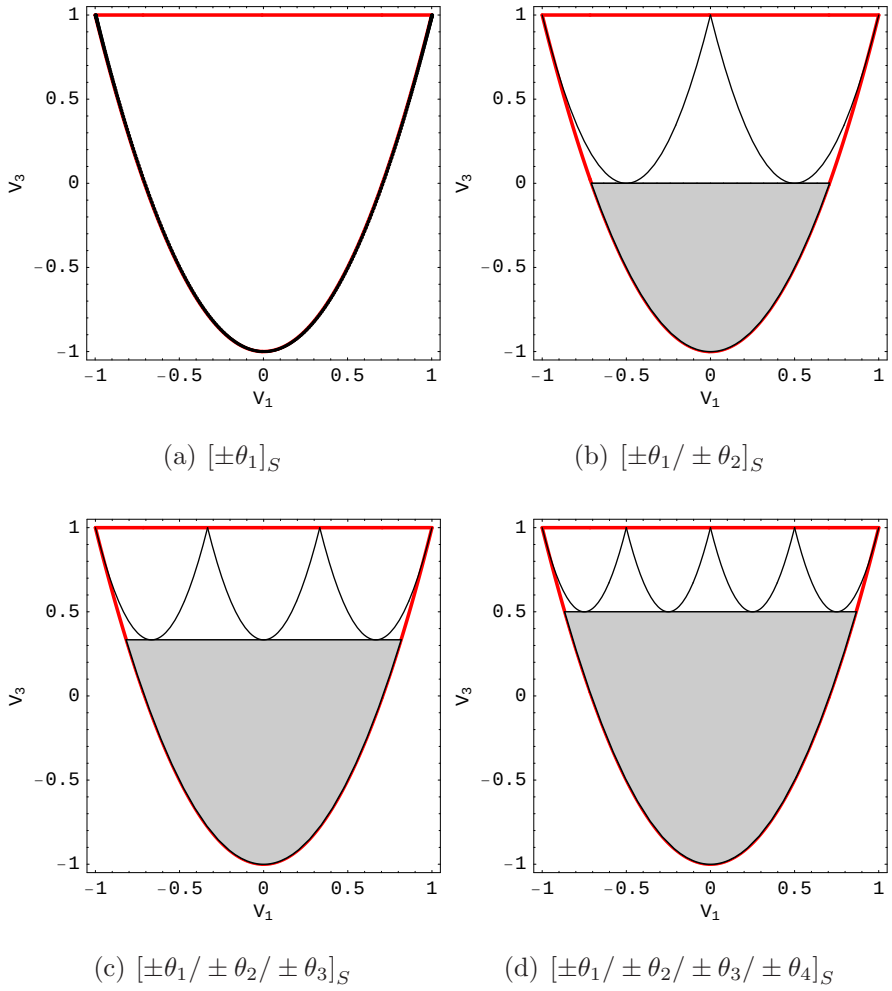

(a) $[\pm\theta_1]_S$ (b) $[\pm\theta_1/\pm\theta_2]_S$

(c) $[\pm\theta_1/\pm\theta_2/\pm\theta_3]_S$ (d) $[\pm\theta_1/\pm\theta_2/\pm\theta_3/\pm\theta_4]_S$

Figure 3.5: Restricted domain for equi-thickness balanced symmetric laminates.

3.5.8 Computing Fiber Angles for Balanced Symmetric Laminates with Equal Thickness Layers

Lipton [41] showed that only a maximum of three layers are required to obtain any feasible point in the in-plane lamination parameters space. Autio [5] demonstrated that bending lamination parameters can be realized by at most a six layered symmetric laminate. Fukunaga [17] on the other hand, presented a solution methodology to obtain laminate configurations from lamination parameters for balanced symmetric laminates. For variable-stiffness laminates however, these techniques are not directly applicable from the manufacturing point of view since they will generate adjacent points with completely different layer thicknesses. In this section, a recursive formulation is presented to obtain fiber orientation angles for balanced symmetric laminates with constant layer thicknesses.

Suppose a point (V_1, V_3) is given in the balanced symmetric lamination parameters space. The first step is to compute the number of equal thickness layers required to generate this point. According to restricted problem formulation of Equation 3.71, the minimum value of $k > 2$ which satisfies $V_3 \leq \frac{k-2}{k}$ gives the required number of layers. Now depending on whether $k = 1$, or $k = 2$, or $k > 2$ we tackle the problem differently.

For the simple case of a $[\pm\theta_1]_s$ lay-up where $V_3 = 2V_1^2 - 1$, the fiber angle can be easily computed from the following simple relation

$$\theta_1 = \frac{1}{2}\arccos(V_1). \tag{3.72}$$

In case of a $[\pm\theta_1/\pm\theta_2]_s$ lay-up, according to the definition of lamination parameters we have

$$\begin{aligned} \cos(2\theta_1) + \cos(2\theta_2) &= 2V_1, \\ \cos(4\theta_1) + \cos(4\theta_2) &= 2V_3. \end{aligned} \tag{3.73}$$

The solution of the above system of two equations and two unknowns gives us the fiber angles θ_1 and θ_2 as

$$\theta_{1,2} = \arccos[V_1 \pm \sqrt{2(V_3 - 2V_1^2 + 1)/2}]/2. \tag{3.74}$$

Next let us consider the general case of $[\pm\theta_1/\pm\theta_2\ldots/\pm\theta_n]_s$ of a restricted equithickness lay-up where $n > 2$. In this case, we have only two equations to solve for n unknown fiber orientation, therefore there potentially exists an infinite number of solutions. The proposed methodology here suggests acceptable ranges for values of θ_i, for $i = n, \ldots, 3$. Then the last two unknown orientations, namely θ_1 and θ_2, are computed from the exact solution as given in Equation 3.74. To clarify this approach, consider the following problem

$$\begin{aligned} \cos(2\theta_1) + \cos(2\theta_2) + \ldots + \cos(2\theta_n) &= nV_1^{(n)}, \\ \cos(4\theta_1) + \cos(4\theta_2) + \ldots + \cos(4\theta_n) &= nV_3^{(n)}, \end{aligned} \tag{3.75}$$

where the superscript in the parenthesis represents number of $[\pm\theta_i]_s$ layers. The restricted feasible domain in this case would be

$$\begin{aligned} V_3^{(n)} &\leq \tfrac{n-2}{n}, \\ V_3^{(n)} &\geq 2{V_1^{(n)}}^2 - 1. \end{aligned} \tag{3.76}$$

Now suppose θ_n is known, we will have the following reduced problem for $n-1$ equithickness laminate

$$\begin{aligned}
\cos(2\theta_1)+\cos(2\theta_2)+\ldots+\cos(2\theta_{n-1}) &= nV_1-\cos(2\theta_n)\\
&= (n-1)V_1^{(n-1)},\\
\cos(4\theta_1)+\cos(4\theta_2)+\ldots+\cos(4\theta_{n-1}) &= nV_3-\cos(4\theta_n)\\
&= (n-1)V_3^{(n-1)},
\end{aligned} \tag{3.77}$$

for which a new set of the lamination parameters can be defined

$$\begin{aligned}
V_1^{(n-1)} &= (nV_1^{(n)}-\cos(2\theta_n))/(n-1),\\
V_3^{(n-1)} &= (nV_3^{(n)}-\cos(4\theta_n))/(n-1).
\end{aligned} \tag{3.78}$$

For this problem to have a solution, $V_1^{(n-1)}$ and $V_3^{(n-1)}$ should satisfy Equation 3.71 for $k=n-1$

$$\begin{aligned}
V_3^{(n-1)} &\leq \frac{n-3}{n-1},\\
V_3^{(n-1)} &\geq 2{V_1^{(n-1)}}^2-1,
\end{aligned} \tag{3.79}$$

after simplifying, we conclude that θ_n should be chosen such that the following conditions are satisfied

$$\begin{aligned}
\cos(2\theta_n)\geq q_1 \vee \cos(2\theta_n)\leq -q_1,\\
q_2\leq\cos(2\theta_n)\leq q_3,
\end{aligned} \tag{3.80}$$

where

$$\begin{aligned}
q_1 &= \sqrt{\frac{1}{2}(nV_3^{(n)}-n+4)},\\
q_2 &= V_1^{(n)}-\sqrt{\frac{1}{2}(n-1)(V_3^{(n)}-2{V_1^{(n)}}^2+1)},\\
q_3 &= V_1^{(n)}+\sqrt{\frac{1}{2}(n-1)(V_3^{(n)}-2{V_1^{(n)}}^2+1)}.
\end{aligned} \tag{3.81}$$

Depending on the values of q_1, q_2, and q_3, feasible interval or intervals for $\cos(2\theta)$ can be found. Any fiber orientation angle for which $\cos(2\theta)$ falls into such interval(s) is an accepted angle, however, in this study, the mid-point of the interval is chosen. Once θ_n is selected, a new set of lamination parameters are computed according to Equation 3.78 and the process is repeated in a recursive fashion until θ_3 is selected. Then Equation 3.74 is used to computed θ_1 and θ_2. Such a methodology can potentially be used to retrieve fiber orientation angles from the optimal distribution of the lamination parameters. However, among possibly different lay-up configurations, one should be chosen that maintains the continuity of the fiber paths the most. Table 3.1 lists computed fiber orientation angles for two typical points.

Table 3.1: Fiber orientation angles computed using the present recursive formulation.

V_1	V_3	n	Lay-up
-0.30	- 0.55	2	$[\pm 43.1/\pm 65.9]_s$
0.20	0.48	4	$[\pm 2.9/\pm 6.0/\pm 50.3/\pm 85.9]_s$

3.6 Bending Analysis Rule

In this section, design of variable-stiffness composite laminates is studied for maximum bending stiffness. First order shear deformation theory (FSDT) [58] is used for the deformation analysis and the same bilinear model as Figure 3.1(b) is considered to obtain the analysis update rule.

The cell state in this case is defined as follows

$$\phi_i = \{(w_i, \psi_i^x, \psi_i^y), (f_i^z, M_i^{xx}, M_i^{yy}, M_i^{xy}), (\rho_i, \boldsymbol{\theta}_i), \mathbf{A}_i, \mathbf{D}_i\}, \tag{3.82}$$

where generalized displacements and generalized forces are denoted by $(w_i, \psi_i^x,\ \psi_i^y)$ and $(M_i^{xx}, M_i^{yy},\ M_i^{xy})$ respectively, ρ_i is the density measure, $\boldsymbol{\theta}_i = \{\theta_i^1, \theta_i^2, ..., \theta_i^{n_h}\}$ is the vector of the cell fiber angles, and n_h is half the number of layers for symmetric laminates.

3.6.1 A Numeric Analysis Rule

The displacement update rule is governed by the equilibrium of the local Moore neighborhood as defined in Figure 3.1(b) similar to Equation 3.7. In such an analysis model, the bilinear elements have constant material properties as proposed in Equation 3.3. The 12×12 stiffness matrix of each bilinear element can be written in the following form

$$\mathbf{K}^e = \begin{bmatrix} \mathbf{K}^{33} & \mathbf{K}^{34} & \mathbf{K}^{35} \\ & \mathbf{K}^{44} & \mathbf{K}^{45} \\ Sym. & & \mathbf{K}^{55} \end{bmatrix},$$

where elements of the above hyper-matrix are each 3×3 matrices defined by

$$\begin{aligned} \mathbf{K}^{33} &= A_{33}\mathbf{S}^{yy} + A_{34}(\mathbf{S}^{xy} + \mathbf{S}^{yx}) + A_{44}\mathbf{S}^{xx}, \\ \mathbf{K}^{34} &= sA_{34}\mathbf{S}^{y0} + sA_{44}\mathbf{S}^{x0}, \\ \mathbf{K}^{35} &= sA_{33}\mathbf{S}^{y0} + sA_{34}\mathbf{S}^{x0}, \\ \mathbf{K}^{44} &= D_{11}\mathbf{S}^{xx} + D_{15}(\mathbf{S}^{xy} + \mathbf{S}^{yx}) + D_{55}\mathbf{S}^{yy} + s^2A_{44}\mathbf{S}^{00}, \\ \mathbf{K}^{45} &= D_{12}\mathbf{S}^{xy} + D_{15}\mathbf{S}^{xx} + D_{25}\mathbf{S}^{yy} + D_{55}\mathbf{S}^{yx} + s^2A_{34}\mathbf{S}^{00}, \\ \mathbf{K}^{55} &= D_{22}\mathbf{S}^{yy} + D_{25}(\mathbf{S}^{xy} + \mathbf{S}^{yx}) + D_{55}\mathbf{S}^{xx} + s^2A_{33}\mathbf{S}^{00}. \end{aligned} \tag{3.83}$$

The common $\mathbf{S}$ matrices with the in-plane stiffness are the same as Equation 3.9 and the remaining terms are computed by full integration in closed form as follows

$$\mathbf{S}^{x0} = \begin{bmatrix} -\frac{1}{6} & \frac{1}{6} & \frac{1}{12} & -\frac{1}{12} \\ -\frac{1}{6} & \frac{1}{6} & \frac{1}{12} & -\frac{1}{12} \\ -\frac{1}{12} & \frac{1}{12} & \frac{1}{6} & -\frac{1}{6} \\ -\frac{1}{12} & \frac{1}{12} & \frac{1}{6} & -\frac{1}{6} \end{bmatrix}, \mathbf{S}^{y0} = \begin{bmatrix} -\frac{1}{6} & -\frac{1}{12} & \frac{1}{12} & \frac{1}{6} \\ -\frac{1}{12} & -\frac{1}{6} & \frac{1}{6} & \frac{1}{12} \\ -\frac{1}{12} & -\frac{1}{6} & \frac{1}{6} & \frac{1}{12} \\ -\frac{1}{6} & -\frac{1}{12} & \frac{1}{12} & \frac{1}{6} \end{bmatrix},$$

$$\mathbf{S}^{00} = \begin{bmatrix} \frac{1}{9} & \frac{1}{18} & \frac{1}{36} & \frac{1}{18} \\ \frac{1}{18} & \frac{1}{9} & \frac{1}{18} & \frac{1}{36} \\ \frac{1}{36} & \frac{1}{18} & \frac{1}{9} & \frac{1}{18} \\ \frac{1}{18} & \frac{1}{36} & \frac{1}{18} & \frac{1}{9} \end{bmatrix}. \tag{3.84}$$

In the case of selective integration, the $\mathbf{S}$ matrices corresponding to out of plane stiffness terms in Equation 3.83 are replaced by their corresponding $\mathbf{S}_R$ matrices computed exactly by reduced integration as follows

$$\mathbf{S}_R^{xx} = \begin{bmatrix} \frac{1}{4} & -\frac{1}{4} & -\frac{1}{4} & \frac{1}{4} \\ -\frac{1}{4} & \frac{1}{4} & \frac{1}{4} & -\frac{1}{4} \\ -\frac{1}{4} & \frac{1}{4} & \frac{1}{4} & -\frac{1}{4} \\ \frac{1}{4} & -\frac{1}{4} & -\frac{1}{4} & \frac{1}{4} \end{bmatrix}, \mathbf{S}_R^{yy} = \begin{bmatrix} \frac{1}{4} & \frac{1}{4} & -\frac{1}{4} & -\frac{1}{4} \\ \frac{1}{4} & \frac{1}{4} & -\frac{1}{4} & -\frac{1}{4} \\ -\frac{1}{4} & -\frac{1}{4} & \frac{1}{4} & \frac{1}{4} \\ -\frac{1}{4} & -\frac{1}{4} & \frac{1}{4} & \frac{1}{4} \end{bmatrix},$$

$$\mathbf{S}_R^{x0} = \begin{bmatrix} -\frac{1}{8} & \frac{1}{8} & \frac{1}{8} & -\frac{1}{8} \\ -\frac{1}{8} & \frac{1}{8} & \frac{1}{8} & -\frac{1}{8} \\ -\frac{1}{8} & \frac{1}{8} & \frac{1}{8} & -\frac{1}{8} \\ -\frac{1}{8} & \frac{1}{8} & \frac{1}{8} & -\frac{1}{8} \end{bmatrix}, \mathbf{S}_R^{y0} = \begin{bmatrix} -\frac{1}{8} & -\frac{1}{8} & \frac{1}{8} & \frac{1}{8} \\ -\frac{1}{8} & -\frac{1}{8} & \frac{1}{8} & \frac{1}{8} \\ -\frac{1}{8} & -\frac{1}{8} & \frac{1}{8} & \frac{1}{8} \\ -\frac{1}{8} & -\frac{1}{8} & \frac{1}{8} & \frac{1}{8} \end{bmatrix},$$

$$\mathbf{S}_R^{00} = \begin{bmatrix} \frac{1}{16} & \frac{1}{16} & \frac{1}{16} & \frac{1}{16} \\ \frac{1}{16} & \frac{1}{16} & \frac{1}{16} & \frac{1}{16} \\ \frac{1}{16} & \frac{1}{16} & \frac{1}{16} & \frac{1}{16} \\ \frac{1}{16} & \frac{1}{16} & \frac{1}{16} & \frac{1}{16} \end{bmatrix}.$$

$$(\mathbf{S}_R^{xy} + \mathbf{S}_R^{yx}) = (\mathbf{S}^{xy} + \mathbf{S}^{yx}) \tag{3.85}$$

3.7 Bending Design Using Fiber Angles

The objective is to design a variable-stiffness laminate for maximum bending stiffness. This stiffness maximization problem is well known to be equivalent to compliance minimization. Consider that the fiber angle of the m-th layer relative to a fixed reference x-y coordinate system for any point (x, y) is $\theta^m(x, y)$. The design problem is to find $\theta^m(x, y)$ for $m = 1, \ldots, n_h$ such that the work done by external forces is minimized where n_h is the half number of layers. Local interpretation of the optimality criteria for compliance minimization will reduce to the following minimization of the complimentary strain energy density $\bar{\Phi}_c(\boldsymbol{\theta})$ at any cell in the domain (see Section 3.3). In case of bending of symmetric laminates, this minimization problem is formulated as follows:

$$\min_{\boldsymbol{\theta}_i} \ \frac{1}{2}\mathbf{N}_i^T \cdot \mathbf{A}^{-1}(\boldsymbol{\theta}_i) \cdot \mathbf{N}_i + \frac{1}{2}\mathbf{M}_i^T \cdot \mathbf{D}^{-1}(\boldsymbol{\theta}_i) \cdot \mathbf{M}_i$$

subject to

$$-90^\circ \leq \theta_i^1, \theta_i^2, \ldots, \theta_i^{n_h} \leq 90^\circ \tag{3.86}$$

where the resultant forces and moments are computed from the following laminate constitutive relation:

$$\begin{Bmatrix} \mathbf{N} \\ \mathbf{M} \end{Bmatrix} = \begin{bmatrix} \mathbf{A} & \mathbf{0} \\ \mathbf{0} & \mathbf{D} \end{bmatrix} \begin{Bmatrix} \boldsymbol{\epsilon} \\ \boldsymbol{\kappa} \end{Bmatrix}. \tag{3.87}$$

In which the membrane strains and curvatures are denoted by $\boldsymbol{\epsilon}$ and $\boldsymbol{\kappa}$, respectively and are computed from the mid-surface generalized displacements by

$$\begin{aligned} \boldsymbol{\epsilon} &= \begin{Bmatrix} u_{,x} & v_{,y} & w_{,y} + \psi^y & w_{,x} + \psi^x & u_{,y} + v_{,x} \end{Bmatrix}^T, \\ \boldsymbol{\kappa} &= \begin{Bmatrix} \psi^x_{,x} & \psi^y_{,y} & 0 & 0 & \psi^x_{,y} + \psi^y_{,x} \end{Bmatrix}^T. \end{aligned} \tag{3.88}$$

For variable-stiffness laminates, the classical laminate stiffnesses **ABD** vary at any point, and are functions of $\theta^m(x, y)$. Keeping the resultant forces and moments fixed, cell fiber angles are updated by numerical solution of Problem 3.86. In this study, a numeric solver[3] is used to solve the minimization problem of Equation 3.86. This numeric solver starts from a random point in each cell design update and computes a new candidate design. Cell fiber angles are updated by this candidate point only if it results in a smaller value of the objective function as compared to the previous design point. Numerical experiments show that this elite type design strategy is convergent.

A more robust methodology to tackle the same problem is to use a global minimization routine such as DIRECT [32, 29, 28]. However, a global minimizer is computationally much more expensive than a gradient based solver. To reduce the computational costs of a global minimizer, a hybrid technique is suggested here. In the hybrid approach, only in the first few design iterations, the global minimizer is used. Once the global minimum is approximately located, a gradient-based minimizer is used to fine tune the location of the minimum. Since the changes in the cell resultant forces and moments are rather insignificant after the first few design iterations, such a strategy exhibits good convergence rates.

[3]DBCONG for $n_h > 1$, and DUVMIF for $n_h = 1$; IMSL Version 3.0.

3.7.1 Sensitivity Analysis

The gradient information are supplied by the following exact formulas to the numeric solver

$$\bar{\Phi}_{c,\theta^m}(\boldsymbol{\theta}) = \frac{1}{2}\mathbf{N}^T \cdot \mathbf{A}^{-1}_{,\theta^m} \cdot \mathbf{N} + \frac{1}{2}\mathbf{M}^T \cdot \mathbf{D}^{-1}_{,\theta^m} \cdot \mathbf{M}. \tag{3.89}$$

in which the sensitivity of the **ABD** matrices with respect to m-th layer fiber angle θ^m, can be computed from

$$\begin{aligned} A_{ij,\theta^m} &= Q^m_{ij,\theta_m}(z_m - z_{m-1}), \\ B_{ij,\theta^m} &= \frac{1}{2}Q^m_{ij,\theta_m}(z^2_m - z^2_{m-1}), \\ D_{ij,\theta^m} &= \frac{1}{3}Q^m_{ij,\theta_m}(z^3_m - z^3_{m-1}). \end{aligned} \tag{3.90}$$

where the derivatives of the transformed reduced stiffnesses, Q^m_{ij,θ_m}, are in turn obtained in terms of the laminate invariants

$$\begin{aligned} Q^m_{11,\theta^m} &= -2U^m_2 \sin 2\theta^m - 4U^m_3 \sin 4\theta^m, \\ Q^m_{12,\theta^m} &= 4U^m_3 \sin 4\theta^m, \\ Q^m_{22,\theta^m} &= 2U^m_2 \sin 2\theta^m - 4U^m_3 \sin 4\theta^m, \\ Q^m_{16,\theta^m} &= U^m_2 \cos 2\theta^m + 4U^m_3 \cos 4\theta^m, \\ Q^m_{26,\theta^m} &= U^m_2 \cos 2\theta^m - 4U^m_3 \cos 4\theta^m, \\ Q^m_{66,\theta^m} &= 4U^m_3 \sin 4\theta^m, \\ Q^m_{44,\theta^m} &= K(\bar{Q}^m_{55} - \bar{Q}^m_{44}) \sin 2\theta^m, \\ Q^m_{45,\theta^m} &= K(\bar{Q}^m_{55} - \bar{Q}^m_{44}) \cos 2\theta^m, \\ Q^m_{55,\theta^m} &= K(\bar{Q}^m_{44} - \bar{Q}^m_{55}) \sin 2\theta^m. \end{aligned} \tag{3.91}$$

here $\bar{Q}_{ij},\ (i,j = 4,5)$ denote the out-of-plane reduced stiffness terms, $K = 5/6$ is the shear correction factor, and the laminate invariants $U_i\ (i = 1,..,5)$ for the $m-th$ layer are defined by

$$\begin{aligned} U^m_1 &= (3\bar{Q}^m_{11} + 3\bar{Q}^m_{22} + 2\bar{Q^m}_{12} + 4\bar{Q}^m_{66})/8, \\ U^m_2 &= (\bar{Q}^m_{11} - \bar{Q}^m_{22})/2, \\ U^m_3 &= (\bar{Q}^m_{11} + \bar{Q}^m_{22} - 2\bar{Q}^m_{12} - 4\bar{Q}^m_{66})/8, \\ U^m_4 &= (\bar{Q}^m_{11} + \bar{Q}^m_{22} + 6\bar{Q}^m_{12} - 4\bar{Q}^m_{66})/8, \\ U^m_5 &= (\bar{Q}^m_{11} + \bar{Q}^m_{22} - 2\bar{Q}^m_{12} + 4\bar{Q}^m_{66})/8. \end{aligned} \tag{3.92}$$

Given these sensitivities, the exact gradient of the inverse of **ABD** matrices can be computed simply from the following relations

$$\begin{aligned} \mathbf{A}^{-1}_{,\theta^m} &= -\mathbf{A}^{-1}\mathbf{A}_{,\theta^m}\mathbf{A}^{-1}, \\ \mathbf{D}^{-1}_{,\theta^m} &= -\mathbf{D}^{-1}\mathbf{D}_{,\theta^m}\mathbf{D}^{-1}. \end{aligned} \tag{3.93}$$

3.8 Bending Design Using Lamination Parameters

According to the definition, the bending lamination parameters are computed from

$$(W_1, W_2, W_3, W_4) = \int_{-1/2}^{1/2} \bar{z}^2(\cos 2\theta(\bar{z}), \sin 2\theta(\bar{z}), \cos 4\theta(\bar{z}), \sin 4\theta(\bar{z}))d\bar{z}. \tag{3.94}$$

The bending stiffness matrix **D** is computed in a similar way as the in-plane stiffness (see Equation 3.56) by

$$\mathbf{D} = \frac{h^3}{12}(\mathbf{\Gamma_0} + W_1\mathbf{\Gamma_1} + W_2\mathbf{\Gamma_2} + W_3\mathbf{\Gamma_3} + W_4\mathbf{\Gamma_4}). \tag{3.95}$$

In deformation analysis of laminated plates using FSDT, in addition to the bending lamination parameters W_1, W_2, W_3, W_4, two of the in-plane lamination parameters, namely V_1, V_2, are also required. However, the relationship among these six parameters defining the feasible domain is unknown. Diaconu et al. [13] presented a numeric methodology to obtain feasible designs to maximize of the fundamental frequency of constant-stiffness panels. In the present study however, for the sake of simplicity, the classical lamination plate theory (CLPT) is used instead of FSDT. In CLPT only the bending lamination parameters are required to perform deformation analysis. In this case, the feasible domain is similar to that of the in-plane lamination parameters given in Equation 3.60 and therefore the cell design problem for symmetric laminates is defined as

$$\min_{\mathbf{W}_i} \frac{1}{2}\mathbf{M}_i^T \cdot \mathbf{D}^{-1}(\mathbf{W}_i) \cdot \mathbf{M}_i$$

Subject to:

$$\begin{gathered} 2W_1^2(1 - W_3) + 2W_2^2(1 + W_3) + W_3^2 + W_4^2 - 4W_1W_2W_4 \leq 1 \\ W_1^2 + W_2^2 \leq 1 \\ -1 \leq W_i \leq 1 \ (i = 1, \ldots, 4), \end{gathered} \tag{3.96}$$

in which $\mathbf{M}$ is the vector of the cell resultant moments. The above problem is solved numerically using an FSQP solver. Optimal design of constant-stiffness and variable-stiffness balanced symmetric laminates are defined analogous to Equations 3.62 and 3.69 respectively.

In the next chapter, the update rules discussed in this chapter are applied to design of variable-stiffness laminates for both in-plane and bending deformations using fiber angle and lamination parameters as design variables.

Chapter 4

Numerical Results

4.1 Introduction

The CA framework for analysis and design of 2-D anisotropic continua as explained in the previous chapter was implemented in Fortran 90 and used for numerical studies. The Fortran 90 CA code was initially designed to run on a single processor machine to verify its accuracy and study its performance. However, for an increased number of cells the CA code was adapted for massively parallel computers.

In this chapter, first the generic data type implemented for CA is explained followed by a brief introduction to the basic parallel and hybrid CA implementations. Using the implemented Fortran codes, fully stressed design of truss structures is studied next. Then design of anisotropic continua is considered for in-plane loading using either fiber angles or lamination parameters as spatial design variables. Examples for both single and multiple load case design of cantilever plates are also included. A picture frame test panel for combined loading is also designed as a real-life application. Finally, bending design of single layer as well as multi-layer composites is presented.

4.2 Cellular Automata Software Implementation

Implementation of the Fortran 90 derived data type is the result of collaborations with Prof. Layne T. Watson of the Departments of Computer Science and Mathematics at Virginia Tech. The parallel version of the existing software was implemented with the help of Mr. Dave B. Adams, whose efforts must be acknowledged here. For more details on this section please refer to Setoodeh et al. [64].

4.2.1 A Generic Data Structure for Cellular Automata

A generic Fortran 90 derived data type was developed for cellular automata where cell states can have the following types: string, integer, logical, and real. Such a data structure can be used for any cellular automata problem and has the flexibility to declare any number of entries for either of the above data types. For example, for the 2-D continuum problem under consideration, real type numeric entries are coordinates of the cell center, horizontal and vertical displacements, reaction forces in the x and y directions, cell density measure, and cell fiber angle. The character states are tags representing whether forces or displacements are applied on a cell such that the corresponding displacement update rule can be invoked. Finally, a logical cell state is used to store the convergence status of the cell displacements. Such a data structure is particularly useful in a parallel implementation. For instance, in the present structural problem only the real cell states evolve during the course of CA iterations. Hence at the time of communication between two processors, only that block of data has to be exchanged.

4.2.2 Standard Parallel Implementation

The initial parallel implementation followed that of Slotta et al. [68]. It is a straightforward application of parallel resources to the cell domain in which each processor iterates independently over the cells in its domain in a Gauss-Seidel iteration style. Processors communicate boundary information with their neighbors (above and below) between iterations in a lock-step communication phase and advance in parallel (cf. 4.1(a)). As the number of processors used in the calculation increases, the iteration style becomes a hybrid of Gauss-Seidel style and Jacobi style iterations. Gauss-Seidel style updates for the interior of a processors cell domain and Jacobi style updates across communication boundaries cause the rate of convergence for different numbers of processors to vary. The task graph, representing the initiation dependencies between processor dependent iterations, is given in Figure 4.1(b). This implementation, though trivial, has the advantage that each processor must only communicate with two neighboring processors. This eliminates some of the message passing overhead as an entire row of state information can be passed in a single message. The iteration style for such a parallel implementation is neither Gauss-Seidel nor Jacobi but rather a mixture of the two. Each processor iterates using new state information where available (Gauss-Seidel style) and uses old, previous iteration, state information in a Jacobi style across partition/processor boundaries.

4.2.3 Hybrid Cellular Automata

A CA-based analysis is computationally expensive compared to an analysis using modern tools on a serial machine. Therefore, it is essential to implement CA in a parallel environment

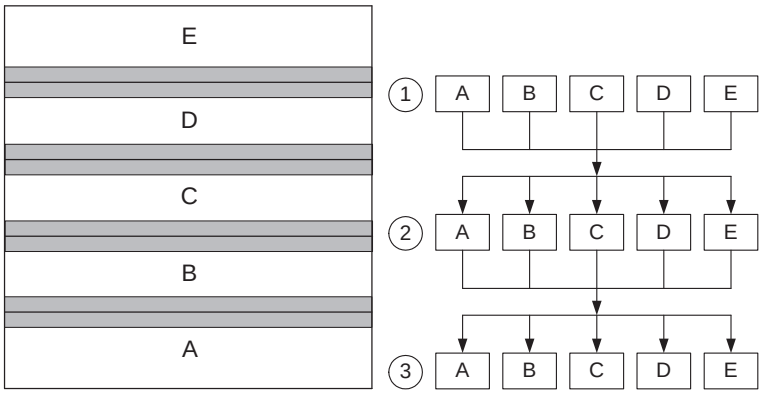

Figure 4.1: (a) Decomposition of the cell domain into five regions. Shaded rows are shared by adjacent processors; (b) Standard parallel implementation. The circles denote computation steps (iteration) between communication. Tasks located on the same horizontal line can be performed in parallel with communication being performed in lock-step after each iteration. The letters AE represent the compute tasks of the partition shown in (a).

to exploit the true merits of a CA-based structural analysis and design. However, parallel computing machines are not as easily accessible as serial ones. To resolve this issue, some researchers [39, 74] have used a global finite element analysis instead of iterative updates of cell displacements and then use the design update in a CA framework. This type of strategy is often called hybrid cellular automata (HCA) in the literature.

4.3 Fully Stressed Design of Trusses

Fully stressed design of truss structures is equivalent to the minimum weight design of statically determinant trusses [25]. To verify the implemented code, design of a 17×9 lattice truss structure with both symmetric and asymmetric loadings as shown in Figures 4.2(a) and 4.2(c) is considered. The following material properties were used in the simulations

$$E = 200GPa, \qquad \nu = 0.3, \qquad \sigma^{all} = 250MPa.$$

Figures 4.2(b) and 4.2(d) depict the obtained results which are in good agreement with typical designs reported in the literature [10].

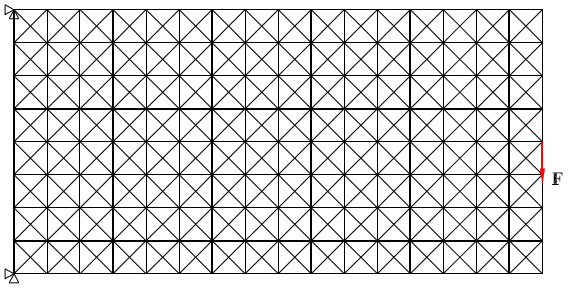

(a) Ground structure; symmetric cantilever.

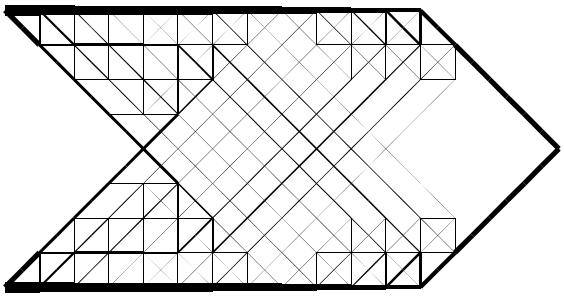

(b) Optimal symmetric cantilever.

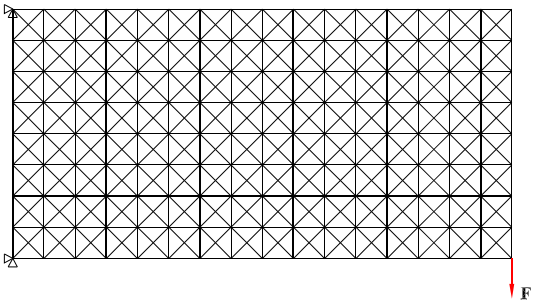

(c) Ground structure; asymmetric cantilever.

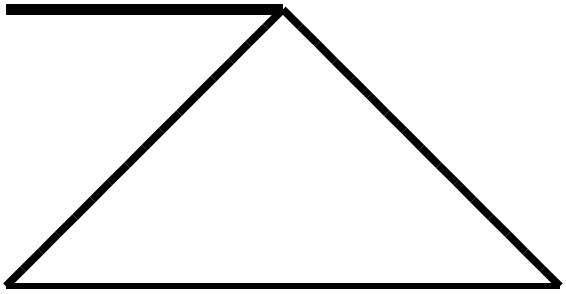

(d) Optimal asymmetric cantilever.

Figure 4.2: Fully stressed design of symmetric and asymmetric truss structures (17×9 CA lattice).

4.4 In-Plane Design Using Fiber Angles

To demonstrate performance of the proposed fiber angle update rule, several examples are considered here. All of the numerical results reported here are obtained using a Fortran 90 hybrid cellular automaton code running on a serial machine. The following material properties were used in simulations unless specified otherwise;

$$E_1 = 135.2\ GPa,\ E_2 = 9.241\ GPa,\ G_{12} = 6.276\ GPa,\ \nu_{12} = 0.318.$$

4.4.1 Fiber Angle Design of a Short Cantilever

Fiber-angle design of a short cantilever with aspect ratio of three and a uniformly distributed load of 1.0 kN/m (cf. Figure 4.3(a)) is considered as suggested by Pedersen [56]. The material properties used in the simulations are

$$\frac{E_1}{E_2} = 8.0, \qquad \frac{G_{12}}{E_2} = 0.35, \qquad \nu_{12} = 0.3.$$

Optimal designs for different CA lattice densities are depicted in Figure 4.3(b) through Figure 4.3(d). In the graphical representation, a small line is used in the center of each cell to represent the fiber orientation along with a color coding which reflects the orientation angle. For finer lattices where the line is not visually evident, the color coding scheme becomes specially useful.

The compliances for 46×16, 91×31, and 301×101 lattices are improved by a factor of $2.6 = 746.2/290.5$, $2.7 = 813.3/298.4$, and $3.0 = 929.0/310.6$, respectively (see Table 4.1). These results show that the optimal distribution of the fiber orientations is independent of the lattice density with more details emerging as the mesh density is increased without changing the overall pattern. The sudden change in the optimal fiber orientation as seen in the figure (for example the sudden change from blue to green near the center of the plate) happens where the two principal stresses are approximately equal in magnitude and opposite in sign [71]. Such phenomenon was explained in Section 3.4.1 as well. Although tow-placement technology requires continuous variation of the fiber orientation angle, based on the tow cutting and restarting capabilities of the current machines, the kind of discontinuities depicted in the resulting designs with clearly defined boundaries are expected to be manufacturable.

Table 4.1: Compliance of the short cantilever for different cell densities.

	Compliance $(N \cdot m)$	
CA Lattice	0° **Fibers**	**Optimal Design**
46×16	746.2	290.5
91×31	813.3	298.4
301×101	929.0	310.6

4.4.2 Fiber Angle Design of a Cutout Example

The CA methodology can be easily used to design irregular geometries as well. To demonstrate this, a square plate with a center cutout is studied next. The ratio of the width to the hole diameter for this plate is 3, and it is loaded with a uniform shear load. It is presumed here that a quarter plate, as shown in Figure 4.4(a) can be used to model the shear loading case. A 61×61 CA lattice is used for the analysis and minimum compliance design of this quarter model. Figure 4.4(b) shows the final CA fiber design obtained by using only the optimality criteria (OC) with 65% improvements in the compliance as compared to a 0° ply plate. Table 4.2 shows the quantitative results for the optimality criteria compared to a nominal design with 0° fibers. Finally, the v displacement profile of the cells on the loaded edge of the model is plotted in Figure 4.5. As this profile shows, the maximum v displacement is reduced by more than 65%.

Table 4.2: Compliance of the cutout example (61×61 cells).

Design	**Normalized Compliance**
0° Fibers	1.0
$[\pm 45^\circ]_s$ laminate	0.40
Optimality Criteria	0.35
Pattern Matching	0.36
Discrete Pattern Matching	0.46

4.4.3 A Heuristic Pattern Matching Technique

For complex geometries in which the stress state changes rapidly in some regions of the layer, the optimal fiber orientation angle can also change rapidly. For example, in the case of layers with a hole or cutout, stress concentration near the hole boundary may cause the fiber

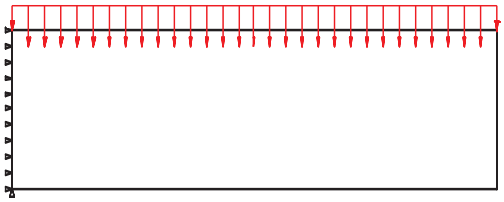

(a) Short cantilever with uniformly distributed loading.

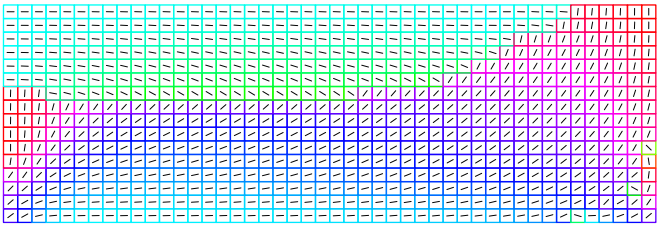

(b) 46×16 CA lattice.

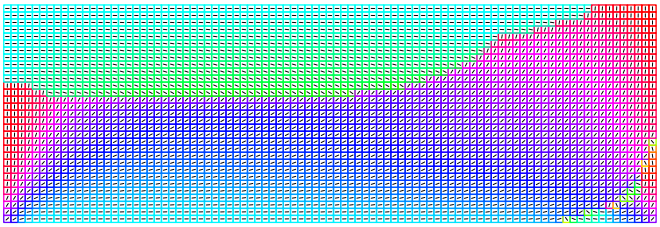

(c) 91×31 CA lattice.

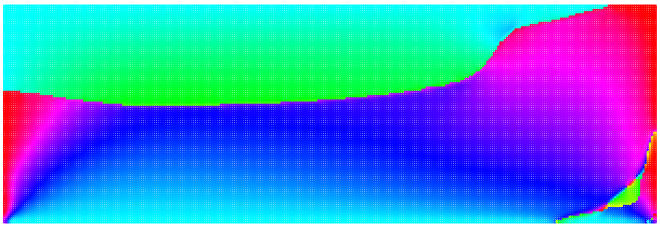

(d) 301×101 CA lattice.

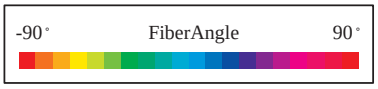

Figure 4.3: Short cantilever design with different CA cell densities.

orientation to change rapidly. It is also observed that in some cases, at locations where the stresses are very low, the principal stress direction varies erratically due to round-off error. In either case, fabricating such laminates with rapidly varying fiber orientation angles may be difficult, if not impossible, if curvilinear fiber orientation designs are sought.

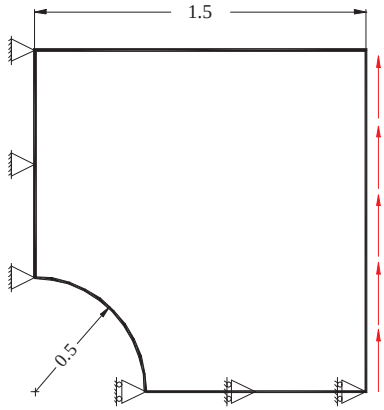

(a) Geometry and loading.

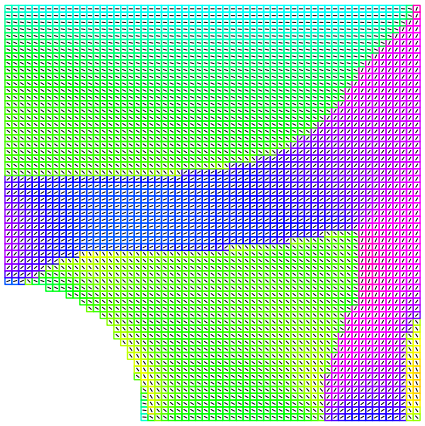

(b) Optimality criteria.

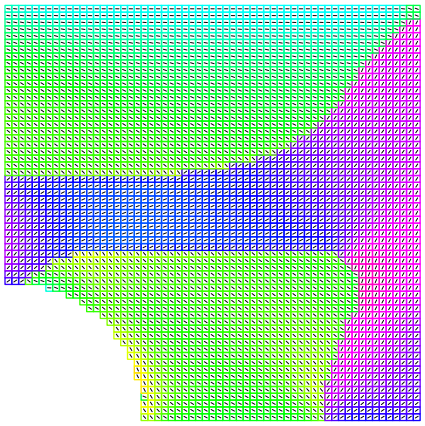

(c) Pattern matching.

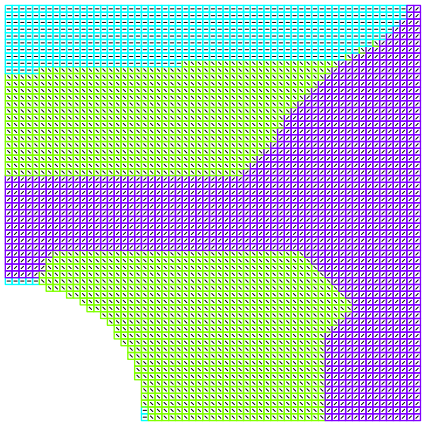

(d) Discrete pattern matching.

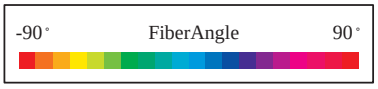

Figure 4.4: Quarter model for the cutout example loaded in shear (61×61 CA cells).

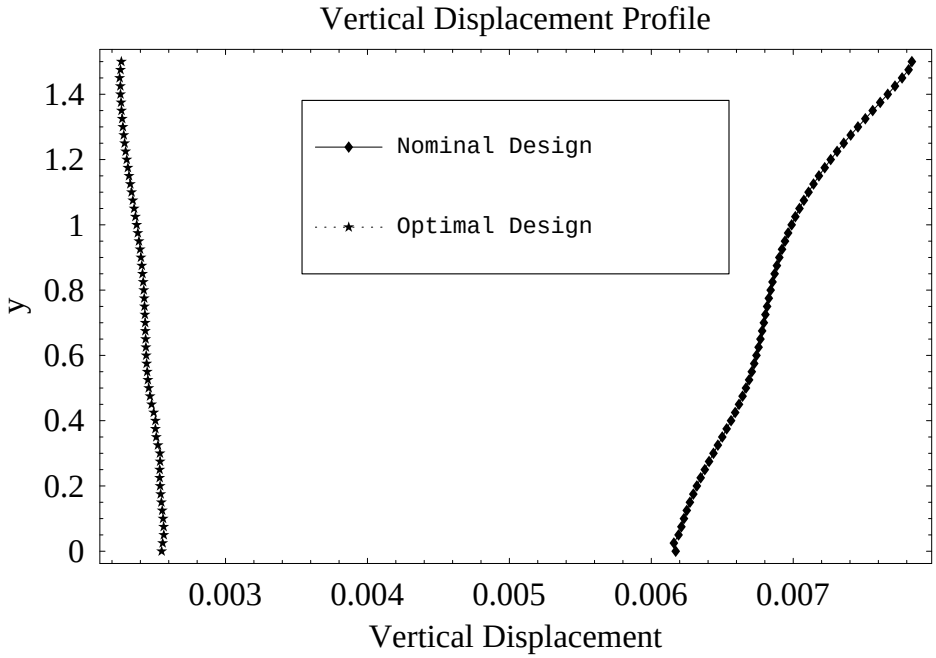

Figure 4.5: Displacement profile along the loaded edge for the square plate with center cutout.

In general, fiber discontinuities occur at two different types of locations. First, in locations where the absolute values of the two principal stresses are almost equal [71]. Second, in the regions of low stress values where the local fiber orientation has practically no effect on the stiffness of the structure. To resolve the discontinuities of the second kind a cell level heuristic manufacturing improvement update scheme is applied along with the strain energy minimization design scheme. In this heuristic approach, in some cases the optimal cell fiber angle, computed from the optimality criteria, is replaced with a new angle that matches the orientation of the neighboring cells. This is accomplished by using a *pattern matching* technique to establish a neighborhood pattern if one exists. To form the neighborhood pattern, the continuous fiber angles for the Moore neighborhood are first rounded to the nearest discrete orientations according to the rule

$$\theta^* = \begin{cases} 90°; & \theta \geq 67.5° \ \vee \ \theta < -67.5°, \\ -45°; & -67.5° \leq \theta < -22.5°, \\ 0°; & -22.5° \leq \theta < 22.5°, \\ 45°; & 22.5° \leq \theta < 67.5°. \end{cases} \tag{4.1}$$

Note that the rounded neighborhood angles are only used for the pattern matching process,

and the angles of the neighboring cells are left unchanged. Once the neighborhood fiber angles are rounded, if any five *contiguous neighborhood cells* (not counting the center cell) have the same discrete fiber orientation, then a pattern is said to be formed. For the Moore neighborhood with nine cells, there are eight possible pattern shapes. Four of the patterns are "C" shaped (e.g., N-NW-W-SW-S or W-NW-N-NE-E) and four are "L" shaped (e.g., NW-W-SW-S-SE or NE-E-SE-S-SW), see Figure 2.1(b). For a neighborhood with a formed pattern, the optimal angle is also rounded using Equation 4.1, then it is checked against the matched direction. If they disagree, the site cell angle is replaced with the average value of the continuous angles of the cells that formed the pattern. If they agree, or if the neighborhood does not form a pattern, then the optimal angle is used to update the cell angle.

In order to enhance the convergence of the algorithm, the pattern matching scheme is activated when the displacement field is loosely converged compared to the CA convergence criterion. This ensures that the information has reached every part of the domain and all possible patterns have been formed. Figures 4.4(c)-4.4(d) show the modified CA design with a 64% stiffness gain using continuous and discrete pattern matching techniques.

4.4.4 Combined Topology and Fiber Angle Design of a Symmetric Cantilever

The minimum compliance topology design problem is known to be convex when the penalization parameter p is set to 1.0, however, it is nonconvex for $p > 1$ [10]. Convexity of the problem guarantees success of a gradient based minimizer to find the global minimum. This property is the basis of the so-called *continuation method* [10, 81] used in this study. In continuation methods, the penalization parameter p is increased gradually from 1.0 to 3.0 in the course of the design iterations to steer the final design towards a local optimum of the nonconvex problem even though the final design for $p > 1$ is not guaranteed to be a global optimum point.

The symmetric cantilever plate in Figure 4.6(a) with an aspect ratio of 4 is modeled with a regular lattice of 325×82 CA cells. Figures 4.6(b) through 4.6(e) show the topology of the optimal designs along with the color-coded fiber orientation angles for different volume fractions. These designs, as expected, are quite similar to classical optimal topologies of isotropic material [2].

The corresponding normalized compliances with respect to a 0° fiber design are tabulated in Table 4.3. These figures show that with the present choice of density interpolation scheme checkerboards are readily suppressed. Besides, for lower volume fractions, fibers are aligned with thin members similar to Mitchell type of structures.

Table 4.3: Normalized compliance of the symmetric cantilever for different volume fractions.

Volume Fraction	Normalized Compliance
100%	0.74
70%	0.88
50%	1.14
30%	2.22

4.4.5 Multiple Load Case Design of an Asymmetric Cantilever

The asymmetric cantilever of Figure 4.7 is next considered for a multiple load case. The first load case is a downward load as denoted by F_1 in Figure 4.7(a), and the upward load F_2 with the same magnitude is the second load case. Optimal design for several volume fractions for both single and multiple load cases are depicted in the same figure and numerical values for the corresponding normalized compliance are tabulated Table 4.4. For 100% volume fraction, the fiber orientation angle can be tailored for the two load-case design such that no loss in stiffness performance occurs compared to the single-load case. As the volume fraction is reduced, however, the stiffness of the two-load case designs are smaller than those of the single-load case designs. For example, for a volume fraction of 50% the two-load case design is 16% softer than the single-load design.

Table 4.4: Normalized compliance of the asymmetric cantilever for different volume fractions (203×102 CA cells).

	Normalized Compliance	
Volume Fraction	Single Load Case	Multiple Load Case
100%	0.32	0.32
90%	0.32	0.33
70%	0.36	0.39
50%	0.47	0.53

Figure 4.8 depicts a quantitative measure of the pertinent fiber orientations along the normalized length of the asymmetric cantilever for the 100% volume fraction multiple load case design. As this figure shows, the fiber orientation angle for different levels of the cantilever depth is constant up to about 70% of the length where a sudden change in the sign of fiber orientation angle occurs. Such erratic changes in the fiber orientational angle are of similar nature to the case of almost equal absolute value of principal stresses for the single load

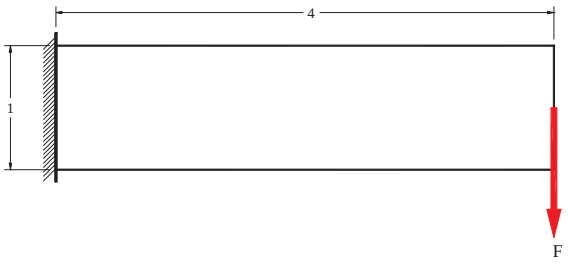

(a) Geometry and loading.

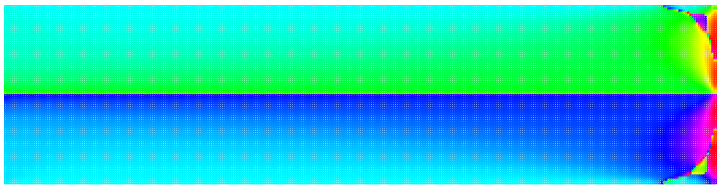

(b) 100% Volume fraction.

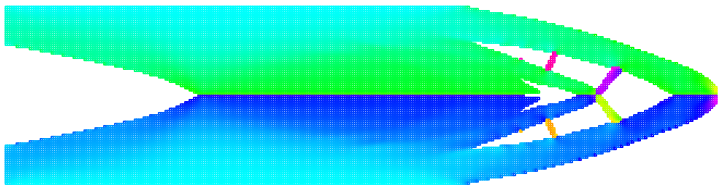

(c) 70% Volume fraction.

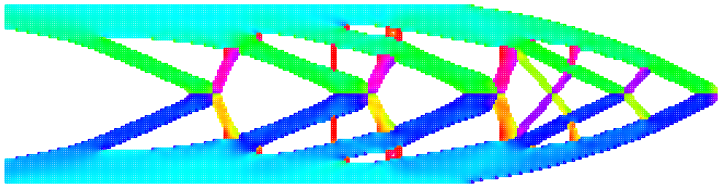

(d) 50% Volume fraction.

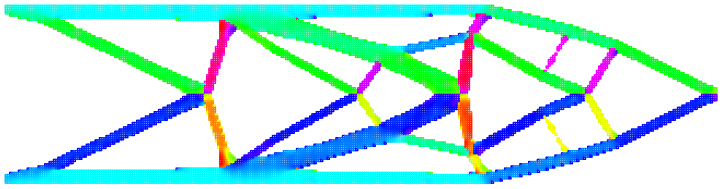

(e) 30% Volume fraction.

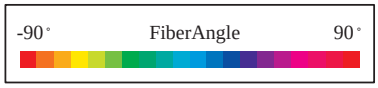

Figure 4.6: CA-converged topology of the symmetric cantilever (325×82 cells).

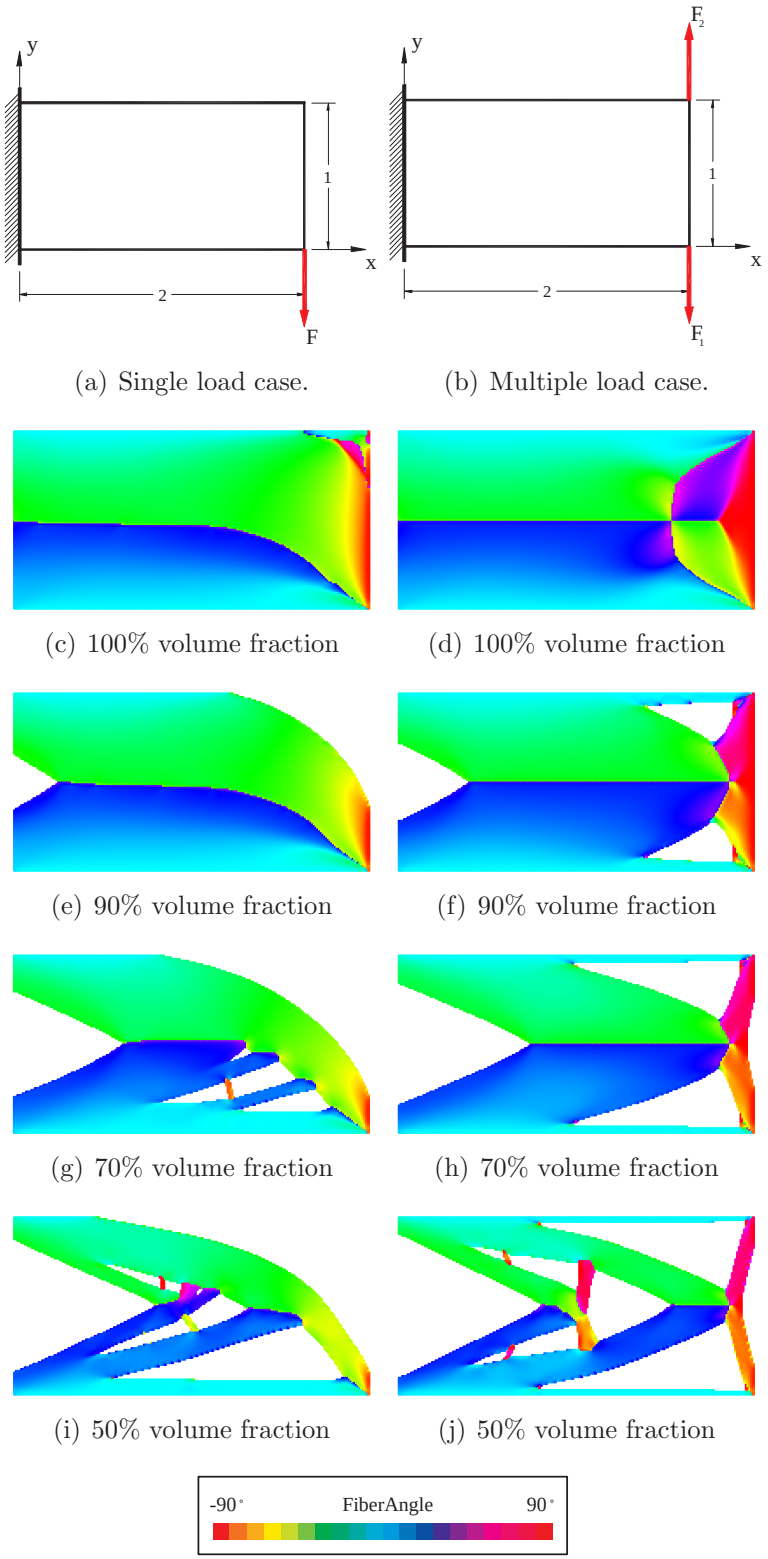

(a) Single load case. (b) Multiple load case.

(c) 100% volume fraction (d) 100% volume fraction

(e) 90% volume fraction (f) 90% volume fraction

(g) 70% volume fraction (h) 70% volume fraction

(i) 50% volume fraction (j) 50% volume fraction

Figure 4.7: CA-converged topologies of the asymmetric cantilever. Left column; single load case, right column; multiple load case (203×102 CA cells).

case. Such a phenomenon is attributed to the fact that complimentary strain energy is not unimodal in fiber angle design space. In other words, the optimal fiber orientation is not a continuous function of principal stresses since the objective function is nonconvex.

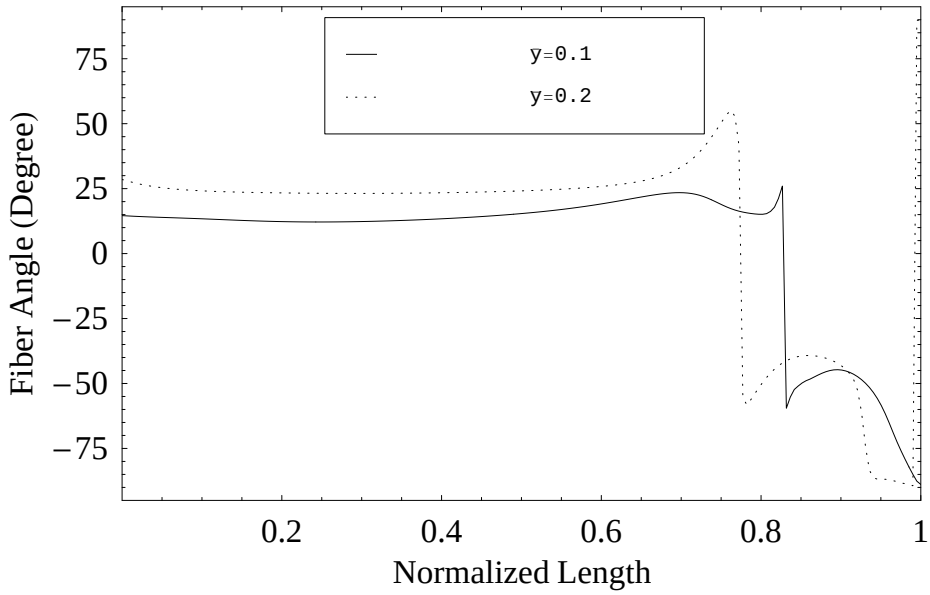

Figure 4.8: Fiber angle along normalized length for the asymmetric cantilever with multiple load cases.

4.4.6 Extended Optimality

The optimum topology can be obtained for different volume fractions. Clearly, as the volume fraction decreases, the compliance will increase. This behavior can also be viewed as a tradeoff between compliance and volume fraction [37]. To examine this phenomenon further, consider a nondimensional compliance defined by:

$$\overline{C} = \frac{C_i \eta_i}{C_0} \tag{4.2}$$

where C_i is the corresponding compliance for a volume fraction of η_i and C_0 is the optimal compliance for $\eta = 1.0$. Figure 4.9 shows variations of this nondimensional compliance for different cantilever problems as a function of volume fraction. In the present formulation where compliance is minimized with a given volume fraction for prescribed loads, it makes practical sense to minimize the nondimensional compliance as defined in Equation (4.2). Following Rozvany et al. [59], this new design is optimal in an *extended optimality* sense.

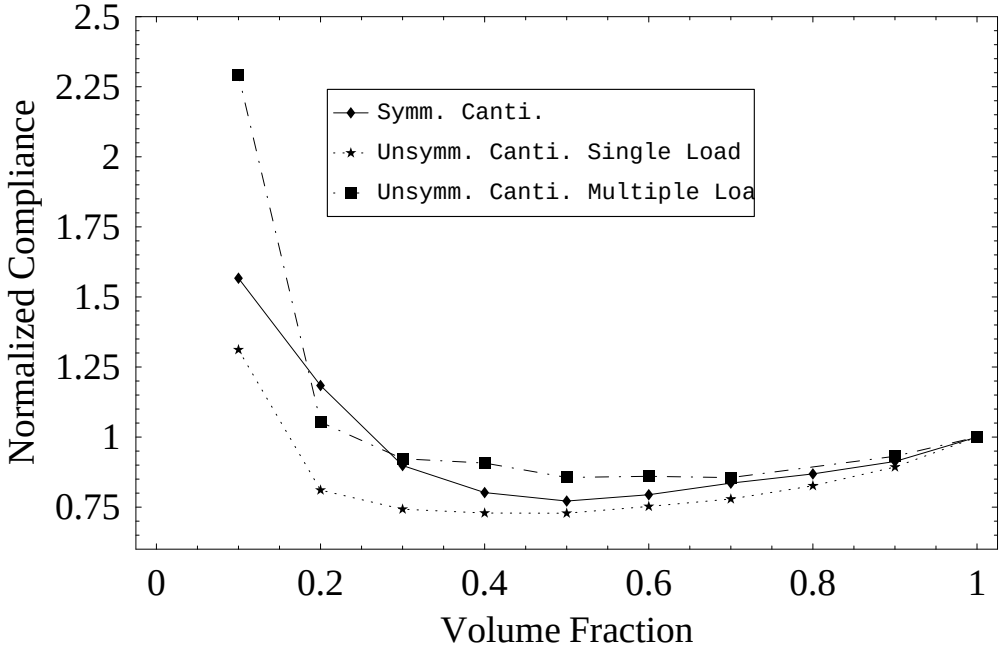

Figure 4.9: Nondimensional compliance as a function of volume fraction.

This can also be interpreted as maximization of the performance index of the design as described in [40]. Figure 4.9 predicts that the optimal designs in the sense of extended optimality for the symmetric, asymmetric single load case, and asymmetric multiple load case correspond approximately to $\eta = 0.50$, $\eta = 0.50$, and $\eta = 0.40$ respectively.

4.4.7 NASA Picture Frame Design for Combined Loading

The next problem under consideration consists of a flat panel with a 3 inch diameter central hole loaded by combined forces of compression and shear. This example is chosen to demonstrate the performance of the presented methodology to design more realistic structures under combined loading conditions. The simplified model was generated in collaboration with Dr. Brian Tatting of ADOPTECH, Inc., whose inputs are acknowledged here.

Model Description

A complete STAGS (Structural Analysis of General Shells finite element code) model detailing the structure was supplied by NASA Langley, and subsequently transformed into a slightly simpler model (in terms of edge conditions and additional elements required for

accurate modeling) to facilitate the design techniques. A three-dimensional representation of the finite element model is shown in Figure 4.10(a) (without the central hole). The model consists of a test panel (the regular grid in the center region) attached on each side to a picture frame type fixture that is connected by pins, which is attached to appropriate loading frames to achieve the combined loading stress state. During testing, the top edge of the upper frame is held fixed, while the bottom frame undergoes a vertical force from below and a horizontal force through an L extension of the bottom frame (not shown here). This results in a horizontal force as well as a bending moment, which is represented in the STAGS model by the force couple shown. The test panel area is 24 inches wide and 28 inches high, with a CA lattice size of one-half inch in both directions. One element is removed at each corner of the test coupon to alleviate stress. Tabs are present on all four sides. The top and bottom tabs measure 23 inches wide (due to the 1/2 cut-out in each corner) by 2.94 inches high, while the sides are 27 inches high and 2.25 inches wide. The tabs are constructed with a layer of steel ($E = 30.0\ Msi, \nu_{12} = 0.30$, 0.19 inches thick) bonded to each side. The test panel and tabs are shown in the Figure 4.10(b) with the other components removed. The origin of the axes is in the bottom left corner of the test panel. Note that the meshing within the tabbed regions is quite erratic, which is due to the fact that earlier models possessed higher density meshes within the test panel region along with the fact that certain points within the tab had to be defined as nodes. These nodes are denoted by the colored dots in the figure, and represent the points of attachment between the tabbed regions and the fixture. The blue dots represent nodes in the tabs which are defined within the model as having identical displacements (horizontal u, and vertical v) as the corresponding point in the frame. The green dots are similarly defined, but are only constrained in the u displacement direction (the connections in the side fixtures are slotted to allow vertical movement). The red dots shown here represent the pinned connections between horizontal and vertical components of the fixture, and indicate that the displacements for each connected component are identical at that point (note that no connection to the test panel or tabbed areas exist for these red points, but are shown for completeness).

Analysis Methodology

In the present simplified 2-D model, to simulate the actual test condition, the connection points on the bottom tab (shown by blue dots in Figure 4.10(b)) are all assumed to have the same horizontal displacement u_O while the vertical displacements vary linearly:

$$\begin{aligned} u_C &= u_O, \\ v_C &= v_O + (x_C - x_O)(v_{O'} - v_O)/9.5, \end{aligned} \tag{4.3}$$

where coordinates of points O and O' are $x_O = 12$, $y_O = -1$, $x_{O'} = 21.5$, $y_{O'} = -1.5$ (see Figure 4.10(b) for the reference coordinate system). The horizontal and vertical displacements of these points are denoted by u_O, v_O, $u_{O'}$, $v_{O'}$ respectively. On the other hand,

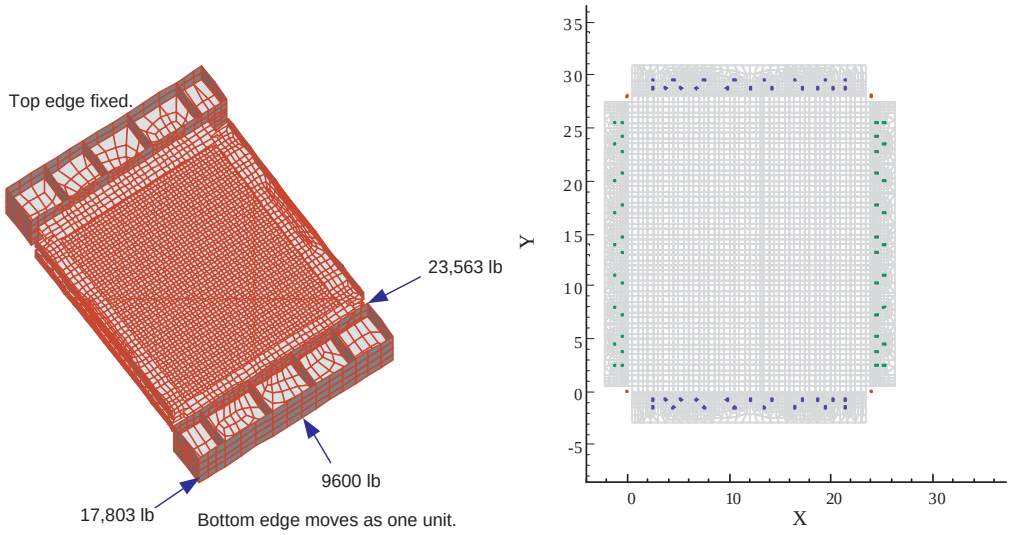

(a) 3-D STAGS model. (b) Simplified 2-D model.

Figure 4.10: Picture frame panel for combined compression and shear loading.

the connection points on the vertical tabs, are assumed to have linearly varying horizontal displacement according to the relation

$$u_C = -(y_C - y_{hinge})u_O/28.0, \tag{4.4}$$

in which the hinge points are the upper red dots shown in Figure 4.10(b). The combined loading on the picture frame fixture is modeled by the following equivalent loads:

$$\begin{aligned} N_{xy} &= -5760.0\ lb, \\ N_{yy} &= 9600.0\ lb, \\ M_{xy} &= 86400.0\ lb \cdot in. \end{aligned}$$

Deformation analysis of this panel with the applied loads and constraints is performed based on a linear superposition approach using a global FE model. First it is assumed that the reaction forces N_{xy}, N_{yy}, and moment M_{xy} on the bottom tab depend linearly on the three independent applied displacements u_O, v_O, and $v_{O'}$ of Equations 4.3 and 4.4 as

$$\begin{aligned} N_{xy} &= Au_O + Bv_O + Cv_{O'}, \\ N_{yy} &= Du_O + Ev_O + Fv_{O'}, \\ M_{xy} &= Gu_O + Hv_O + Iv_{O'}, \end{aligned} \tag{4.5}$$

where the reaction forces and moment are computed by summing the forces and moments on the bottom tab over the number of the bolts ($nb = 19$):

$$\begin{aligned} N_{xy} &= \sum_{i=1}^{nb} f^x_{c(i)}, \\ N_{yy} &= \sum_{i=1}^{nb} f^y_{c(i)}, \\ M_{xy} &= \sum_{i=1}^{nb} (f^y_{c(i)}(x_i - x_O) + f^x_{c(i)}(y_i - y_O)), \end{aligned} \tag{4.6}$$

in which $c(i)$ is the index of the i-th cell coinciding on a connection point. Now, three sets of linearly independent displacements are applied to $(u_O, v_O, v_{O'})$ and separate analyses are performed. Then, Equation 4.5 is solved for the "apparent stiffness" of the panel, i.e., $A, B, ..., I$. Next, given the actual applied forces, and the picture frame stiffness terms, Equation (4.5) is solved for $(u_O, v_O, v_{O'})$. Finally, the computed set of displacements are applied on the model, and another analysis is performed to find the displacements of all the cells in the domain.

In practical working conditions, the direction of the shear load could be either positive or negative. Designing for either case would generate direction sensitive designs which are usually undesirable. To resolve this issue, the panel is designed for the following two separate load cases:

$$\begin{aligned} N_{xy} &= -5760.0\ lb, \\ N_{yy} &= 9600.0\ lb, \\ M_{xy} &= 86400.0\ lb \cdot in, \end{aligned}$$

and

$$\begin{aligned} N_{xy} &= 5760.0\ lb, \\ N_{yy} &= 9600.0\ lb, \\ M_{xy} &= -86400.0\ lb \cdot in. \end{aligned}$$

Each analysis step in the iterative analysis and design process is composed of four simple analyses. Clearly, during the design process, the stiffness of the panel will change. This would require repeated calculation of the panel stiffness as defined in (4.5) in the course of the optimization.

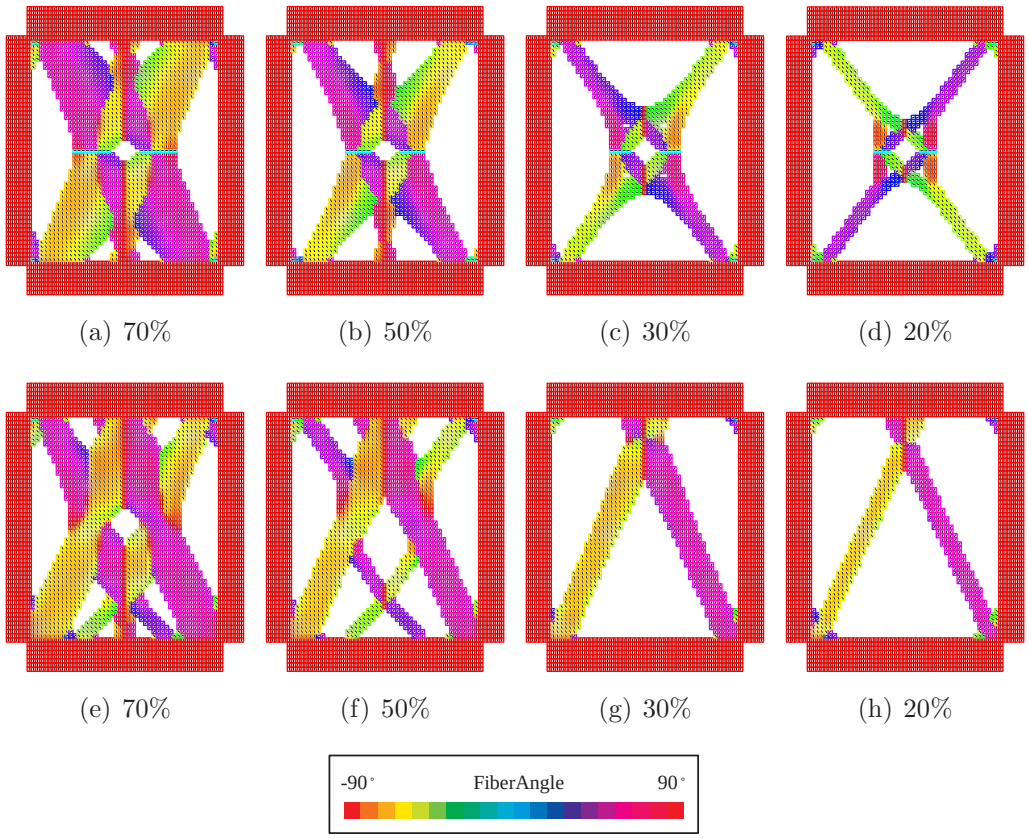

Figure 4.11: Partial coverage designs for the NASA panel. First row; imposed symmetry for both horizontal and vertical center axes, second row; imposed symmetry for the vertical axes only.

Partial Coverage Design

The same principle of minimum compliance design is applied to design the picture frame panel, considering the fact that the tabs have two layers of 0.19in thick steel bounded on each side. Besides, tabbed areas are not to be designed. Due to the combined loading condition, multiple load case design, and anisotropy of the material a full model will not readily capture the inherent symmetry of the design problem. Therefore, the symmetry is imposed for designs for two separate cases of X and Y axis symmetry and Y axis symmetry where the origin of the X-Y coordinate system is located in the center of the cutout hole. Figure 4.11 depicts partial coverage designs for different volume fractions, and Table 4.5 lists the corresponding normalized compliances.

Table 4.5: Normalized CA-converged compliances for the NASA panel.

Volume Fraction	XY**-axes Symmetric**	Y**-axis Symmetric**
70%	0.670	0.732
50%	0.975	1.008
30%	1.543	1.354
20%	2.177	1.693

4.5 In-Plane Design Using Lamination Parameters

In this section, the formulation presented in Section 3.5 is used to design laminates with different lay-up configurations and geometries. In the following examples, first design of the cutout problem of Section 4.4.2 is considered and then the effect of lattice density is studied using a cantilever example.

4.5.1 Optimal Design of the Cutout Example

The cutout example of Section 4.2.2 is considered here to show the stiffness improvements using the proposed lamination parameter formulations. First, the simplest balanced symmetric configuration of $[\pm\theta]_s$ is investigated for which only one lamination parameter V_1 ($V_3 = 2V_1^2 - 1$) is required to fully represent the in-plane stiffness properties. This reduces the problem to a simple 1-D minimization problem. Such a laminate configuration is graphically represented by the parabolic portion of the Miki diagram. Numerical experiments showed that this new formulation has an improved rate of convergence and generates a design with a normalized compliance of 0.27. For such a laminate lay-up configuration, the fiber angles can be easily retrieved using the formula

$$\theta = \frac{1}{2}\arccos(V_1). \tag{4.7}$$

The optimal $\pm\theta$ for this example is shown in Figure 4.12.

The same problem is solved again for a general balanced symmetric configuration where $V_3 \geq 2V_1^2 - 1$. Such a laminated configuration could have a $[\pm\theta_1/\pm\theta_2/.../\pm\theta_{n_h}]_s$ lay-up. However, the thickness of the layers might or might not be the same. Since the equality constraint is relaxed to an inequality one, we are expecting a smaller (or at least the same) compliance. However, a similar compliance of 0.27 is obtained. This means that for this particular example, additional layers will not improve the stiffness of the structure as compared to a $[\pm\theta]_s$ variable-stiffness design. Next, a general lamination parameters case with four design variables per cell is consider which predicts the best design by far with a compliance of 0.20.

Numerical values of the compliance are list in Table 4.6 for comparisons. Finally, it should also be pointed out here that as shown in Chapter 2, optimal topology can be obtained once the lay-up design is completed. In other words, optimal topologies can be obtained regardless of the fact that retrieving the actual stacking sequence remains as a post processing step.

Table 4.6: CA-converged compliance of the cutout example for balanced symmetric and general lay-ups (61×61 cells).

Design	**Normalized Compliance**
0° Fibers	1.0
$[\pm 45^\circ]_s$ laminate	0.40
Constant stiffness, balanced symmetric	0.36
Constant stiffness, general	0.33
Variable-stiffness, single layer	0.35
Variable-stiffness, $[\pm\theta]_s$ lay-up	0.27
Variable-stiffness, balanced symmetric	0.27
Variable-stiffness, general	0.20

4.5.2 Design of a Cantilever Plate

In-plane design of a cantilever plate with thickness h, loaded with uniform load q_0 (as considered in Section 4.4.1 for $a/b = 3$; initially suggested by Pedersen [56]) is studied here to demonstrate the improvements in stiffness by a variable-stiffness design (see Figure 4.13). The cantilever is discretized using a regular grid of bilinear elements with 11 nodes on the shorter side of the rectangular domain, b, fixed for all aspect ratios. The following material properties are used in all numerical simulations,

$$E_{11} = 181.0GPa,\ E_{22} = 10.3GPa$$
$$G_{12} = 7.17GPa,\ \nu_{12} = 0.25$$

For the problem suggested by Pedersen [56], the aspect ratio is $a/b = 3$. In that case, the nondimensional compliance of the optimal general constant-stiffness design $\bar{C}_{gc} = 0.0935$ and the value of optimal lamination parameters of $V_1 = 0.4779, V_2 = 0.3926, V_3 = 0.2015, V_4 = -0.06850$. The optimal single layer variable-stiffness design improves the compliance by 30% to $\bar{C}_{sv} = 0.0654$. The distribution of the fiber angles for this example is depicted in Figure 4.14(a). The optimal general variable-stiffness design based on four lamination parameters at each node yield a normalized compliance of $\bar{C}_{gv} = 0.0592$, while the locally balanced

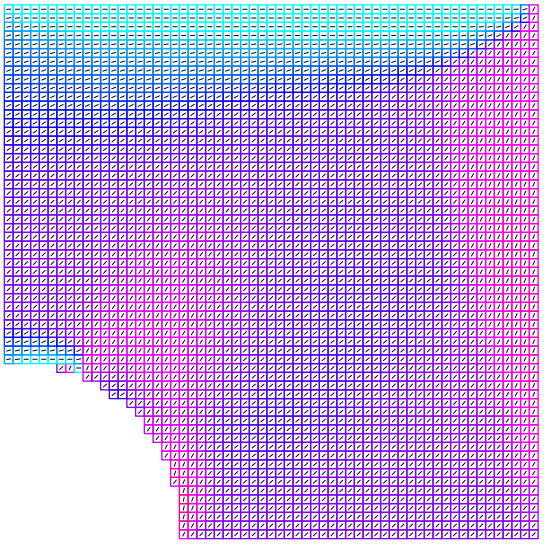

(a) $+\theta$ layer.

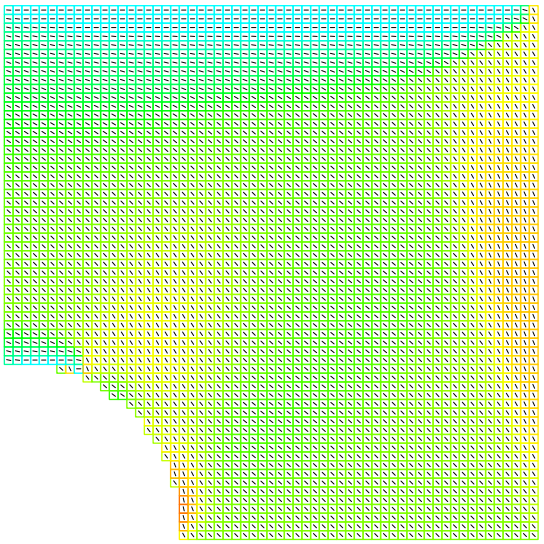

(b) $-\theta$ layer.

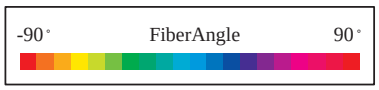

Figure 4.12: Balanced symmetric $[\pm\theta]_s$ design for the cutout example with shear loading(61×61 CA cells.)

variable-stiffness design based on two lamination parameters yields a normalized compliance of $\bar{C}_{bv} = 0.0788$. The optimal distribution of the lamination parameters are depicted in

Table 4.7: Nondimensional CA-converged compliance of cantilevered plates under uniform loading for different aspect ratios. $\bar{C} = C\frac{E_2 h b^3}{q_0^2 a^5}$

$\frac{a}{b}$	$\bar{C}_{bc}$	$\bar{C}_{gc}$	$\bar{C}_{bv}$	$\bar{C}_{sv}$	$\bar{C}_{gv}$
1.0	0.7591	0.5687	0.6121	0.4429	0.3915
2.0	0.1854	0.1592	0.1443	0.1114	0.0978
3.0	0.1019	0.0935	0.0788	0.0654	0.0592
5.0	0.0620	0.0597	0.0500	0.0447	0.0425
10.0	0.0419	0.0417	0.0386	0.0363	0.0360

bc: balanced constant-stiffness, *gc*: general constant-stiffness, *bv*: balanced variable stiffness *sv*: single layer variable-stiffness, *gv*: general variable stiffness

Figures 4.14(b) through 4.14(e) for the general lamination case. For general lamination, the compliance is improved by 36% compared to the optimal constant-stiffness laminate.

The nondimensional optimal compliances for cantilevers with different aspect ratios are given in Table 4.5.2. The second column lists the values for constant-stiffness balanced lamination, while the third column is for generally laminated constant-stiffness designs. The fourth, fifth and sixth columns list the optimal values for variable-stiffness designs based on single layer, balanced lamination (two lamination parameters), and general lamination, respectively. A comparison of constant and variable-stiffness designs also indicate that variable-stiffness designs are significantly better than constant-stiffness designs. The difference between balanced and general designs, and constant and variable-stiffness designs, decreases as the aspect ratio is increased. To explain this trend, notice that as the aspect ratio is increased, the cantilever approximates a slender beam where the optimal fiber orientation is constant along the beam axis. For this case, the optimal solution for all the five different design variants are almost identical.

4.5.3 Design of the Symmetric Cantilever

To investigate dependency of the results on the lattice size, design of the symmetric cantilever of Figure 4.15(a) with an aspect ratio of 2, is studied with two different lattice sizes of 83×42 and 203×102 cells. The cantilever is designed for the general lamination parameters with V_1, V_2, V_3, and V_4 as spatial design variables. Figures 4.15(b) through 4.15(e) depict the optimal distribution of the lamination parameters for the 83×42, and Figures 4.15(f) through 4.15(i) show the same results for the 203×102 lattice. As these figures demonstrate, the results are

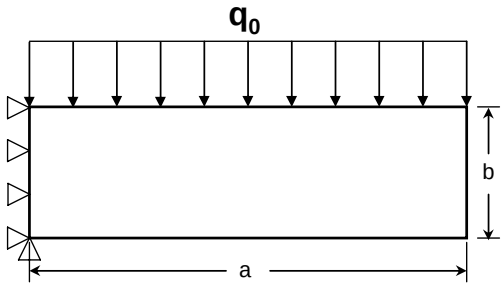

Figure 4.13: Cantilever plate problem.

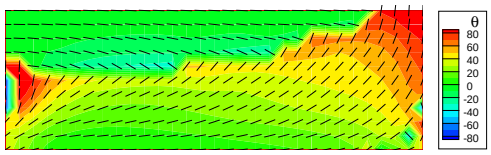

(a) Fiber angle distribution for single layer lamina.

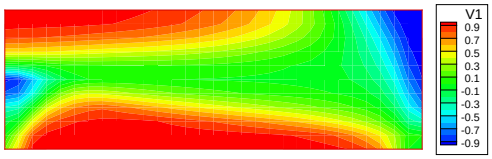

(b) V_1

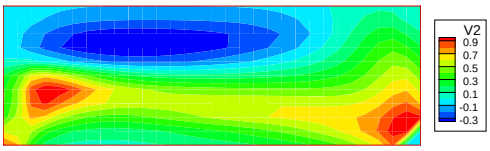

(c) V_2

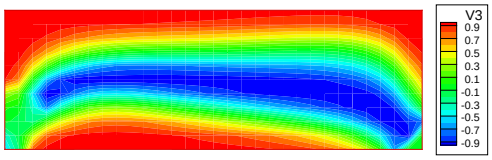

(d) V_3

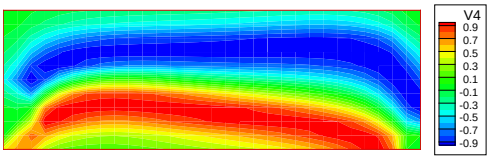

(e) V_4

Figure 4.14: CA-converged distribution of the fiber orientation angle and lamination parameters for the cantilever plate with $a/b = 3$ (31×11 nodes).

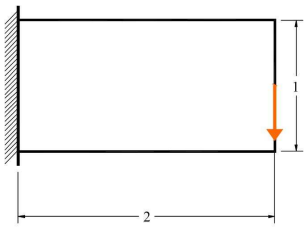

(a) Geometry and loading.

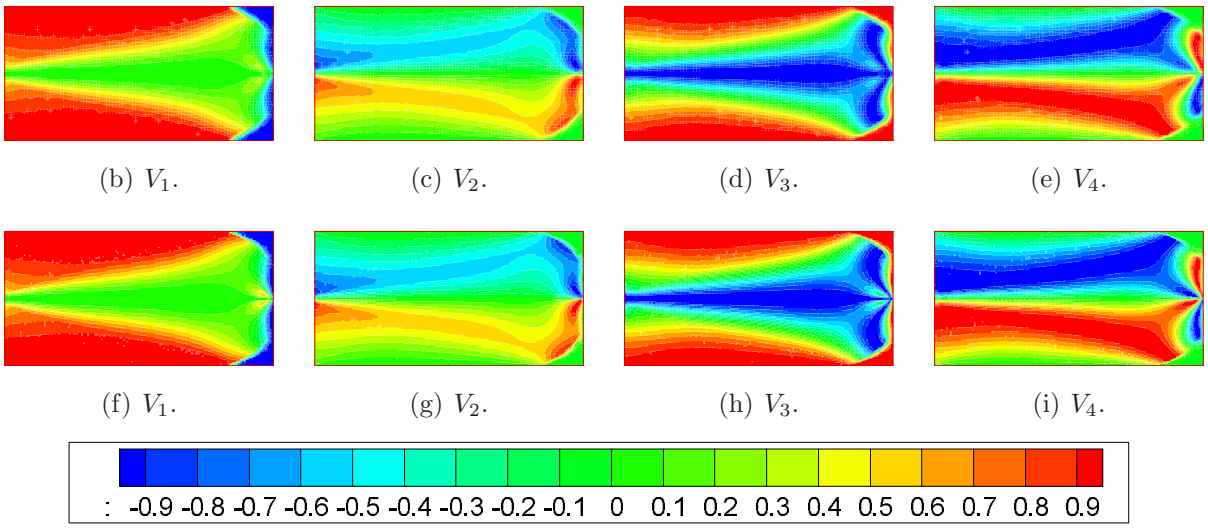

(b) V_1. (c) V_2. (d) V_3. (e) V_4.

(f) V_1. (g) V_2. (h) V_3. (i) V_4.

Figure 4.15: CA-converged distribution of the lamination parameters for the symmetric cantilever. (a)-(d) 83×42 CA cells; (e)-(h) 203×102 CA cells

nearly independent of the lattice size. Moreover, the optimal distribution of the lamination does not exhibit erratic behavior in the regions of low stress level, e.g. upper and lower right corners of the beam, as it is usually seen in the optimal distribution of fiber angle orientation (see Section 4.4.4).

4.5.4 Restricted Balanced Symmetric Lay-up Design of the Symmetric Cantilever

The restricted design formulation for equithickness balanced symmetric variable-stiffness laminates as explained in Section 3.5.7 is applied to design of the symmetric cantilever of the section 4.5.3. Table 4.8 lists the normalized compliance for an increasing number of equithickness layers. The normalized compliance of the optimal balanced symmetric constant-stiffness design for this example is 0.711. This table shows that using a few (about 4 to 6) layers of constant thickness laminate in the restricted formulation one can more or less benefit from a variable-stiffness design. More recent studies [60] present a comparison in design parameterizations using fiber angles versus lamination parameters.

Table 4.8: CA-converged compliance of the symmetric cantilever for an increasing number of equal thickness layers.

Number of $[\pm\theta_i]_s$ layers	**Normalized Compliance**
2	0.646
3	0.571
4	0.546
5	0.534
10	0.516
50	0.507
100	0.506
∞	0.505

4.6 Bending Design Using Fiber Angles

Optimal design of variable-stiffness composite plates using fiber angles as continuous spatial design variables is considered in this section. The methodology presented in Section 3.7 is used to design both single layer and multiple layer laminates. The deformation analysis is based on the shear deformable theory for these examples.

4.6.1 A Benchmark Example

In order to validate the present methodology, the benchmark example of Lund and Stegmann [43] is studied first. This problem is a single-layer 0.1m$\times$0.1m $\times$ 0.05m clamped plate uniformly loaded with downward pressure. Figure 4.16, shows the fiber angle distribution for

Table 4.9: Normalized compliance for benchmark problem.

Design	**Normalized Compliance**
0° Fibers	1.0000
Radial Fibers	0.9545
Circumferential Fibers	1.0110
Optimal Fibers	0.9428

the full plate (symmetry enforced) for several nominal designs as well as the optimal design. The optimal design as depicted in Figure 4.16(d) is in good agreement with the results reported by Lund and Stegmann [43]. Normalized compliances as listed in Table 4.9 shows that the presented optimal design has an improved compliance as compared to the nominal designs. The deformed shape and the rotational deformation about the y-axis along the horizontal centerline ($y = 0.5$) are plotted in Figures 4.17(a) and 4.17(b) respectively. These figures show the continuity of the deformations across the fiber angle discontinuities.

4.6.2 Design of Single Layer Laminae

Now, design of a square laminated plate with a center load is considered. Aspect and side to thickness ratios are 1.0 and 10.0 respectively and the edge supports are either simply supported or clamped. Due to the symmetry, only a quarter model is used in the numerical simulations, however, a full plate is used to demonstrate the fiber angle distributions. The following orthotropic material properties are used in the simulation [34]:

$$\frac{E_1}{E_0} = 181.0, \frac{E_2}{E_0} = 10.3, \frac{G_{12}}{E_0} = 7.17$$

$$\frac{G_{23}}{E_0} = 3.0, \nu_{12} = 0.25, G_{12} = G_{13}, E_0 = 1.0GPa$$

Figure 4.18 depicts the optimal designs for both simply supported and clamped square plates with a concentrated center load for different lattice sizes (51×51 and 101×101). These figures show that the optimal design do not depend on the lattice sizes, therefore in the next examples, the coarser 51×51 CA lattice is used.

Combined Fiber Angle and Topology Design of Laminae

The clamped lamina plate of the previous section is considered here for combined topology and fiber angle design. Table 4.11 lists the optimal compliance for different volume fractions

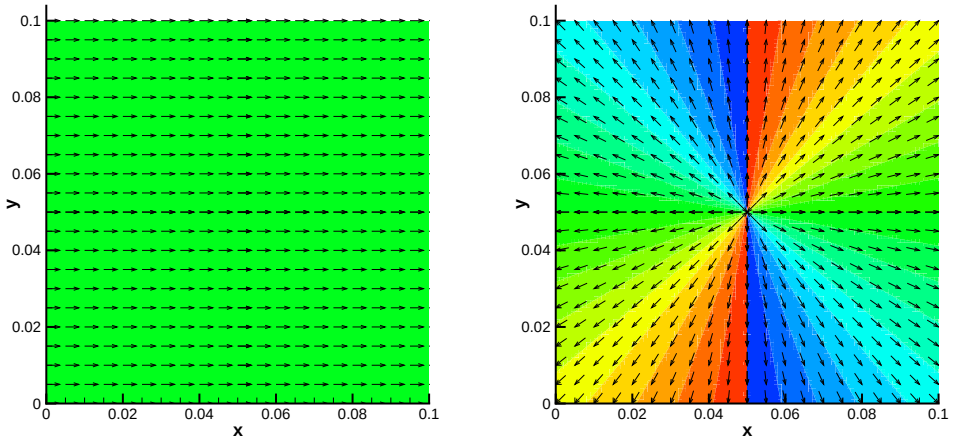

(a) 0° fibers.

(b) Radial fibers.

(c) Circumferential fibers.

(d) Optimal design.

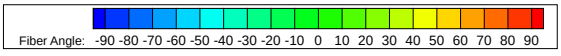

Figure 4.16: Design of a single layer clamped square plate with uniform pressure.

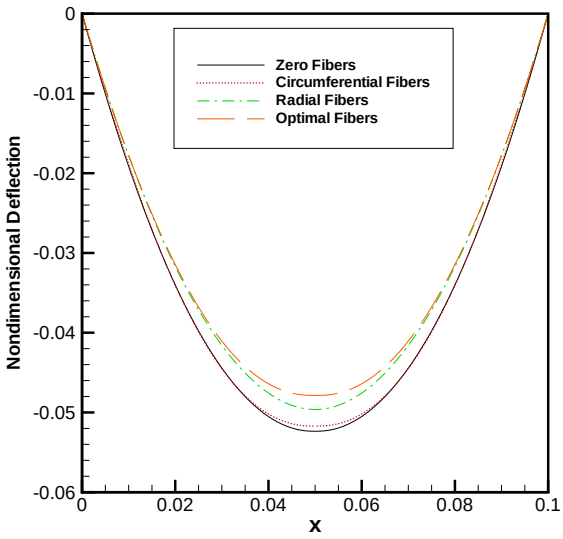

(a) Nondimensional deflection; $\bar{w} = \frac{wE_2h^3}{b^4q_0}$.

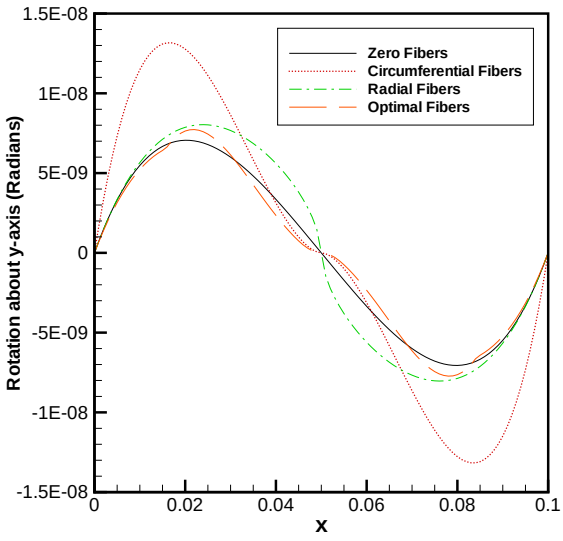

(b) Rotational about the y-axis; ψ^x.

Figure 4.17: Generalized deformations along the horizontal centerline.

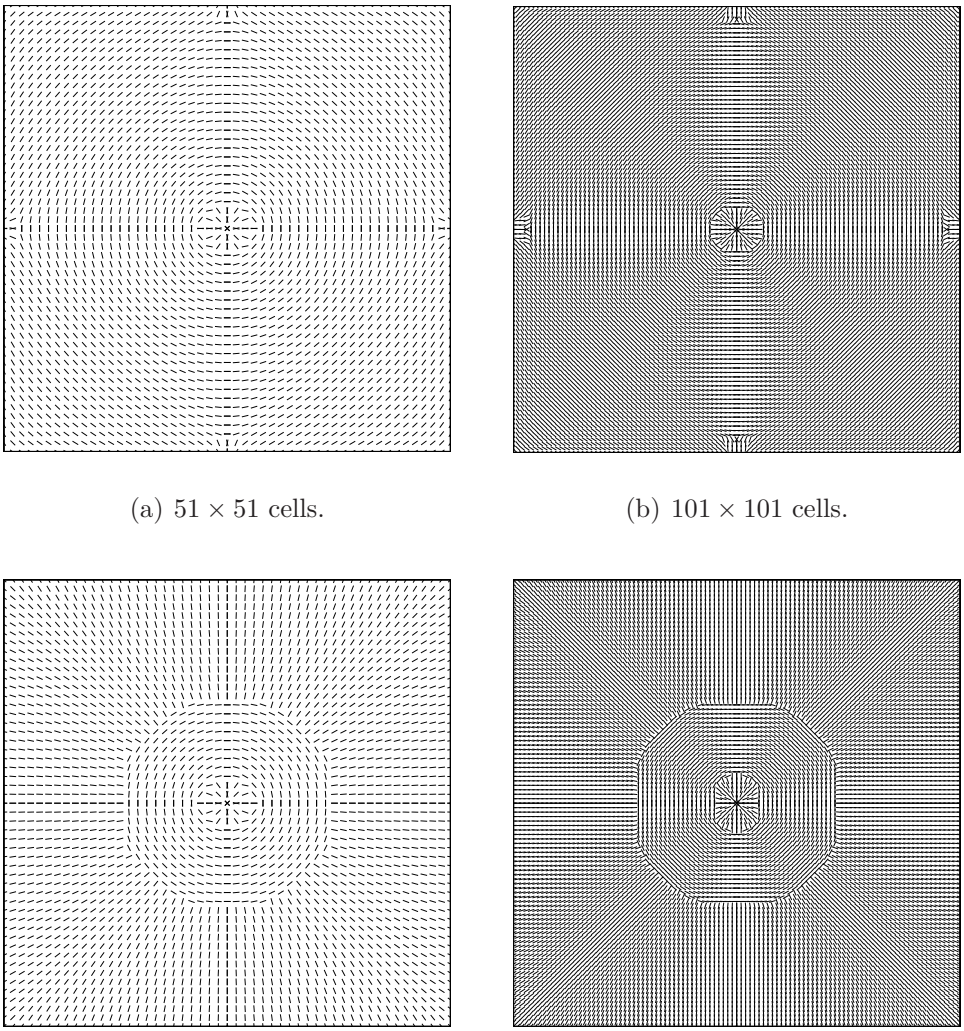

(a) 51×51 cells.

(b) 101×101 cells.

(c) 51×51 cells.

(d) 101×101 cells.

Figure 4.18: CA-converged variable-stiffness laminae for different lattice sizes. (a-b) simply supported; (c-d) clamped.

and the corresponding designs are depicted in Figure 4.19.

4.6.3 Multiple-Layer Laminates

Next, the square laminate of the previous section is designed for an increasing number of layers while the total thickness of the plate is kept fixed . Table 4.12 lists the optimal compliances for symmetric laminates with up to 5 layers for both simply supported and

Table 4.10: Normalized optimal compliance for simply supported/clamped laminae with different discretization.

	Normalized Compliance	
CA cells	**Simply Supported**	**Clamped**
51×51	0.7019	0.7327
101×101	0.7026	0.7278

Table 4.11: Optimal compliances for combined topology and fiber angle design of the clamped square lamina for different volume fractions.

Volume Fraction	**Normalized Compliance**
100%	0.7327
90%	0.7456
70%	0.7683
50%	0.8363

clamped edge boundary conditions. The corresponding CA-converged fiber distributions are depicted in Figures 4.20 and 4.21 (Note: the CA-converged points are not known to be optimal, or even Kuhn-Tucker, points). In these figures, layers are numbered starting from the outmost layer as 1 and ending to the innermost layer as n_h where n_h is half number of layers for symmetric laminates. The optimal compliances show that the gain in the bending stiffness is rather insignificant beyond $n_h = 4$ for symmetric laminates.

Table 4.12: Normalized compliance for simply supported/clamped square symmetric laminates (51×51 CA cells for the quarter model.)

	Normalized Compliance	
Half Number of Layers	**Simply Supported**	**Clamped**
1	0.7019	0.7327
2	0.6019	0.6522
3	0.5917	0.6396
4	0.5888	0.6413
5	0.5866	0.6374

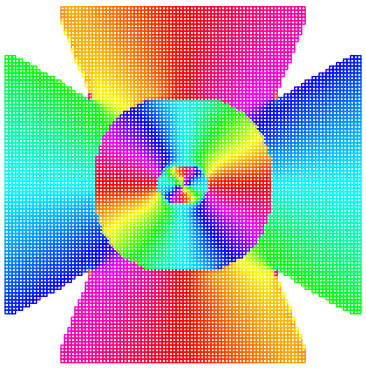

(a) 90% Volume.

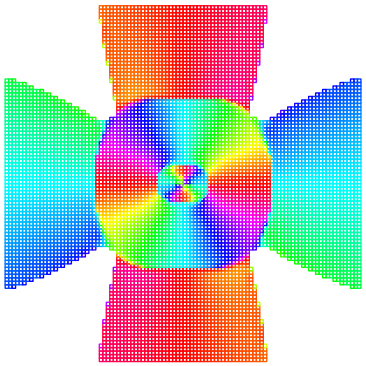

(b) 70% Volume.

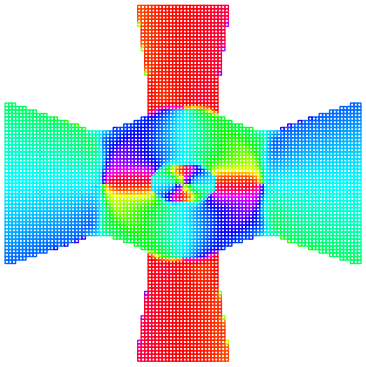

(c) 50% Volume.

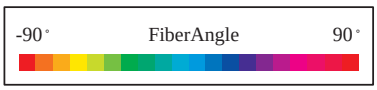

Figure 4.19: Combined topology and fiber angle design of a variable-stiffness clamped plate with a concentrated center load.

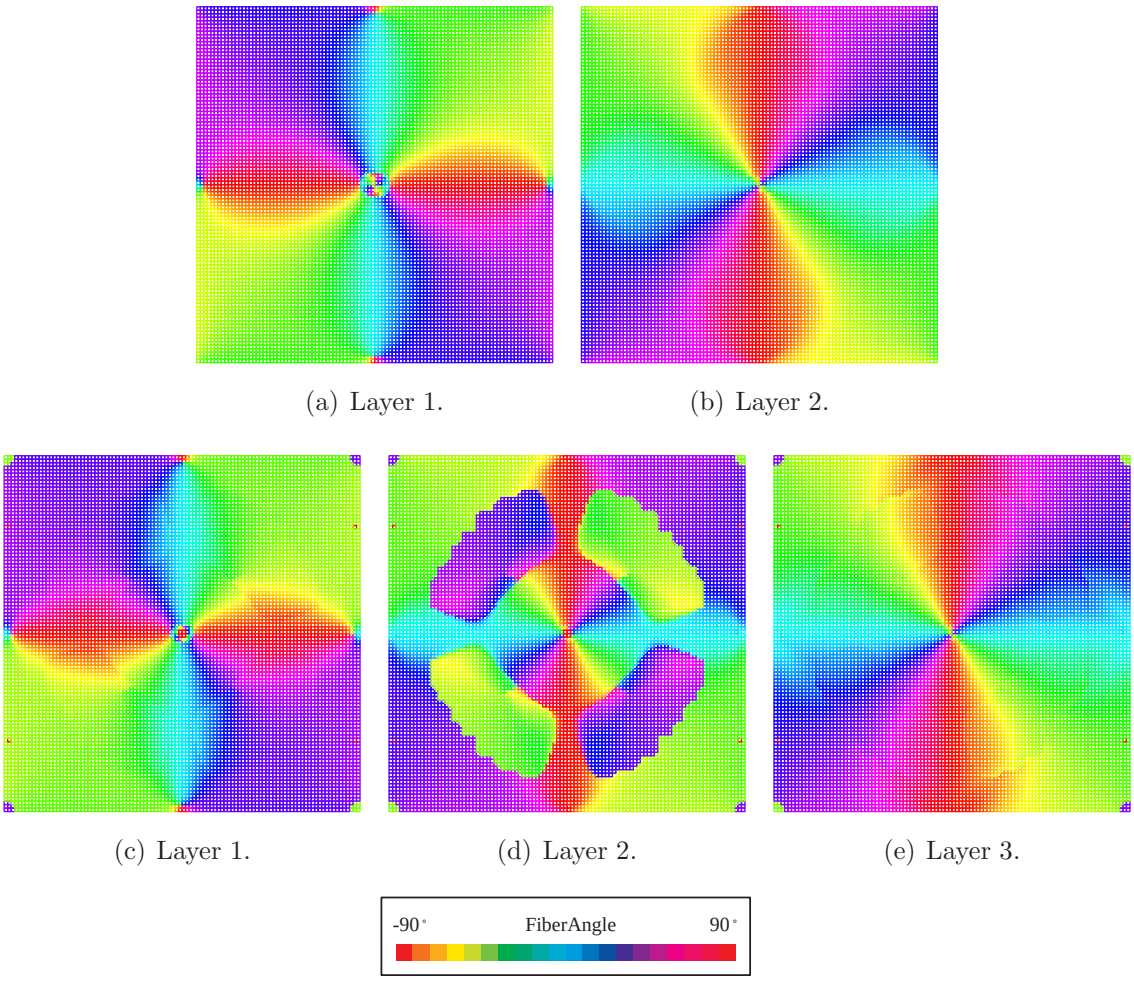

(a) Layer 1. (b) Layer 2.

(c) Layer 1. (d) Layer 2. (e) Layer 3.

Figure 4.20: CA-converged design of simply supported symmetric laminates; 51×51 CA lattice. (a-b) 4 layer symmetric laminate; (c-e) 6 layer symmetric laminate.

4.7 Bending Design Using Lamination Parameters

Fukunaga et al. [18, 19] studied optimal design of constant-stiffness laminates for natural frequency and buckling using 4 lamination parameters based on a CLPT (Classical Lamination Plate Theory) deformation analysis. Six lamination parameters (4 for bending and two for out of plane shear) were used by Diaconu et al. [13] to design laminated plates for fundamental frequency using a FSDT (First Order Shear Deformation Theory) deformation analysis engine. In this study, only the bending lamination parameters are used to design variable-stiffness plates for minimum compliance. Analysis is based on a conforming rectangular element [58] and the number of nodes is kept fixed on the shorter side of the plate to maintain the same level of accuracy for different aspect ratios. Tables 4.13 and 4.14 list

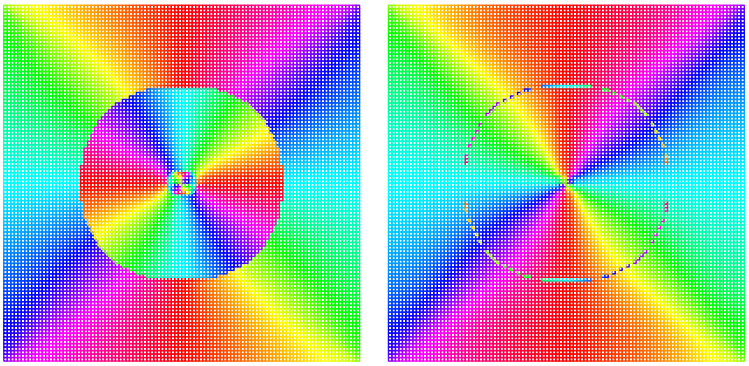

(a) Layer 1. (b) Layer 2.

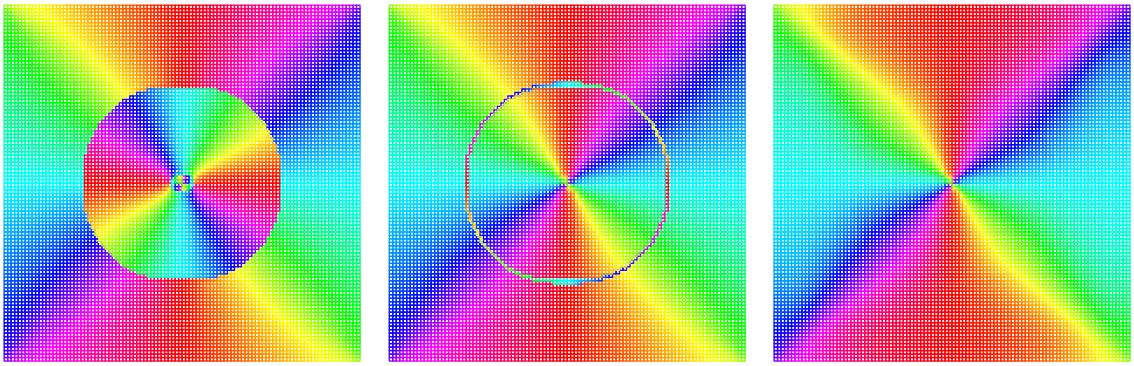

(c) Layer 1. (d) Layer 2. (e) Layer 3.

Figure 4.21: CA-converged design of clamped laminates; 51×51 CA lattice. (a-b) 4 layer symmetric laminate, (c-e) 6 layer symmetric laminate.

optimal nondimensional compliances for simply supported and clamped rectangular plates for different aspect ratios respectively.

Table 4.13: Effect of the aspect ratio on nondimensional compliance for simply supported rectangular plates with uniformly distributed loading. $\bar{C} = \frac{E_2 h^3 C}{q_0^2 b^5} \times 10^2$

$\frac{a}{b}$	$\bar{C}_{gc}$	$\bar{C}_{bv}$	$\bar{C}_{sv}$	$\bar{C}_{gv}$
1.0	0.2179	0.2165	0.1978	0.1787
1.2	0.3642	0.3307	0.2914	0.2721
1.4	0.5291	0.4423	0.3929	0.3715
1.6	0.6898	0.5551	0.4991	0.4763
1.8	0.8265	0.6682	0.6081	0.5843
2.0	0.9435	0.7811	0.7186	0.6943

Table 4.14: Nondimensional compliance for clamped rectangular plates with uniformly distributed loading. $\bar{C} = \frac{E_2 h^3 C}{q_0^2 b^5} \times 10^2$.

$\frac{a}{b}$	$\bar{C}_{gc}$	$\bar{C}_{bv}$	$\bar{C}_{sv}$	$\bar{C}_{gv}$
1.0	0.0602	0.0366	0.0337	0.0332
1.2	0.0827	0.0569	0.0523	0.0519
1.4	0.1021	0.0760	0.0711	0.0706
1.6	0.1212	0.0949	0.0902	0.0893
1.8	0.1400	0.1138	0.1090	0.1083
2.0	0.1587	0.1326	0.1279	0.1272

$\bar{C}_{gc}$: general lamination parameters; constant-stiffness.
$\bar{C}_{bv}$: balanced symmetric; variable-stiffness.
$\bar{C}_{sv}$: single layer, variable-stiffness.
$\bar{C}_{gv}$: general lamination parameters, variable-stiffness.

4.8 Parallel Results

The update rules presented in Chapter 3 are implemented as described in Section 4.2.2. Numerical studies reveal convergence problems with such an implementation as described

in the next sections. To resolve the convergence problem, a pipeline implementation is suggested. Finally, timing results are provided to demonstrate the gains made in terms of computational speed.

4.8.1 Design of the Asymmetric Cantilever

The same asymmetric cantilever of Section 4.4.5 is considered again here to investigate the performance of the standard parallel implementation. Analysis of the structure without design updates converged after 211,938 iterations and yielded a compliance of $C = 129.30N \cdot m$ using 32 processors. The optimal design for 50% volume fraction was obtained after 347,764 iterations resulting in a compliance of $C = 62.86N \cdot m$. Attempts to employ more than 32 processors in this case fail due to divergence of the CA iterations.

4.8.2 Convergence Issues

To investigate the divergence problem, consider the following linear system of equations:

$$\mathbf{KX} = \mathbf{F}. \tag{4.8}$$

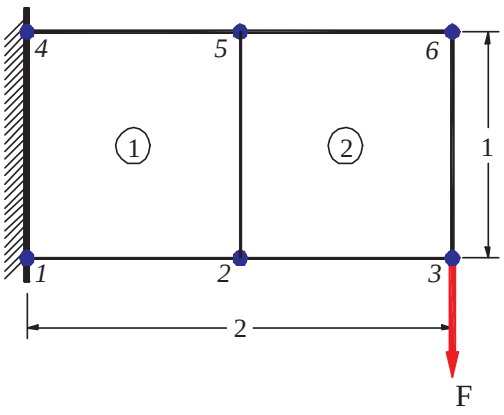

Figure 4.22: The prototype problem.

The CA analysis in a serial environment is identical to the Gauss-Seidel iterative solution of this system where **K** is the stiffness matrix obtained by an equivalent global finite element model, **X** is the unknown vector of displacements, and **F** is the given vector of applied forces. It is known that the finite element stiffness matrix is symmetric, positive definite, and non-singular for well-restrained structures, therefore convergence of a Gauss-Seidel iteration is guaranteed regardless of the starting point [38]. However, a Jacobi iteration might or might

not converge. To illustrate this issue, following Slotta et al. [68],consider a prototype problem as shown in Figure 4.22 modeled by six nodes and two bilinear finite elements.

The global stiffness matrix of Equation 4.8 can be written as the summation of the diagonal, lower triangular, and upper triangular matrices as:

$$\mathbf{K} = \mathbf{L} + \mathbf{D} + \mathbf{U}. \tag{4.9}$$

The Jacobi and Gauss-Seidel iteration matrices are given by, respectively,

$$\mathbf{J} = -\mathbf{D}^{-1}(\mathbf{L} + \mathbf{U}), \tag{4.10}$$
$$\mathbf{G} = -(\mathbf{L} + \mathbf{D})^{-1}\mathbf{U}. \tag{4.11}$$

By definition, the spectral radius is the maximum absolute value of the eigenvalues of the iteration matrix. For this prototype problem, the numerical values of the spectral radii for the Jacobi and Gauss-Seidel iteration matrices are

$$\begin{aligned} \lambda_J &= \quad 1.46596, \\ \lambda_{GS} &= \quad 0.834054. \end{aligned}$$

The fact that the spectral radius for the Jacobi iteration matrix is larger than one implies that Jacobi iteration for Equation 4.8 will not in general converge, and thus neither may the equivalent Jacobi CA iterations. On the other hand, Gauss-Seidel iteration always converges since the spectral radius in that case is less than one. However, the present block synchronous parallel implementation is a mixture of Jacobi and Gauss-Seidel iteration modes, where it is Gauss-Seidel style within each processor, and Jacobi style between processors. Hence, the iteration is more Jacobi like as the number of processors increases. For a single processor, the update environment is a pure Gauss-Seidel style, and when there are as many processors as the number of cells, it is a pure Jacobi style update scheme. Anywhere between those two extremes, the iteration is a mixture of Jacobi and Gauss-Seidel update styles. Numerical experiments showed divergence for the parallel code as the number of processors exceeded a certain value. The above spectral radii calculations for the prototype problem explain this divergence. It is important to mention here that such a phenomenon was not seen in the analysis of trusses since the spectral radii are less than one for both Gauss-Seidel and Jacobi iteration matrices [68]. The case for a 2-D continuum is attributed to the interpolation functions used and the nature of the problem. To resolve this convergence issue, a pipeline implementation which simulates a pure Gauss-Seidel iteration is suggested in the next section.

4.8.3 Pipeline Implementation

The initial parallel implementation given in Section 4.2.2 resulted in divergence of the CA as outlined above through hybrid Jacobi Gauss-Seidel style update schemes. An additional parallel implementation was developed to preserve the convergence of a pure Gauss-Seidel iteration through pipelined updates. This pipelined parallel code was created in Fortran 90 using the MPI (Message Passing Interface) communication library to guarantee Gauss-Seidel style iteration for the entire cell domain regardless of the number of processors used in the calculation. Cells are distributed, as for the standard implementation, in horizontal contiguous rows but the global iteration of the cell domain is pipelined across the processors (see Setoodeh et al. [64] for details).

The primary contribution of such an implementation is not in a novel parallelization of a CA, but rather to emphasize the need to maintain the convergence properties of the algorithm as the number of processors increases for a simultaneous analysis and design CA. The point is that convergence for parallel CA simultaneous analysis and design can be preserved through the simple use of pipelined computation provided that the serial CA simultaneous analysis and design iteration converges.

4.8.4 Timing Results

Execution time for the pipeline code with asynchronous message passing was measured for a cell domain grid of 751×1501 cells. The start up time and time required to flush the pipe at the end of the calculation grow as the number of processors increases. Since the pipeline code emulates a serial Gauss-Seidel iteration, the number of iterations to convergence are the same regardless of the number of processors used in the calculation. Timing results giving the speedup for the pipeline with asynchronous message passing are given in Figure 4.23 with computation time until convergence measured in seconds. Performance of the algorithm is expected to drop severely as the number of processors used in the calculation increase beyond half the number of available rows. In the case of the 751×1501 lattice, using more than 751 processors causes at least one processor in the pipe to have a single row to update and will result in an oscillation behavior. The model is rotated to maximize the number of rows available in the partitioning of work if the number of columns of cells is greater than the number of rows.

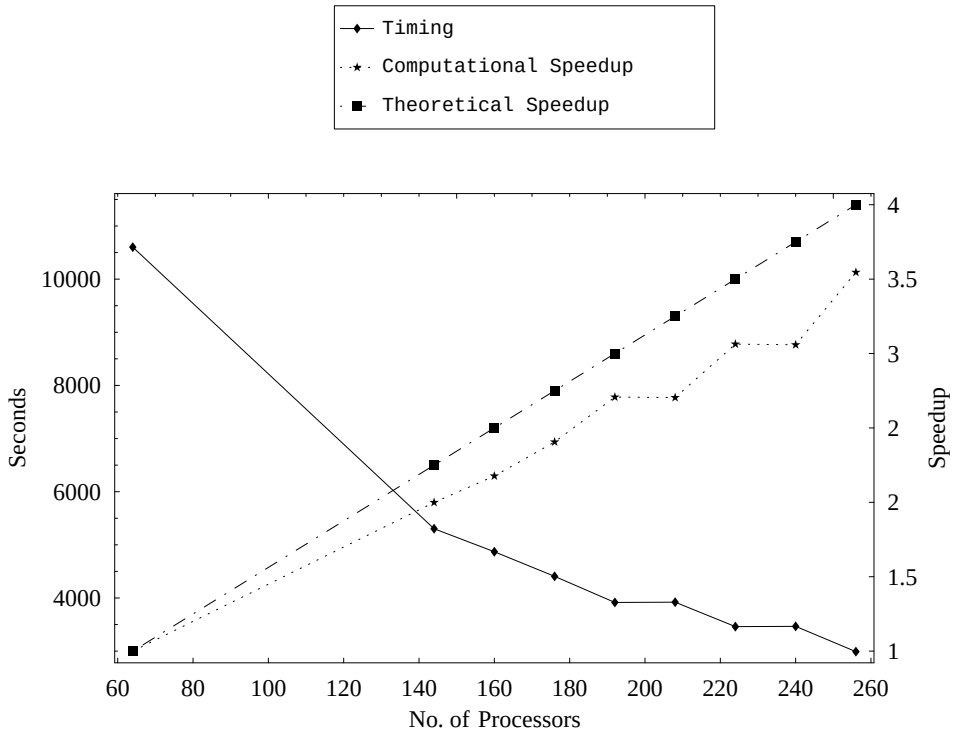

Figure 4.23: Timings performed at the Maui High Performance Computing Center on the P3 partition of Tempest consisting of 16-way, 375Mhz Nighthawk-2 nodes, each with 8Gbytes of shared memory.

Chapter 5

Conclusions

5.1 Summary

Applications of composite materials in aerospace and naval structures are growing more than ever. Manufacturing technologies of composites, on the other hand, are also evolving. This would demand innovative design approaches to fully benefit from directional properties of fiber-reinforced composite materials. In this thesis, design of variable-stiffness composites was studied for different types of problems and it was shown that significant improvements can be gained in the mechanical properties of structures by spatially optimal lay-up configurations.

In the first chapter, the concept of variable-stiffness laminates was reviewed. Design of composite laminates with variable fiber orientation is well studied in the literature. Global curve fitting [35] and linear variation of the fiber angle [22] are used in the literature to simplify the design problem by reducing the number of the design variables to a few design parameters defining the global curvilinear paths. In this study, however, fiber orientation angles were treated as continuous design variables at any point without the restriction of predefined curve fitting.

The computational burden has always been a restricting factor in structural optimization and therefore a robust parallel scheme which can significantly reduce the computational time is very compelling. The cellular automata (CA) paradigm is known for its parallelism and has recently been used in structural design [23, 69, 68, 2, 3]. In Chapter 2, elements and previous applications of cellular automata (CA) in structural design were reviewed. The cellular automaton algorithm proposed here is based on iterative updates of both field and design variables until convergence. Essential elements of CA in structural design are CA cell, cell state, CA lattice, cell neighborhood, and update rules. CA cells are used to discretize the domain. Field and design variables constitute the cell state and are updated using the update rules. The key feature of update rules is that only local information is required to

update a cell and therefore such a rule is expected to have a simple form. Besides, the fact that no information other than local neighbors' states is required makes CA inherently suitable for parallel implementation.

In Chapter 3, the CA formulation for topology design of isotropic continua as initially presented by Abdalla and Gürdal [2] was extended to combined fiber angle and topology design of anisotropic laminates. The CA update rule in structural design has two parts analysis rule and design rule. The analysis rule updates the cell displacement using only displacements of the neighboring cells based on the local equilibrium. Design variables, e.g., fiber orientation angles and thickness, are updated using a design rule derived from optimality criteria. It was shown that a closed form analysis update rule can be obtained for constant thickness isotropic media; however, for a general anisotropic continuum with variable thickness, a numeric analysis rule was used.

The optimality criteria for minimum compliance design subject to a volume constraint were used to derive local design rules. It was shown that the design update at any point splits into two separate levels. In the first level, the optimal lay-up configuration is found such that the local complimentary strain energy is minimized, and then in the second level, the density measure is updated using the optimal lay-up configuration obtained.

To represent the lay-up configuration, both fiber angles and lamination parameters were used. For a single layer laminae, closed form solutions exist that provide the global minimum of the complimentary strain energy. However, for laminates with multiple layers no closed form solution exists and therefore a numerical minimizer was used. Since the local design problem is not convex when parametrized using fiber orientation angles, special attention was required in numerical implementations. To avoid local optima, an elite type of strategy was used in this study. Each design iteration starts from a random point and obtains a candidate new design. This candidate design was used only if it generates a smaller value of the objective function for the same values of resultant forces. Since changes in the resultant forces are rather insignificant after the first few design iterations, such a strategy proved to be convergent.

A more robust methodology to tackle the issue of local minima is to use a global minimization routine such as DIRECT [32, 29, 28]. However, a global minimizer is computationally much more expensive than a gradient based solver. To reduce the computational costs of a global minimizer, a hybrid technique was suggested. In the hybrid approach, only in the first few design iterations, the global minimizer was used. Once the global minimum was approximately located, a gradient-based minimizer was used to fine tune the location of the minimum. Such a strategy exhibits good convergence rates in the bending examples used in this study.

Numerical studies show that the CA-converged distributions of the fiber angles exhibit discontinuities in parts of the domain with clearly defined boundaries. An in-depth study of the minimization problem reveals that, under special circumstances, the local design problem of minimization of the complimentary strain energy can have multiple minima. For

instance, in the case of single layer lamina, when principal stresses have approximately the same magnitude with opposite signs, both the principal stress direction and the direction perpendicular to that result in the same minimum value of the complimentary strain energy (the objective function). This behavior explains discontinuities between adjacent points in the domain where the resultant forces are very close, however, the sum of principal stresses is approximately zero. Although tow-placement technology requires continuous variation of the fiber orientation angle, based on the tow cutting and restarting capabilities of the current machines, the kind of discontinuities depicted in the resulting designs with clearly defined boundaries are expected to be manufacturable.

In general, fiber discontinuities occur at two different types of locations. First, as described in the previous paragraph, in locations where the absolute values of the two principal stresses are almost equal [71]. Second, in the regions of low stress values where the local fiber orientation has practically no effect on the stiffness of the structure. To resolve the discontinuities of the second kind a cell level heuristic manufacturing improvement update scheme is presented in this study. This heuristic manufacturing improvement smooths local fiber orientations in the regions of low stress while preserving the clear boundaries due to the case of multiple optimum fiber directions.

5.2 Future Research

The design objective in this study was minimizing the compliance. In other words, the proposed design methodology maximizes the stiffness of the structure. In many practical applications however, design for maximum strength is required. Even though maximum stiffness designs usually have improved strength properties, they are not optimal in general. A heuristic approach based on minimization of a local failure function was used by Majak [44] to design for strength. A more rigorous mathematical formulation is required to handle local stress constraint.

Usually laminated sandwich plates are used where plates are expected to have a high bending stiffness. Miki and Sugiyama [47] designed laminated sandwich plates with isotropic core and orthotropic surface materials. They presented the feasible lamination parameters domain for different core thicknesses and used two lamination parameters, i.e. W_1 and W_3, and core thickness as design variables for optimal design of constant-stiffness panels. A similar formulation can be used to design variable-stiffness sandwich panels.

In many aerospace structures, laminated plates have to be designed to withstand vibration and buckling in addition to static deformations. The concept of variable-stiffness laminates can be also be extended to design laminated plates for buckling and vibration[4]. Tatting and Gürdal [70] used a three parameter curvilinear fiber path definition to model variable-stiffness laminates along with genetic algorithm to design for buckling load. Wu et al. [85] designed variable-stiffness plates for buckling and post-buckling using a linear variation of

the fiber angle along the panel length. A general variable-stiffness formulation where stiffness properties are allowed to vary independently over the domain has yet to be studied. Composite shell structures such as aircraft fuselage can also benefit from the concept of variable-stiffness laminates. This application is particularly compelling since filament winding and tow-placement are the primary manufacturing techniques used to build composite shells.

In Chapter 5, numerical examples were given for the optimal distribution of the lamination parameters. In those examples however, the actual lay-up configurations were not computed and were left for the future work. The restricted problem formulation of Chapter 3 was an attempt to compute the lay-up configuration for balanced symmetric laminates with equal thickness layers which are practical from manufacturing point of view. Using such a formulation and taking into account the fiber orientation of the neighboring cells, it is believed that meaningful fiber angles can be obtained in a post-processing level. Besides the idea of balanced symmetric laminates with equal thickness layers can potentially be extended to general case of the lamination parameters. Eventually, this approach can be extended to bending lamination parameters. It is also believed that it is possible to retrieve a continuous fiber path from the lamination parameters in a post processing step [65]. Future research should concentrate on using curve fitting techniques to find fiber angle distributions for arbitrary number of plies that approximate the optimized lamination parameters distribution. In such a scheme, manufacturing constraints such as minimum allowed radius of curvature, can be included as well.

A more in-depth knowledge of manufacturing innovations and their limitations can provide us with better insights to steer our design formulation. For example, the kind of fiber angle discontinuities depicted in the resulting designs, with clearly defined boundaries, are expected to be manufacturable. Nonetheless, even if there are still manufacturing obstacles to build such panels, the optimal distribution of the fiber orientations provides us with guidelines on how to define continuous fiber paths which are consistent with the optimal distributions and reformulate the design problem using continuous fiber path representations.

On the CA front on the other hand, there are many different areas that require additional research work. For example, the merit of CA in structural design is essentially in its ease of parallel implementation. However, it is very important to have an efficient parallel implementation to fully benefit from CA. To enhance the convergence properties of CA, Abdalla et al. [1] used multi-grid acceleration for analysis and design of beams on FPGA hardware. Similar approaches are essential for 2-D problems. Finally, efficient domain decomposition in CA is very crucial to balance load between processors.

Bibliography

[1] M. Abdalla, S. Kim, and Z. Gürdal. Multigrid accelerated cellular automata for structural design optimization: A 1-d implementation. In *45th AIAA/ASME/ASCE/AHS/ASC Structures, Structural Dynamics and Materials Conference*, Palm Spring, California, April 18-22 2004.

[2] M. M. Abdalla and Z. Gürdal. Structural design using optimality based cellular automata. In *Proceedings of the 43rd AIAA/ASME/ASCE/AHS Structures, Structural Mechanics and Materials Conference*, Denver, CO, 2002. AIAA.

[3] M. M. Abdalla and Z. Gürdal. Structural design using cellular automata for eigenvalue problems. *Structural and Multidisciplinary Optimization*, 26(3-4):200–208, 2004.

[4] M. M. Abdalla, S. Setoodeh, and Z. Gürdal. Design of variable stiffness composite panels for maximum fundamental frequency using lamination parameters. In *European Conference on Spacecraft Structures, Materials & Mechanical Testing*, Noordwijk, The Netherlands, May 2005.

[5] M. Autio. Optimization of coupled thermal-structural problems of laminated plates with lamination parameters. *Structural and Multidisciplinary Optimization*, 21:40–51, 2001.

[6] N. V. Banichuk. Optimization of anisotropic properties of deformable media in plane problems of elasticity. *Mechanics of Solids*, 14(1):63–68, 1979.

[7] N. V. Banichuk, V. Saurin, and A. A. Barsuk. Optimal orientation of orthotropic materials for plates designed against buckling. *Structural Optimization*, 10:191–196, 1995.

[8] J. Barlow. Optimal stress locations in finite element models. *International Journal for Numerical Methods in Engineering*, 10:243–251, 1976.

[9] M. P. Bendøe, A. R. Díaz, R. Lipton, and J. E. Taylor. Optimal design of material properties and material distribuation for multiple loading conditions. *International Journal for Numerical Method in Engineering*, 38(7):1149–1170, 1995.

[10] M. P. Bendsøe and O. Sigmund. *Topology Optimization, Theory, Methods and Applications*. Springer-Verlag, Berlin Heidelberg New York, 2003.

[11] H. Brandmaier. Optimum filament orientation criteria. *J. Composite Materials*, 4:422–425, July 1970.

[12] A. A. G. Cooper. *Trajectorial Fiber Reinforcement of Composite Structures*. PhD thesis, Washington University, St. Louis, Missouri, 1972.

[13] C. G. Diaconu, M. Sato, and H. Sekine. Layup optimization of symmetrically laminated thick plates for fundamental frequencies using lamination parameters. *Structural and Multidisciplinary Optimization*, 24:302–311, 2002.

[14] G. Duvaut, G. Terrel, F. Léné, and V. E. Verijenko. Optimization of fiber reinforced composites. *Composite Structures*, 48:83–89, 2000.

[15] D. O. Evans, M. M. Vaniglia, and P. C. Hopkins. Fiber placement process study. In *34th International SAMPE Symposium and Exhibition*, pages 1822–1833, May 1989.

[16] J. Foldager, J. S. Hansen, and N. Olhoff. A general approach forcing convexity of ply angle optimization in composite laminates. *Structural Optimization*, 16:201–211, 1998.

[17] H. Fukunaga. A solution procedure for determining laminate configurations from lamination parameters. *Advanced Composite Materials*, 1(3):209–224, 1991.

[18] H. Fukunaga, H. Sekine, and M. Sato. Optimal design of symmetric laminated plates for fundamental frequency. *Journal of Sound and Vibration*, 171(2):219–229, 1994.

[19] H. Fukunaga, H. Sekine, M. Sato, and A. Iino. Buckling design of symmetrically laminated plates using lamination parameters. *Computers & Structure*, 57(4):643–649, 1995.

[20] H. C. Gea and J. H. Luo. On the stress-based and strain-based methods for predicting optimal orientation of orthotropic materials. *Structural and Multidisciplinary Optimization*, 26(3-4):229–234, 2004.

[21] Z. Gürdal, R. T. Haftka, and P. Hajela. *Design and Optimization of Laminated Composite Materials*. John Wiley & Sons Inc., 1999.

[22] Z. Gürdal and R. Olmedo. In-plane response of laminates with spatially varying fibre orientations: Variable stiffness concept. *AIAA Journal*, 31(4):751–758, 1993.

[23] Z. Gürdal and B. Tatting. Cellular automata for design of truss structures with linear and nonlinear response. In *Proceedings of the 41st AIAA/ASME/ASCE/AHS Structures, Structural Mechanics and Materials Conference*, pages 2000–1580, Atlanta, GA, 2000. AIAA Paper.

[24] R. T. Haftka. Simultaneous analysis and design. *AIAA Journal*, 23(7):1099–1103, 1985.

[25] R. T. Haftka and Z. Gürdal. *Elements of Structural Optimization (Solid Mechanics and Its Applications)*. Kluwer Academic Publishers, 1992.

[26] V. B. Hammer, M. P. Bendsøe, R. Lipton, and P. Pedersen. Parametrization in laminate design for optimal compliance. *International Journal of Solids and Structures*, 34(4):415–434, 1997.

[27] W. Hansel and W. Becker. Layerwise adaptive topology optimization of laminate structures. *Engineering Computations*, 16(7):841–851, 1999.

[28] J. He, A. Verstak, L. T. Watson, T. S. Rappaport, C. R. Anderson, N. Ramakrishnan, C. A. Shaffer, W. H. Tranter, K. Bae, and J. Jiang. Global optimization of transmitter placement in wireless communication systems. In *Proceedings of High Performance Computing Symposium*, San Diego, CA, 2002.

[29] J. He, L. T. Watson, N. Ramakrishnan, C. A. Shaffer, A. Verstak, J. Jiang, K. Bae, and W. H. Tranter. Dynamic data structures for a direct search algorithm. *Computational Optimization and Applications*, 23(1):5–25, 2002.

[30] M. W. Hyer and R. F. Charette. Use of curvilinear fiber format in composite structure design. In *30th Structures, Structural Dynamics, and Material Conference*, pages 1011–1015, Mobile, AL, April 1989. AIAA.

[31] M. W. Hyer and H. H. Lee. The use of curvilinear-fiber format to improve buckling resistance of composite plates with central holes. *Composite Structures*, 18(3):239–261, 1991.

[32] D. R. Jones. The direct global optimization algorithm. In *Encyclopedia of Optimization*, volume 1, pages 431–440, Boston, 2001.

[33] R. M. Jones. *Mechanics of Composite Materials*. Taylor & Francis, Inc., second edition, 1998.

[34] T. Y. Kam and F. M. Lai. Maximum stiffness design of laminated composite plates via a constrained global optimization approach. *Composite Structures*, 32:391–398, 1995.

[35] Y. Katz, R. T. Haftka, and E. Altus. Optimization of fiber directions for increasing the failure load of a plate with a hole. In *ASC Technical Conference*, volume 4, pages 62–71, 1989.

[36] D. W. Kelly and M. W. Tosh. Interpreting load paths and stress trajectories. *Engineering Computations*, 17(2):117–135, 2000.

[37] I. Y. Kim and O. de Weck. Variable chromosome length genetic algorithm for structural topology design optimization. In *45th AIAA/ASME/ASCE/AHS/ASC Structures, Structural Dynamics & Materials Conference*, Palm Springs, CA, April 19-22 2004.

[38] D. Kincaid and W. Cheney. *Numerical Analysis*. Brooks/Cole, Pacific Grove, CA, 1996.

[39] E. Kita and T. Toyoda. Structural design using cellular automata. *Journal of Structural and Multidisciplinary Optimization*, (19):64–73, 2000.

[40] Q. Q. Liang and G. P. Steven. A performance-based optimization method for topology design of continuum structures with mean compliance constraints. *Computer Methods in Applied Mechanics and Engineering*, 191:1471–1489, 2002.

[41] R. P. Lipton. On optimal reinforcement of plates and choice of design parameters. *Control and Cybernetic*, 23(3):481–492, 1994.

[42] B. B. Lowekamp, L. T. Watson, and M. S. Cramer. The cellular automata paradigm for the parallel solution of heat transfer problems. *Parallel Algorithms and Applications*, 9:119–130, 1995.

[43] E. Lund and J. Stegman. On structural optimization of composite shell structures using a discrete constitutive parameterization. In *American Society for Composites 18th Technical Conference, ASC 18*, page 110, Gainesville, FL, October 19-22 2003.

[44] J. Majak and S. Hannus. Orientational design of anisotropic materials using the hill and tsai-wu strength criteria. *Mechanics of Composite Materials*, 39(6):509–520, 2003.

[45] M. Miki. Material design of composite laminates with required in-plane elastic properties. In *Progress in Science and Engineering of Composites, ICCM-IV*, pages 1725–1731, Tokyo, 1982.

[46] M. Miki. A graphical method for designing fibrous laminated composite with required in-plane stiffness. In *Trans. JSCM 9*, volume 2, pages 51–55, 1983.

[47] M. Miki and Y. Sugiyama. Optimum design of laminated composite plates using lamination parameters. *AIAA Journal*, 113:275–283, 1991.

[48] M. Miki and Y. Sugiyama. Optimum design of laminated composite plates using lamination parameters. *AIAA Journal*, 31:921–922, 1993.

[49] S. Missoum, Z. Gürdal, and S. Setoodeh. Study of a new local update scheme for cellular automata in structural design. *Structural and Multidisciplinary Optimization, accepted for publication*, 29(2):103–112, 2005.

[50] S. Nagendra, S. Kodiyalam, and J. E. Davis. Optimization of tow fiber paths for composite design. In *Proceedings of the AIAA/ASME/ASCE/AHS/ASC* 36^{th} *SDM Conference*, pages 1031–1041, New Orleans, LA, April 10-13 1995.

[51] L. Parnas, S. Oral, and U. Ceyhan. Optimum design of composite structures with curved fiber courses. *Composite Science and Technology*, 63:1071–1082, 2003.

[52] P. Pedersen. On optimal orientation of orthotropic materials. *Structural Optimization*, (1):101–106, 1989.

[53] P. Pedersen. Bounds on elastic energy in solids of orthotropic materials. *Structural Optimization*, 2:55–63, 1990.

[54] P. Pedersen. On thickness and orientational design with orthotropic materials. *Structural Optimization*, 3:69–78, 1991.

[55] P. Pedersen. Optimal orientation of anisotropic materials, optimal distribution of anisotropic materials, optimal shape design with anisotropic materials, optimal design for a class of non-linear elasticity. In G. I. N. Rozvany, editor, *Optimization of Large Structural Systems*, volume II, pages 649–681, 1993.

[56] P. Pedersen. Examples of density, orientation, and shape-optimal 2d-design for stiffness and/or strength with orthotropic materials. *Structural Optimization*, 26(1-2):37–49, 2003.

[57] K. Preston and M. J. B. Duff. *Modern Cellular Automata, Theory and Applications.* Plenum Press, New York, 1984.

[58] J. N. Reddy. *Mechanics of Laminate Composite Plates, Theory and Analysis.* CRC Press, 1997.

[59] G. Rozvany, O. Querin, and V. Pomezanski. Extended optimality in topology design. *Structural and Multidisciplinary Optimization*, 24:257–261, 2002.

[60] S. Setoodeh, M. M. Abdalla, and Z. Gürdal. Comparison of design parameterization of variable-stiffness panels using fiber angles and lamination parameters. in preparation.

[61] S. Setoodeh, M. M. Abdalla, and Z. Gürdal. Design of variable-stiffness laminates using lamination parameters. submitted to Composites Part B: Engineering.

[62] S. Setoodeh, M. M. Abdalla, and Z. Gürdal. Simultaneous topology and curvilinear fiber path design of composite layers using cellular automata. In *45th AIAA/ASME/ASCE/AHS/ASC SDM Conference*, Palm Spring, California, April 18-22 2004.

[63] S. Setoodeh, M. M. Abdalla, and Z. Gürdal. Combined topology and fiber path design of composite layers using cellular automata. *Structural and Multidisciplinary Optimization*, Onlie First, July 2005.

[64] S. Setoodeh, D. B. Adams, Z. Gürdal, and L. T. Watson. Pipeline implementation of cellular automata for structural design on message-passing multiprocessors. *Mathematical and Computer Modeling, to appear*, 2004.

[65] S. Setoodeh, A. W. Blom, M. M. Abdalla, and Z. Gürdal. Generating curvilinear fiber paths from lamination parameters distribution. In *47th AIAA/ASME/ASCE/AHS/ASC Structures, Structural Dynamics, and Materials Conference*, Newport, Rhode Island, May 1-4 2006. submitted.

[66] S. Setoodeh and Z. Gürdal. Design of composite layers with curvilinear fiber paths using cellular automata. In *Proceedings of the 44th AIAA/ASME/ASCE/AHS Structures, Structural Dynamics, and Materials Conference*, Norfolk, Virginia, 7-10 April 2003.

[67] S. Setoodeh, Z. Gürdal, and L. T. Watson. Design of variable-stiffness composite layers using cellular automata. *Computer Methods in Applied Mechanics and Engineering*, Available Online June 2005.

[68] D. J. Slotta, B. Tatting, L. T. Watson, Z. Gürdal, and S. Missoum. Convergence analysis for cellular automata applied to truss design. *Engineering Computations*, 19(8):953–969, 2002.

[69] B. Tatting and Z. Gürdal. Cellular automata for design of two-dimensional continuum structures. In *Proceedings of the 8th AIAA/USAF/NASA/ISSMO Symposium on Multidisciplinary Analysis and Optimization*, pages 2000–4832, Long Beach, CA, 2000. AIAA Paper.

[70] B. F. Tatting and Z. Gürdal. Analysis and design of tow-steered variable stiffness composite laminates. In *AHS Meeting*, Williamsburg, VA, October 30-November 1 2001.

[71] J. Thomsen. Optimization of composite discs. *Structural Optimization*, 3:89–98, 1991.

[72] S. P. Timoshenko and S. Woinowsky-Krieger. *Theory of Plates and Shells*. McGraw-Hill Book Company, New York, 1959.

[73] M. W. Tosh and D. W. Kelly. On the design, manufacture and testing of trajectorial fibre steering for carbon fiber for composite laminates. *Composite Part A: Applied Science & Manufacturing*, 31(10):1047–1060, 2000.

[74] A. Tovar, G. L. Niebur, M. Sen, and J. E. Renaud. Bone structure adaptation as a cellular automaton optimization process. In *45th AIAA/ASME/ASCE/AHS/ASC Structures, Structural Dynamics & Materials Conference*, Palm Springs, CA, April 19-22 2004.

[75] S. W. Tsai and H. T. Hahn. *Introduction of Composite Materials*. Technomic, Lancaster, 1980.

[76] S. W. Tsai and N. J. Pagano. Invariant properties of composite materials. In *Composite Materials Workshop*, pages 233–253, Westport, 1968. Technomic.

[77] S. Ulam. Random processes and transformations. In *Proceedings of the International Congress of Mathematics*, volume 2, pages 85–87, 1952.

[78] J. von Neumann. *Theory of Self-Reproducing Automata*. University of Illinois Press, 1996.

[79] J. Wahle, L. Neubert, J. Esser, and M. Schreckenberg. A cellular automaton traffice flow model for online simulation of traffice. *Parallel Computing*, 27:719–735, 2001.

[80] C. Waldhart, Z. Gürdal, and C. Ribbens. Analysis of tow placed, parallel fiber, variable stiffness laminates. In *37th AIAA/ASME/ASCE/AHS/ASC Structures, Structural Dynamics and Material Conference*, pages 2210–2220, Salt Lake City, UT, Apr.15-17 1996.

[81] L. T. Watson. Theory of globally convergent probability-one homotopies for nonlinear programming. *SIAM Journal on Optimization*, (11):761–780, 2000.

[82] J. R. Wiener and A. Rosenbluth. The mathematical formulation of the problem of conduction of impulses in a network of connected excitable elements, specifically in cardiac muscle. In *Arch. Inst. Cardiol*, volume 16, pages 205–265, Mexico, 1946.

[83] S. Wolfram. *Cellular Automata and Complexity: Collected Papers*. Addison-Wesley Publishing Company, 1994.

[84] S. Wolfram. *A New Kind of Science*. Wolfram Media, 2002.

[85] K. Wu, Z. Gürdal, and J. Starnes. Buckling and postbuckling of tow-placed variable stiffness panels. In *Proceedings of the 43rd AIAA/ASME/ASCE/AHS/ASC Structures, Structural Dynamics and Materials (SDM) Conference*, Denver, CO, 2002.

Vita

Shahriar Setoodeh was born in 1972 in Shiraz, Iran. After graduating from high school in 1990, he entered Shiraz University majoring in Mechanical Engineering. In 1995 he started his masters degree program at Shiraz University. In 2001, he started his PhD degree program at Virginia Tech under supervision of Professor Zafer Gürdal.